Effects of Autonomous Vehicles on Pavement Distress & Road Safety and Pavement Distress Optimization

by

© Md Masud Rana

A Thesis Submitted to the

School of Graduate Studies

In partial fulfillment of the requirements for the degree of

Master of Engineering

Faculty of Engineering and Applied Science

Memorial University of Newfoundland

May 2021

St. John's Newfoundland and Labrador Canada

Abstract

The commercial application of automation technology in passenger and freight transport will bring positive revolutionary changes in transportation mobility. Despite having more advantages, automation in trucking technology has some detrimental effects on the performance of asphalt pavement and highway safety. This study focuses on optimization of asphalt pavement distresses and prediction of rutting induced traffic safety factors for movement of autonomous trucks. This study optimizes the asphalt concrete (AC) pavement distresses by devising traffic input in Mechanistic-Empirical Pavement Design Software, AASHTOWare. An increase in pavement distresses was observed for a small increase in the standard deviation of wheel wander, uniform distribution of truck traffic loading, and equal distribution of vehicle positioning on the road lanes. Permanent deformation of the asphalt concrete layer for roads (PEDRO) model was incorporated to predict AC pavement rutting for a typical pavement section. Hydroplaning speed and skid resistance as traffic safety factors were evaluated from widely accepted empirical equations for the induced rutting. A standard tire rather than a truck tire was considered due to its high susceptibility to traffic safety. A graphical relationship has been proposed to obtain a design threshold value for hydroplaning speed, water film depth and autonomous truck speed. An attempt was made to improve pavement performance by increasing frequency of truck load in low-temperature period of a day.

.

Keywords: Autonomous Truck, Pavement Distresses, Optimization, Traffic Safety, Low-Temperature Duration.

Acknowledgments

First and foremost, the author would like to express his deep praise and gratitude to the Almighty Allah for giving strength and means for completing the thesis work successfully. The author also would like to acknowledge profound gratitude and indebtedness to the supervisor, Dr. Kamal Hossain for his continuous guidance, valuable suggestions, and co-operation throughout the study.

Special thanks to Dr. Ashutosh Sutra Dhar for being supportive in many times of the journey in this university. The author gratefully acknowledges the support provided by Professor Elie Hajj from the University of Nevada, USA for allowing us to use the AASHTOWare ME Pavement design software and Mr. Piratheepan from the University of Nevada for his time and effort throughout this study and software usage.

The author thankfully acknowledges the support from the team members of the Advanced Road & Transportation Engineering Lab (ARTEL) at the Memorial University of Newfoundland. Their continuous encouragement and knowledge sharing mentality helped the author a lot to develop research ideas and implement them in studies. The author also would like to thank the Bangladeshi community in St. John's for being a source of inspiration at a place thousands of miles away from my beloved home country.

Finally, the author would like to convey his thanks, love and gratitude to his beloved parents and family members due to their encouragement and sacrifice for his personal and academic life. Last but not the least, the author would like to thank his dearest wife, Atika for her motivation and dedication throughout this journey.

Table of Contents

List of Figures

List of Tables

Co-authorship Statement

As the principal author, Md. Masud Rana has conducted all the research of the manuscripts presented in this thesis under the supervision of Dr. Kamal Hossain. Mr. Rana also prepared the draft manuscript. The co-author supervised the research and reviewed the manuscript.

Chapter 1 Introduction and Overview

1.1 Background

Rapid growth in information and communication technology is accelerating the implementation of automation techniques in transportation mobility. Center for Automotive Research predicted the increment of autonomous vehicles sales up to 55 percent of all vehicles by 2040 (Fee, 2020). Some places of the world witnessed the successful application of autonomous vehicles in the time of Covid-19 to deliver necessary foods and medical equipment to the infected people (Donelson, 2020). Automation in transportation mobility has reached out to trucking sectors, crossing the border of the passenger car (Noorvand et al., 2017). An autonomous truck was deployed to deliver butter in California, making a country trip (Linder, 2019). Different organizations worldwide announced schedules to perform field tests of autonomous trucks (Wanek-Libman, 2020). Successful implementation of automation techniques in transportation sectors will bring potential impacts on transportation planning and pavement design.

Autonomous vehicles, including trucks, significantly reduce crash rates due to human error, relieving drivers stress, improved productivity, and mobility being used as mobile office and bedrooms, minimizing traffic congestion, parking costs, pollution emissions, etc. (Litman, 2020). Automatic braking configured in AV technologies will increase the highway infrastructure capacity through the reduction of safe distance between vehicles at an increased speed (Chen et al., 2016; Lu et al., 2020; Shladover et al., 2012; Simko, 2016; Tientrakool et al., 2011). This automation will overcome the shortage of

truck drivers also (Gungor & Al-Qadi, 2020a). Despite having a lot of advantages, pavement infrastructures will be negatively affected with the implementation of AV technology. Researchers encountered the necessity to change the road markings, lane width, roadway capacity, and pavement design for AV (Litman, 2020).

Pavement engineers and researchers are working on the structural performance of AC pavement for minimization of additional distresses induced by AT. The influences of AT on the performance of asphalt concrete (AC) pavement are induced from channelized or less wander traffic loading, reduced inter-vehicle distances, and constant speeds and less stop/start actions (Steyn & Maina, 2019). A very limited number of studies on the optimization of pavement distresses for AT movement are observed. The optimization of distress was introduced controlling wheel load distribution in a lane of pavement section (Noorvand et al., 2017; Zhou et al., 2019; Chen et al., 2019, 2020) and changing the positioning of vehicles on the different lane of a road section (Noorvand et al., 2017).

Noorvand et al. devised traffic input in the Mechanistic-Empirical Pavement Design Guide (MEPDG) for the mixing of the human-driven truck and autonomous trucks (ATs). The authors devised traffic input to control wheel loading distribution and vehicle positioning on different lanes of a road section. They observed a significant reduction in rutting and fatigue for the uniformly distributed wheel on a pavement lane compared with AT (Noorvand et al., 2017). Chen et al. conducted finite element studies to observe zero-wander, double peak gaussian and two-section uniform distribution of wheel load on pavement fatigue and rutting. The authors found two-section uniform mode as efficient in distress reduction mode (Chen et al., 2019). Chen et al. also introduced fatigue damage

growth mode to allow the movement of the vehicle on a pavement lane. The basis of this technique is to allow vehicle movement in a controlled manner to induce equal fatigue on the entire width of the lane (Chen et al., 2020).

1.2 Research Gap

The impact of autonomous trucks (AT) on pavement performance and their remediation have not been extensively studied yet. Researchers have performed some studies to estimate pavement distresses due to the movement of AT on asphalt concrete pavement. Researchers found that the lane-centering tendency of AT affects pavement performance significantly. This lane-centering tendency reduces the standard deviation of wheel loading distribution (wheel wander) on pavement lane. Some of them introduced techniques to minimize pavement distresses from AT (Noorvand et al., 2017; Chen et al., 2019, 2020). Chen et al. (2019, 2020) performed finite element analysis to minimize pavement distresses of AT movement through the control on wheel loading distribution patterns. But, there is less possibility for AT to occupy the pavement lane very soon. Noorvand et al. (2017) introduced mechanisms to improve pavement performance for combination of AT and human-driven trucks. This analysis data was compared with fully autonomous or zero wander trucks. Zhou et al. (2019) performed field tests on AT and observed that AT could be modeled for loading distribution of standard deviation ranging from 0.25 cm (1 inch) to 0.76 cm (3 inches). Pavement performance for the combination of human-driven trucks and AT with a wide range of wheel wander has not been studied yet.

A significant reduction in the road accident is encountered by Stakeholders through the implementation of automation technology in the transportation sectors. Channelized truck traffic seriously deteriorates asphalt pavement rutting. Increased rut depth are crucial factors for traffic safety in wet weather conditions. The effects of AT implementation on hydroplaning potential and skid resistance (traffic safety parameters) for different wheel wanders have not been analyzed so far.

Climatic factors greatly affect asphalt pavement performance. Pavement temperature changes with air temperature and other climatic factors. Resilient modulus, a critical variable in asphalt pavement design, varies with pavement temperature. (Ghao et al., 2019; Zhao et al., 2020). Asphalt mixtures are found to show higher resilient modulus at low temperature. Pavement performance evaluation due to the movement of AT at the low-temperature duration of a day has not been analyzed so far.

1.3 Objectives and Contribution

The objective of this research is to evaluate the effects of autonomous truck (AT) and their optimization for asphalt concrete (AC) pavement performance and traffic safety factors. More specifically, the goals of this thesis project are presented as follows:

- To optimize the additional distresses from AT through explicit control of i) wheel load distribution in a lane and ii) vehicle positioning on different AC pavement lanes.
- To evaluate the pavement rutting, leading to hydroplaning potential and skid resistance for the movement of AT on AC pavement and establish a threshold value.

The first objective of this study is to evaluate the additional distress induced by autonomous trucks and their optimization based on vehicle positioning in the lanes of a road section and a wide range of truck wander within a lane. Based on traffic distribution, baseline, separated and integrated scenarios were considered in this study. The baseline scenario is designated for the movement of human-driven trucks. A dedicated lane was allocated for AT and human-driven trucks separately in case of the separated scenario. The integrated scenario was simulated to share the same lane by both AT and human-driven trucks. Vehicle positioning on the lane along with the wander of AT was replicated for 24 simulations. Simulations were devised by equivalency factors (EF) obtained using multilayer elastic theory for AC rutting and bottom-up fatigue (BU) cracking separately. Adjusted traffic volume from EFs was inputted in AASHTOWare-a robust pavement analysis software. Comparative studies were performed to obtain an optimized scenario based on performance perspectives. Besides, an attempt has been made to minimize AT impacts on AC pavement by scheduling AT traffic in a low-temperature period of the day.

The second objective of this study is to evaluate the pavement rutting for a wide range of wheel wander for the movement of the autonomous truck on AC pavement. AT was simulated by different standard deviation values of traffic distribution to estimate rutting on the pavement. Each wander condition was replicated for different vehicle speeds. Permanent Deformation of Asphalt Concrete Layer for Roads, PEDRO was employed to assess the rutting of AC pavement due to the movement of AT. Additional rutting of AT was measured compared to the human-driven truck. Hydroplaning potential and skid resistance in wet weather conditions were evaluated in this study from the induced rutting

for all simulations. This research has developed threshold values for truck speed, WFD and HPS parameters for a wide range of autonomous scenarios. An attempt was made to minimize pavement rutting and traffic safety factors by adjusting the frequency of truck traffic loading to get the benefit of the low-temperature duration of a day.

1.4 Thesis Framework

This thesis is written in manuscript format. The outcome of this thesis is presented in four chapters. It includes three peer-reviewed journal manuscripts. One manuscript of chapter 1 is submitted to Construction and Building Materials and other two manuscripts of chapter 3 and chapter 4 are submitted to Road Materials and Pavement Design (RMPD) journal.

Chapter 1 introduces the background, previous research on autonomous vehicles focusing on the evaluation of asphalt pavement performance and traffic safety factors, objectives and contribution of the present study.

Chapter 2 provides a detailed literature review on connected and autonomous vehicles. It describes the influence of connected and autonomous trucks on pavement design. This chapter also explains the research gap for evaluating the effects of connected and autonomous trucks on pavement performance and their optimization. This chapter is submitted to the journal as a review paper.

Chapter 3 includes a journal manuscript submitted to the Road Materials and Pavement Design (RMPD) journal in 2020. It evaluates the asphalt pavement distresses for the movement of autonomous trucks and their optimization through the control of truck wheel wander in a lane and vehicle positioning on lanes of the pavement section. It also studies

the minimization of pavement allowing autonomous trucks in the low-temperature duration of a day.

Chapter 4 presents another manuscript which is also to the Road Materials and Pavement Design (RMPD) recently. This paper predicts the rutting of asphalt pavement for a wide range of wheel wander. Each wheel wander was simulated for different truck speeds. A threshold value was developed among truck speed, hydroplaning speed and water film depth. Optimization was made by increasing truck loading frequency on the low-temperature duration of a day.

Chapter 5 summarizes the general conclusions, recommendations, and suggestions for future works.

1.5 References

Chen, F., Balieu, R., & Kringos, N. (2016). Potential influences on long-term service performance of road infrastructure by automated vehicles. *Transportation Research Record*, 2550(January 2016), 72–79. https://doi.org/10.3141/2550-10

Chen, F., Song, M., & Ma, X. (2020). A lateral control scheme of autonomous vehicles considering pavement sustainability. *Journal of Cleaner Production*, 256, 120669. https://doi.org/10.1016/j.jclepro.2020.120669

Chen, F., Song, M., Ma, X., & Zhu, X. (2019). Assess the impacts of different autonomous trucks' lateral control modes on asphalt pavement performance. *Transportation Research Part C: Emerging Technologies*, 103(September 2018), 17–29. https://doi.org/10.1016/j.trc.2019.04.001

Donelson, B. (2020). *Coronavirus response: Real-World case for expanded autonomous vehicles testing in the U.S*. JDSupra. https://www.jdsupra.com/legalnews-/coronavirus-response-real-world-case-56295/

Fee, G. (2020). Preparing for autonomous vehicles. *Asphalt Magazine*. http://asphaltmagazine.com/autonomous-vehicles/

Ghao, L., Hong, F., & Ren, Y. (2019). Impact of seasonal and annual weather variations on network-level pavement performance. *Infrastructures*, 4(27), 1–13.

Gungor, O. E., & Al-Qadi, I. L. (2020). All for one: Centralized optimization of truck platoons to improve roadway infrastructure sustainability. *Transportation Research Part C: Emerging Technologies*, 114(January), 84–98. https://doi.org/10.1016-/j.trc.2020.02.002

Linder, C. (2019). Self-Driving freight trucks - autonomous trucks. *Popular Mechanics*. https://www.popularmechanics.com/technology/infrastructure/a30196644/self-driving-truck-cross-country/

Litman, T. (2020). *Autonomous vehicle implementation predictions: Implications for transport planning*. In Victoria Transport Policy Institute (Issue 2020).

Lu, Q., Tettamanti, T., Hörcher, D., & Varga, I. (2020). The impact of autonomous vehicles on urban traffic network capacity: an experimental analysis by microscopic traffic simulation. *Transportation Letters*, 12(8), 540–549. https://doi.org/10.1080-/19427867.2019.1662561

Noorvand, H., Karnati, G., & Underwood, B. S. (2017). Autonomous vehicles: Assessment of the implications of truck positioning on flexible pavement performance and design. *Transportation Research Record*, 2640(April 2018), 21–28. https://doi.org/10.3141-/2640-03

Shladover, S. E., Su, D., & Lu, X. Y. (2012). Impacts of cooperative adaptive cruise control on freeway traffic flow. *Transportation Research Record*, 2324(Idm), 63–70. https://doi.org/10.3141/2324-08

Simko, D. J. (2016). *Increasing road infrastructure capacity through the use of autonomous vehicles* [Master's thesis, Naval Postgraduate School]. Proquest Dissertations and Theses.

Steyn, W. J. v. M., & Maina, J. W. (2019). Guidelines for the use of accelerated pavement testing data in autonomous vehicle infrastructure research. J*ournal of Traffic and Transportation Engineering* (English Edition), 6(3), 273–281. https://doi.org/-10.1016/j.jtte.2019.05.001

Tientrakool, P., Ho, Y. C., & Maxemchuk, N. F. (2011). Highway capacity benefits from using vehicle-to-vehicle communication and sensors for collision avoidance. *IEEE Vehicular Technology Conference*, 0–4. https://doi.org/10.1109/VETECF.2011-.6093130

Wanek-Libman, M. (2020). CTDOT scheduled to deploy first full-size automated transit bus in North America. *Mass Transport*. https://www.masstransitmag.com/alt-

mobility/autonomous-vehicles/article/21143509/ctdot-scheduled-to-deploy-first-fullsize-automated-transit-bus-in-north-america

Zhao, X., Shen, A., & Ma, B. (2020). Temperature response of asphalt pavement to low temperatures and large temperature differences. *International Journal of Pavement Engineering*, 21(1), 49–62. https://doi.org/10.1080/10298436.2018.1435883

Zhou, F., Hu, S., Chrysler, S. T., Kim, Y., Damnjanovic, I., Talebpour, A., & Espejo, A. (2019). Optimization of lateral wandering of automated vehicles to improve roadway safety and pavement life. *Transportation Research Record*, 1–9.

Chapter 2 Literature Review

This chapter has been prepared for publication in a Journal as a review paper with the title 'Connected & Autonomous Vehicles and Pavement Performance: A Literature Review' The paper is presented in each chapter.

Abstract

The CAVs are becoming fruitful gradually as some technologies such as advance driver-assist systems (ADAS) integrated into them can help control vehicles in a longitudinal and transverse direction. The most available ADAS in current running vehicles and their functions are summarized in this paper. There are a lot of uncertainties in harnessing the benefits of CAV implementation. The advantages and the uncertainties of the CAVs are presented. The lane-keeping algorithm in ADAS allows the vehicles to move in the reduced width of the lane. Cooperative Adaptive Cruise Control (CACC) has increased in the tendency of truck traffic platooning. The features of automation and connectivity are improving the applicability of CAVs, however they are also posing potential negative impacts on roadway infrastructures. The reduction of lane width and replacement of human drivers by machine greatly impacts the various geometric elements of highways. The reduction of the lane width and truck platooning affect the structural performance of the pavements significantly. This paper presents the effects of connected and automated driving on geometric elements and structural performance of the highway pavements. In

Rana, M., Hossain, K. (2020). Connected & Autonomous Vehicles and Pavement Performance: A Literature Review. Submitted to journal.

addition, various optimization techniques to minimize the additional distresses of connected and automated driving are also explained in this paper.

Keywords: Connected and Autonomous Vehicles, Controls of Autonomous Vehicles, Geometric Elements, Pavement Performance.

Rana, M., Hossain, K. (2020). Connected & Autonomous Vehicles and Pavement Performance: A Literature Review. Submitted to journal.

2.1 Introduction

The commercial application of autonomous technology in passenger and freight transport is growing at a fast pace due to tremendous development in Intelligent Transportation Systems (ITS). The deployment of ITS in Connected Vehicle (CV) and Autonomous Vehicle (AV) will bring revolutionary changes in transportation mobility in the near future. CVs use communication technologies to establish connections with autonomous and non-autonomous vehicles, roadside infrastructures, and other road participants to share the driving information (Figure 2.1(a)). CVs help human or autonomous drivers to make a better choice by supplying information collected by wireless technologies (Atkins, 2017). AV, also known as driverless vehicles, can move from one place to another using sensors and equipment (shown in Figure 2.1(b)) without any human intervention. AVs conduct driving tasks relying on cameras, radar, GPS, LiDAR etc., and reduces human assistance based on the level of autonomy (Presented in the next section). The existence of significant overlapping between AVs and CVs creates difficulties in selecting specific infrastructure requirements for each technology (Hallmark, 2019). There is a belief among transportation stakeholders that CV is the enabler of AV (CAVita LLC, 2017) and CV has a significant influence on AV (Shladover, 2018). Connected and Autonomous Vehicle (CAV) incorporates both AV and CV technology and this combination has more benefits than separated one.

This paper aims to provide a brief overview on features and control of CAVs on the highway, the potential benefits and uncertainties of CAV implementation, the influence of CAV on pavement infrastructures, and recommendations for future studies. The CAV

features and control are presented in the level of autonomy, advanced-driver assist system, and progress in communication and path tracking technologies sections. The potential benefits and associated uncertainties for CAV deployment are explained in terms of road safety, traffic capacity, mobility, environmental effects and economic benefits. The impacts of CAV on pavement infrastructures are presented in detail and divided in two parts: geometric and structural performance. The impacts of CAVs on geometric design mainly presents the change in geometric elements for CAV deployment. The effects of connected and autonomous freight transport on pavement distress and different optimization techniques and study gaps are presented in the last part of this paper.

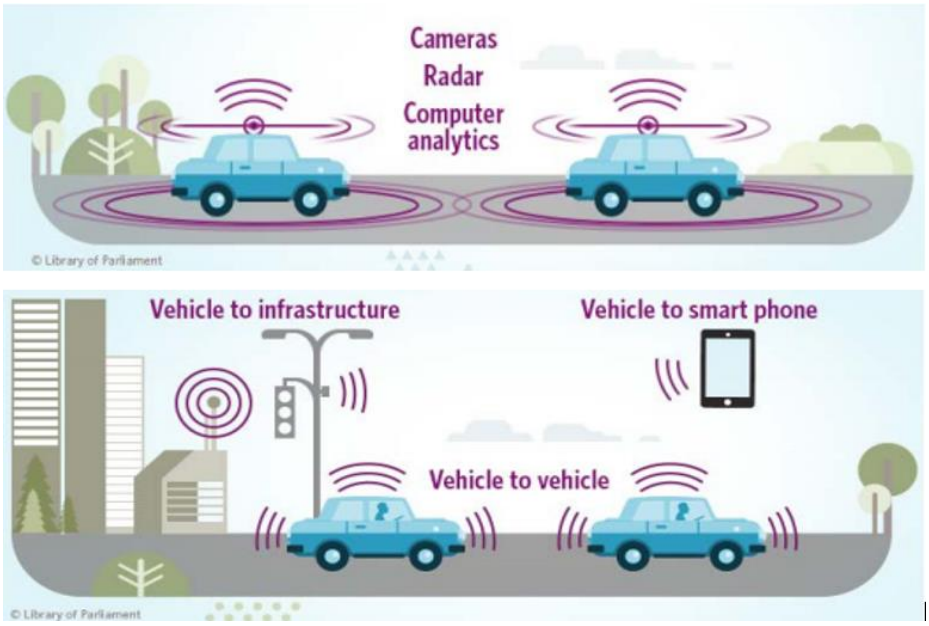

Figure 2.1 (a) Autonomous and (b) Connected Vehicles (Chong, 2016)

2.2 Level of Autonomy

Automation in driving requires the execution of dynamic driving functions related to operational activities and tactical strategies. The steering, braking, accelerating, and

monitoring are part of operational activities, and tactical strategy comprises different decisions about the changing lane, avoiding traffic congestions and construction zones. Society of Automotive Engineers (SAE), a global platform comprising scientists, engineers, and practitioners, classify passenger, and freight transport automation into six levels (SAE International, 2014).

- *Level 0*: No automation- All driving tasks are performed by a human.
- *Level 1*: Driver assistance- Cruise control is incorporated in vehicle design.
- *Level 2*: Conditional automation- Steering and accelerating/decelerating are controlled by the vehicle.
- *Level 3*: Partial automation- Steering, braking, acceleration, and navigation are integrated into vehicles.
- *Level 4*: High automation- All operational and tactical decisions are included in good weather conditions.
- *Level 5*: Full automation- All driving tasks are handled by vehicles. No driver is required.

These automation levels have been adopted by the US Department of Transportation and the United Nations (National Science and Technology Council & US DOT, 2020). The progressive technological development over the last decades has brought the full automation level to the implementation phase.

2.3 Advanced Driver-Assist System

Advanced driver-assist system (ADAS) is an integrated part of ITS and assists the human-driver in driving functions (Belmonte et al., 2020; L. Wang et al., 2020). The level of automation is also characterized based on the relief of human tasks by ADAS. Different ADAS are currently integrated into human-driven vehicles (Lengyel et al., 2020). The common ADAS technologies integrated into current vehicles (Mitchell1, 2019) and their functions (American Automobile Association, 2019) are presented in Table 2.1. The analysis found that the vast majority of new vehicles in the USA in 2018 consist of at least one ADAS function (American Automobile Association, 2019).

Table 2.1 Different ADAS systems and their functions

ADAS	Functions
Adaptive Cruise Control (ACC)	Accelerates or stops the vehicle along with many other functions
Back-Up Cameras/Sensors	Assists in parking and observe the backside
Adaptive Headlights	Make the headlight adjustment to notice at bends and corners in hill
Lane Departure Warning	Warns the driver at the moment of leaving the lane
Lane Keeping System (LKS)	Confines the vehicles in the lane width
Automatic Parking	Parks the cars automatically without any assistance
Blind Spot Monitoring	Alerts the drivers about objects in the blind spot
Emergency Braking	Applies brakes to avoid the collision
Pedestrian Detection	Differentiates between the pedestrians and objests
Drowsy Driver Detect	Prevents accidents by sleeping drivers
Night Vision	Sees clearly at night or adverse weather

The ultimate goal of ADAS is to transform vehicles from human-driven to fully autonomous conditions (Cheong et al., 2017) and increase traffic safety (Hagl & Kouabenan, 2020). Transportation sectors have already entered into a new era of automation technology by successfully transforming ADAS into fully automated driving systems (ADS). The addition of cooperative adaptive cruise control (CACC) features (connectivity with surroundings) with ADS has brought a new dimension to driverless vehicles.

2.4 Current Scenario of CAV Deployment

The experimental program of CAV is growing tremendously, and the feasibility of commercial deployment of AVs has been a reality from the technological point of view (Bell, 2017). Beep and NAVYA partnered with the Jacksonville Transportation Authority, Florida, and a Chinese company, Baidu, successfully deployed AV to control the spreading of Covid-19. AVs successfully supplied necessary medical supplies and foods to the infected areas at the peak period of Covid-19 (Baidu, 2020). Different cities across the U.S. are planning to run the pilot program of AVs on different roads. National Highway Traffic Safety Administration (NHTSA), USA recently published an online tool to track the AV running in the streets (Associated Press, 2020). It is predicted that AVs will occupy 25% of all miles driven in the U.S. by 2030. Estimation of the Center for Automotive Research proclaims that new vehicle sales might get increased up to 55 percent by 2040 (Fee, 2020). The application of automation techniques is not restrained to passenger cars only. Combined efforts of scientists, engineers, and practitioners, to increase efficiency in the shipment of people and goods, initiated to bring public transit and trucks under automation

technology (Andersson & Ivehammar, 2019). In December 2019, an autonomous freight truck made a cross country trip of 2800 mile in California to deliver butter commercially (Linder, 2020). Connecticut Department of Transportation (CTDOT) declared the plan of testing the full-size driverless transit bus by 2021 (Wanek-Libman, 2020)

2.5 Progress in Communication and Path Tracking Technologies

Despite having differences in the design of various manufacturers, CAVs move on the road section based on (i) input devices or sensors to perceive the surrounding environment (ii) control systems comprised of different computer programs to process the inputs and commanding about the travel path and (iii) output devices or actuators for operating steering, wheel, brakes, etc. (Wevolver, 2019). Input devices, control systems and output devices are treated as eye, heart, and hands of the AVs, respectively (Skarbek-Zabkin & Szczepanek, 2018). Figure 2.2 shows the functioning of CAVs for moving on the road.

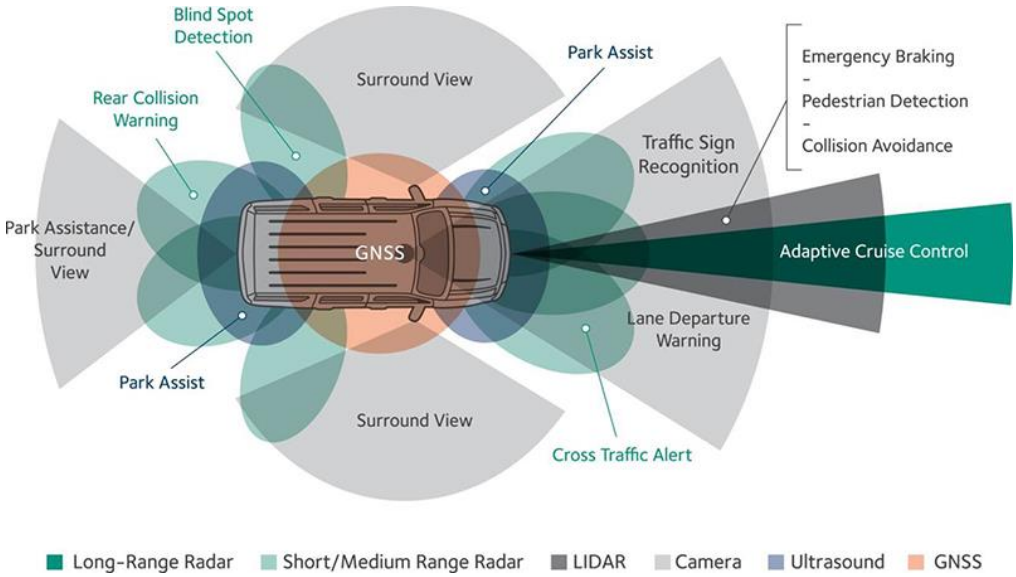

Figure 2.2 Positioning performance by AV (Hexagon, 2020)

Longitudinal and lateral controller systems in AV ensure safe vehicles' movement on a road lane (Filho et al., 2014). Longitudinal control, maintained by cruise controls, works on the vehicle speeds using a brake or accelerator and maintains a safe distance between two vehicles. ACC and CACC are part of the ADAS, and reduce the human drivers' input in the driving of CAV (Mahdinia et al., 2020). ACC senses the surrounding condition based on different sensors and operates in speed control and spacing control modes. CACC integrates dedicated short-range communication (DSRC) technologies to establish the vehicle to vehicle (V2V) and vehicle to infrastructure (V2I) communication (Liu et al., 2020). The recently developed vehicle to everything (V2X) is gaining momentum, being more advantages.

Lateral control bound the vehicles to be confined in the traveled lane (Belmonte et al., 2020; Filho et al., 2014). The camera sensors in the moving vehicles and their algorithms ensure to travel in the specified path (Chandni et al., 2017). The traveled path of CAV can be off-line predefined or online to keep away from the obstacles, to change the lanes, etc. (Dominguez et al., 2016). The dynamic lateral control significantly influences the stability of the CAV. The yaw stability control in the vehicle dynamics maintains the lateral stability of CAVs and this is performed by braking and steering subsystems. The controller system in CAVs instantly controls yaw rate and sideslip angle to allow the vehicles in a specified path by controller and braking (Aripin et al., 2014; Norouzi et al., 2019).

The driving performance of the automated driving system is equipped with the camera, light detection and ranging (LiDAR), millimeter-wave radar (MWR), and the

global navigation satellite system (GNSS) or internal navigation system (INS) (Yoneda et al., 2019). GNSS technology (Figure 3) has decimal level accuracy to keep CAV in its lane and maintain a safe distance from other vehicles (Hexagon, 2020). The adverse weather condition like sun glare, rain, fog and snow poses serious threats to the navigation and traffic condition assessment process of AV (Neumeister & Pape, 2019; Yoneda et al., 2019). The harsh weather (snow and rain) creates obstacles in AVs' movement by confusing sensors, hiding the markings. GNSS also faces difficulties running on the road section due to harsh weather conditions in space, not in the atmosphere (Zhang et al., 2020). Researchers are studying to find out the probable strategies for AVs' movement in adverse weather conditions.

2.6 Positive Effects and Uncertainties

Implementation of autonomous vehicle has potential benefits in various aspects. The positive aspects of CAVs are presented in five major perspectives- road safety, traffic efficiency, mobility, environmental, and economic. Despite having the noticeable progress of automation technology, the implementation of CAVs is facing several issues. Many CAV manufacturers are performing road tests to find out the problems associated with automated driving. Researchers are working to solve the associated problems of CAV deployment from their studies (Future Agenda, 2020; Lim & Taeihagh, 2018; Litman, 2020; Taeihagh & Lim, 2018).

2.6.1 Road Safety

Road safety is a significant consideration for the transition of human drivers to connected and autonomous drivers (European Commission, 2018; Maurer et al., 2015). Human drivers and their driving habits are the most influential factors of the crash on the road (Adanu & Jones, 2017; Bouchihati, 2020). USDOT surveyed national motor vehicle crash causation and found that about 90% of car crashes are occurred due to human errors (US DOT, 2015). USDOT fact sheet reported about 80% of the fatal crashes are due to the impaired connectivity between vehicles. Autonomous driving with connectivity can minimize the drivers' stress (Litman, 2020), and it is expected that AVs will significantly reduce road accidents related to human error (Fagnant & Kockelman, 2015). But, the commercialization of AVs has a safety-related key challenge till now. European Commission (2018) reported the declination of traffic safety in the mixed mode of non-AVs vehicles and AVs. Wang et al. conducted a statistical survey on the testing of AVs by different manufacturers. About 63% of accidents for a total of 3.7 million passing are found to happen in autonomous mode (Wang et al., 2020). Fiber et al. found the truck platooning using CACC has detrimental effects on traffic safety. The regulations for rolling out of CAVs and liability related to road safety have not been addressed properly worldwide (Faber et al., 2020).

2.6.2 Traffic Capacity

The automatic braking configured in the AV system will increase highway capacity along with other advantages. This increased capacity may further induce an overuse of the

practical roads, reducing the safe distance between vehicles and increasing vehicle speed due to the incorporation of ACC and CACC (Simko, 2016; Tientrakool et al., 2011). Commercially deployed AVs reduce traffic congestion delays and subsequently increase traffic flow (Hoogendoorn et al., 2014; Milakis et al., 2017). Applications of ACC and CACC systems in AVs increase highway capacity by 80% compared to human-driven traffic (Shladover et al., 2012). Virginia DOT found the increment in highway capacity as 28% and 92% compared to legacy vehicles for fully AVs and CAVs, respectively. Autonomous trucks in freight transportation systems might be beneficial for transportation stakeholders (Heaslip et al., 2020). Autonomous trucks (ATs) will benefit the transportation system through the improvement in operational frequency in moving goods and overcoming the shortage of truck drivers (Gungor & Al-Qadi, 2020a). Calvert et al. showed that low-level automation negatively affects traffic flow and road capacity from the experimental analysis (Calvert et al., 2017).

2.6.3 Mobility

Improvement in mobility is the consequence of the CAV, leading to a reduction in traffic congestion and emission (Pakusch et al., 2018). The movement of AVs on the road appears to increase the mobility of elder or disabled people. This application will help the disabled peoples for access to educational institutions and employment facilities (Litman, 2020). The ride-sharing tendency of the passengers will be increased with the deployment of CAVs (Narayanan et al., 2020; Thomas, 2018) and appear to be economically viable (Gurumurthy & Kockelman, 2020; Meyer & Beiker, 2019). The users with disabilities are still in doubt about the acceptance of this new technology. Bennet et al. conducted a

questionary survey to know the concerning issue of the people with disabilities about the AVs and found that two-thirds of them have negative views about the use of AVs (Bennett et al., 2019).

2.6.4 Environmental Impacts

The beneficial and detrimental effects of CAVs on energy consumption and greenhouse gas (GHG) emissions co-exist and are related to the occurring scenario (Greenwald & Kornhauser, 2019). The environmental benefits are expected to increase in deploying CAVs by reducing traffic congestion and smoothening traffic from minimizing stop-and-go driving behavior (Kopelias et al., 2020). The use of the dampening function in place of stop-and-go has the capability to reduce GHG. This percentage in GHG decrease was observed to be in the range of 15%-73% (Stern et al., 2019). There is a lower possibility to obtain the optimized GHG emission in the near future for the low CAV penetration rate in the roadway (Liu et al., 2019). Patella et al. integrated traffic simulation and noise assessment tools and observed a significant reduction in noise pollution for 100% AVs. Authors found the deteriorated scenario at different links of the network systems (Patella et al., 2019).

2.6.5 Economic Benefits

The incorporation of automation in driving sectors is beneficial from an economic point of view. The economic benefits of the CAVs are associated with reduced congestion and reduced travel time, and its reliability (Winston & Karpilow, 2020). The comparative cost analysis between the truck platooning of human drivers and autonomous drivers showed

the maximum cost reduction as 46% for 16-ton trucks (Engholm et al., 2020). There is a significant reduction in fuel usage due to the platooning of autonomous trucks (AT) due to the aerodynamic force (Gungor et al., 2020; Zhang et al., 2020). This platooning of AT can significantly affect the pavement performance due to lane centering tendency (Gungor & Al-Qadi, 2020a). AVs could be economically disadvantageous due to increased travel of minors, elderly and disabled people, and avoiding public transport who do not like ride-share.

2.7 Infrastructures for CAVs

Improvement in road infrastructures for the deployment of CAVs is crucial. The most visible development in automated driving for passenger and freight transport is related to digital infrastructure (Farah, 2016). The physical infrastructures as the facilitators of the CAV driving are in the planning/study phase. Planners, designers, engineers, and other road stakeholders continue their studies to obtain the probable impacts of CAV on physical infrastructures and find the way out of these limitations.

The roadway traffic control devices are the essential physical infrastructures and provide the regulatory, warning, and guidance information for driving safely on the road (Boateng et al., 2019). Road signs and markings as the traffic control devices are the basic infrastructure needs for the deployment of CAVs. The CAVs, equipped with cameras and sensors, navigate the travel path with the assistance of pavement markings (Hallmark, 2019). The centerline and edge line markings are the indicators for AVs to confine the vehicles within the lane (Garcia & Camacho-Torregrosa, 2020). The lane marking's

inconsistency is the cause of declination in driving by AVs. The unreadable and non-standardized signs create a confusing situation for road users (Liu et al., 2019). The geometric design and structural design of pavement infrastructures are discussed in the next section of this paper.

The The Transportation Research Board (TRB), USA arranged the National Cooperative Highway Research Program [Project No. NCHRP 20-24(112)] for the development of Connected Roadway Classification System (CRCS) for American Association of State Highway and Transportation Officials (AASHTO). This research program developed the framework with three approaches concerning infrastructure readiness of CAVs for various departments of transportation (DOT), metropolitan planning organizations, and infrastructure owners/operators. The concerning three approaches for the development of the infrastructure facilities are-

- ***Talking with the road:*** The improvement in the roadway infrastructure (i.e. DSRC, C-V2X) for the establishment of the communication of AVs with infrastructures (V2I) and other vehicles (V2V) on the road.
- ***Seeing the road:*** The enhancement of traffic signals and road markings to make it visible to the eyes (i.e. video camera, optical sensors) of the AVs.
- ***Simplifying the road:*** The change in road geometry, the improved pavement design, making the pavement free of defects, etc., to obtain operational design domain (ODD) are the part of this approach.

The CSRC recommended implementing these approaches in different stages over the next 10 (ten) years for the safe operation of CAVs (Poe, 2020). European Union (EU) published the European Technology Platform (ERTRAC) roadmap for the development of roadway infrastructures to accommodate CAVs along with human-driven vehicles. The ENTRAC roadmap introduced infrastructure support levels for automated driving (ISAD) and exhibits infrastructure readiness by classifying it into five levels (A to E). Level E and D are called conventional infrastructures and Level C-A are termed as digital infrastructures (ENTRAC, 2019)..

2.8 Impacts of CAVs on Geometric Design

The geometric design is the controlling factor of operational efficiency and traffic safety in the road transportation system. The geometric design deals with dimensions and layouts of the visible features and the features generally considered are the alignment, sight distance, cross-section and intersection. Washburn and Washburn explained vehicle performance and sight distance as the significant influence factors on highway geometric design (Washburn & Washburn, 2018). The adhesion between the rubber tire of AVs and pavement surface affects the acceleration and deceleration rate, inducing lower vehicle performance for on-ramp and off-ramp steepness. The improvements in braking, achieving a higher coefficient of adhesion in the future, will increase the acceleration rate.

The LiDAR and vision sensors in AVs show lower performance than human eyes in case of obstacles around the horizontal curve and the vertical curve. The Washburn and Washburn (2018) mentioned that connectivity (V2X) integrated into AVs could solve sight

distance problems, but not for the fallen boulder on the highway or vehicles with non-operational V2X on the highways.

The roadway capacity increment is expected for autonomous vehicles by allowing more lanes in the same carriageway through the narrowing down the lane width (National Academies of Sciences, Engineering, 2015). Garcia et al. compared the influence of lane width on the human-driven and semi-AVs' performance and found semi-AV's failure on the narrower lane width. The authors concluded the 100% efficiency of human and semi-AV for the lane width of 2.5 m and 2.75 m, respectively (Garcia & Camacho-Torregrosa, 2020). The lane-keeping system (LKS) was deployed in semi-AV for road testing in Spain for this study and the technical reason for this disengagement was unknown. Binshuang et al. observed that reduced lane width and limitation of vision sensors in downhill or uphill affect the safety of AVs. The reduced lane width causes a reduction in superelevation run-off, and subsequent skid resistance is compromised. The sensors have limitations to capture the road surface conditions in a hilly road. The authors recommended increasing skid resistance to solve the issues and provided the modified braking distance formula to improve traffic safety (Binshuang et al., 2019). The authors introduced Equation 2.1 from the regression analysis of the field test data to obtain the side-force coefficient (SFC). SFC is the measurement of the ability to control the vehicles in the curve (National Academies of Sciences, Engineering, 2009). The obtained SFC is used in Equation 2.2.

$$SFC = -0.85t^2 + 3414t - (3X10^6); \qquad R^2 = 0.9919 \tag{2.1}$$

$$\varphi\,(t) = 0.01(SFC) \tag{2.2}$$

Where,

t =time in years

$\varphi\ (t)$ = frictional coefficient of tire-pavement interface

The frictional coefficient is inputted in Equation 2.3 to determine stopping distance (D). This equation was adopted from Chu and Fwa (Chu & Fwa, 2018).

$$D = v_0 t - \frac{1}{2} G g t^2 - \int_0^T \left[\int_0^t \varphi(t) g dt \right] dt \quad 2.3$$

The American Association of State Highway and Transportation Officials (Hancock & Wright, 2018) provided the design criteria for different geometric elements of the highways. The guidelines introduced Equations 2.4 and 2.5 for stopping sight distance (SSD) (i.e. the distance to stop the vehicle before the stationary object). All equations presented here are valid for metric units only.

SSD on level roads:

$$SSD = 0.278Vt + 0.039\left(\frac{V^2}{a}\right) \quad 2.4$$

SSD on the sloping road:

$$SSD = 0.278Vt + \frac{V^2}{254\left[\left(\frac{a}{9.81}\right) \pm G\right]} \quad 2.5$$

Where,

V = Design speed (km/hr)

t = Driver's PRT (seconds)

a = Deceleration rate (m/s^2)

G = Roadway grade (decimal)

AASHTO (2018) recommends the perception reaction time (PRT) and deceleration rate as 2.5 seconds and 3.4 m/sec^2 to evaluate SSD. The PRT of full AVs was found to be in the order of 0.5 sec from the extensive numerical study (Urmson, 2006).

AASHTO adopts Equation 2.6-2.7 and Equation 2.8-2.9 for the length calculation of the crest curve (L_{crest}) and sag curve (L_{sag}) based on sight distance (S) and recommends the height of the driver's eye above the roadway surface as 1.08 m and headlight height as 0.6 m.

When $S<L_{crest}$:

$$L_{crest} = \frac{AS^2}{100\left(\sqrt{2h_1}+\sqrt{2h_2}\right)^2} \quad 2.6$$

When $S>L_{crest}$:

$$L_{crest} = 2S - \frac{200\left(\sqrt{2h_1}+\sqrt{2h_2}\right)^2}{A} \quad 2.7$$

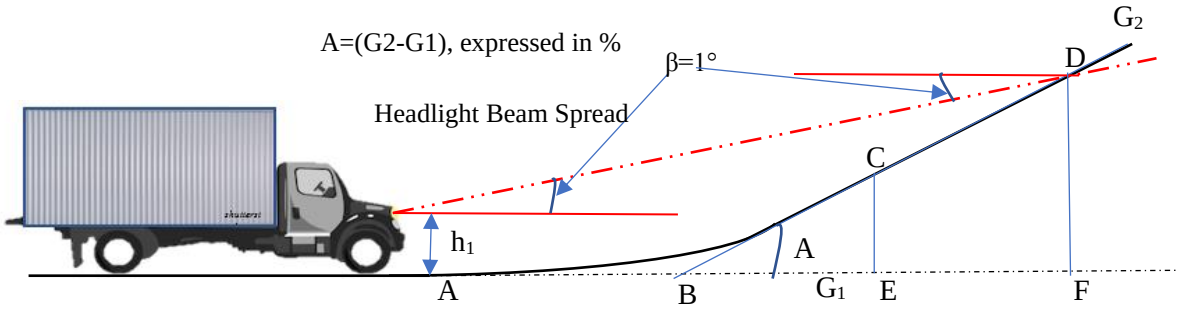

Figure 2.3 Inclined angle of the headlight beam (Khoury et al., 2019)

When $S<L_{sag}$:

$$L_{sag} = \frac{AS^2}{[200(H+Stan\beta)]} \quad 2.8$$

When $S>L_{sag}$:

$$L_{sag} = 2S - \frac{[200(H+Stan\beta)]}{A} \quad 2.9$$

Where,

h_1, h_2, H = The height of eye, object and headlight above the roadway surface

β = The angle of inclination of the headlight beam shown in Figure 2.3

The AVs replace the human eyes with vision sensors such as LiDAR. The h_1 of AVs is obtained by summing the height of the Waymo driverless car (1.55 m) and the height of LiDAR (0.28 m). Khoury et al. (2019) assume the minimum $h_1$value as 1.7 m keeping freight transport height in mind. Velodyne LiDAR Inc., the manufacturer of LiDAR, has a total angle of view from the horizontal axis as 26.8°, as shown in Figure 2.4 (Velodyne LiDAR Inc., 2019). Khoury et al. (2019) consider half of the manufacturer's provided angle as the inclination angle (13.4°).

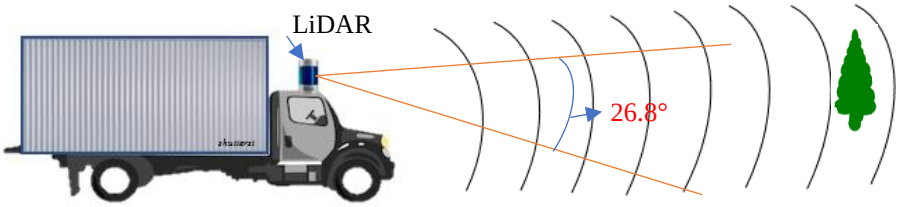

Figure 2.4 Vertical field of view of LiDAR sensor (Velodyne LiDAR Inc., 2019)

Khoury et al. (2019) redesigned the roadway for the proposed values of AVs mentioned in previous section. AASHTO recommendation for the minimum vertical curve length was followed to ensure drivers' comfort. The current geometric elements following the AASHTO standard was compared with the redesigned values. The authors found a significant reduction in SSD, L_{crest} and L_{sag}, and improvement in economic perspectives for less earthwork (lowering 7.67% filling and 47.22% cutting) shown in Figure 2.5.

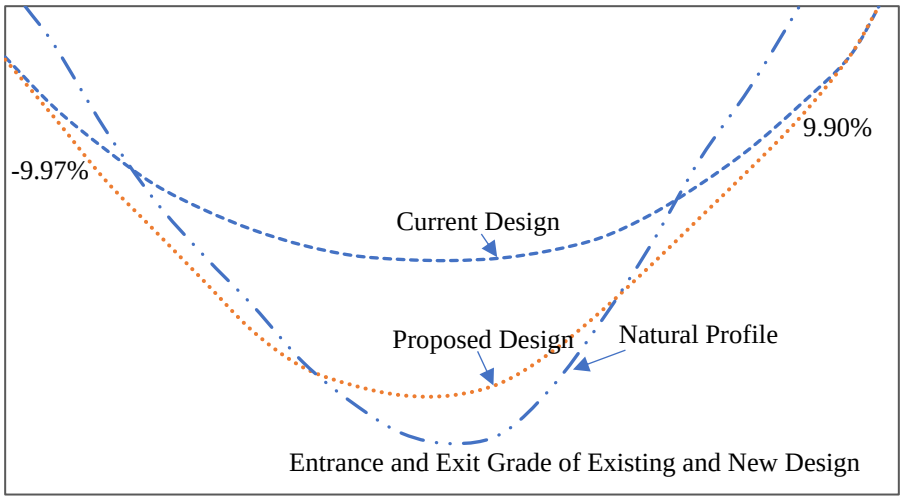

Figure 2.5 Profiles for different designs (Khoury et al., 2019)

Welde and Qiao also re-evaluated SSD, L_{crest} and L_{sag} for two AV scenario and found a significant influence on geometric elements (Welde & Qiao, 2020). In addition to all parameters of Kohury et al. (2019, the authors considered the deceleration rate as 4.5 m/s^2 in scenario 1 (A-1). In scenario 2 (A-2), PRT was assumed as 0.2 sec along with a deceleration rate of 4.5 m/s^2. The authors compared the geometric elements of two scenarios (A-1 and A-2) with the AASHTO standard values for human-driven vehicles, as shown in Figure 2.6. The author found autonomous driving as an economically efficient option due to the decrease in SSD, L_{crest} and L_{sag}.

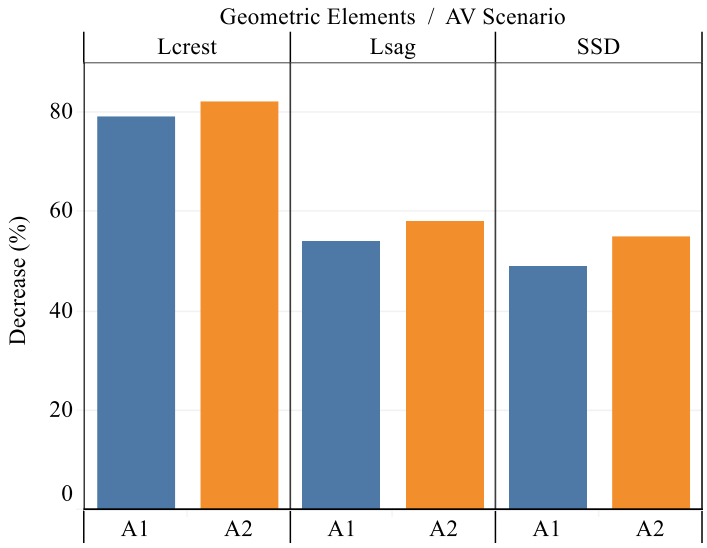

Figure 2.6 Percentage decrease in geometric elements (Welde & Qiao, 2020)

2.9 Effects on Structural Performance

The deployment of CAVs will influence the structural performance of pavements due to reduced wheel wander and platooning of truck traffic. The lane-keeping algorithm will accomplish the wheel moving in a narrower path and platooning will reduce inter-vehicle distance. Different aspects of the effects of CATs on pavement performance are described below.

2.9.1 Human Driven vs Autonomous Vehicles

Human drivers almost always change the lateral positioning of vehicles on a lane of road section during the traveling period. This lateral movement of the wheel along lane width is referred to as wheel wander. Wheel wander is influenced by drivers' habits, wind effects, and mechanical alignment (Buiter et al., 1989) and lane width, vehicle width, speed, and rut depth (Blab & Litzka, 1995). Researchers found that wheel wander of vehicular

movement could be modeled with probabilistic distribution (Gungor & Al-Qadi, 2020b; Siddharthan et al., 2017). Lateral positioning of the wheel on the traveled lane is normally distributed (ARA Inc., 2004; Erlingsson, 2012; Wu & Harvey, 2008) and is statistically modeled with zero mean and known standard deviation following Equation 2.10 (Gungor, 2018)

$$f(x) = \frac{1}{\sqrt{2\pi\sigma^2}} e^{-\frac{(x-\mu)^2}{2\sigma^2}} \quad 2.10$$

Where,

μ=mean of wheel wander distribution

σ=standard deviation of wheel wander

Mechanistic-Empirical (ME) pavement design analyzes the pavement section for the human-driven vehicle for wheel load normally distributed on a lane with zero mean and standard deviation of 0.25 m (10 inches) (ARA Inc., 2004). This standard deviation value differentiates human-driven vehicles from autonomous and semi-autonomous vehicles concerning the loading distribution pattern. Autonomous vehicles are bound to follow the centerline of pavement lanes due to the integrated dynamic control system integrated (Hills & Lee, 2012). This lane-centering tendency compels the lateral positioning of the wheel load to a narrower width, resulting in channelized traffic. This type of channelization for autonomous vehicles is analyzed as zero wander distribution (Noorvand et al., 2017). Zhou et al. quantified wheel wandering of AVs and the standard deviation of wandering was found to range 3.0 (cm) to 7.5 (cm) (1.2" to 3.0") for AV. The

author concluded with three times narrower standard deviation could be modeled for AVs to analyze the pavement section (Zhou et al., 2019).

2.9.2 Wheel Wander in Pavement Analysis

Mechanistic-Empirical Pavement Design Guide (MEPDG) software, also known as AASHTOWare, is widely accepted to predict pavement distresses. This robust pavement analyses pavement performance based on four fundamental inputs. These inputs are material properties for all the layers, traffic details, climate, and structural design. Wheel wander, one of the traffic inputs controls the wheel loading distribution in the pavement lane. The MEPDG approach evaluates the fatigue cracking in pavement by dividing the width of the lane into five portions as shown in Figure 7. The center positioning of truck traffic is fixed and calculated by multiplying standard deviation with standard deviates (0, ±0.5244, ±1.28155). About 20% of all the wheel movement is addressed in predicting fatigue for each segment. Damage accumulations from segments 1-5 are represented as D1, D2, D3, D4, and D5. Cumulative fatigue damage is evaluated using Equation 2.11. No explanation of modified rutting determination procedures is given in the MEPDG guide (Gungor, 2018).

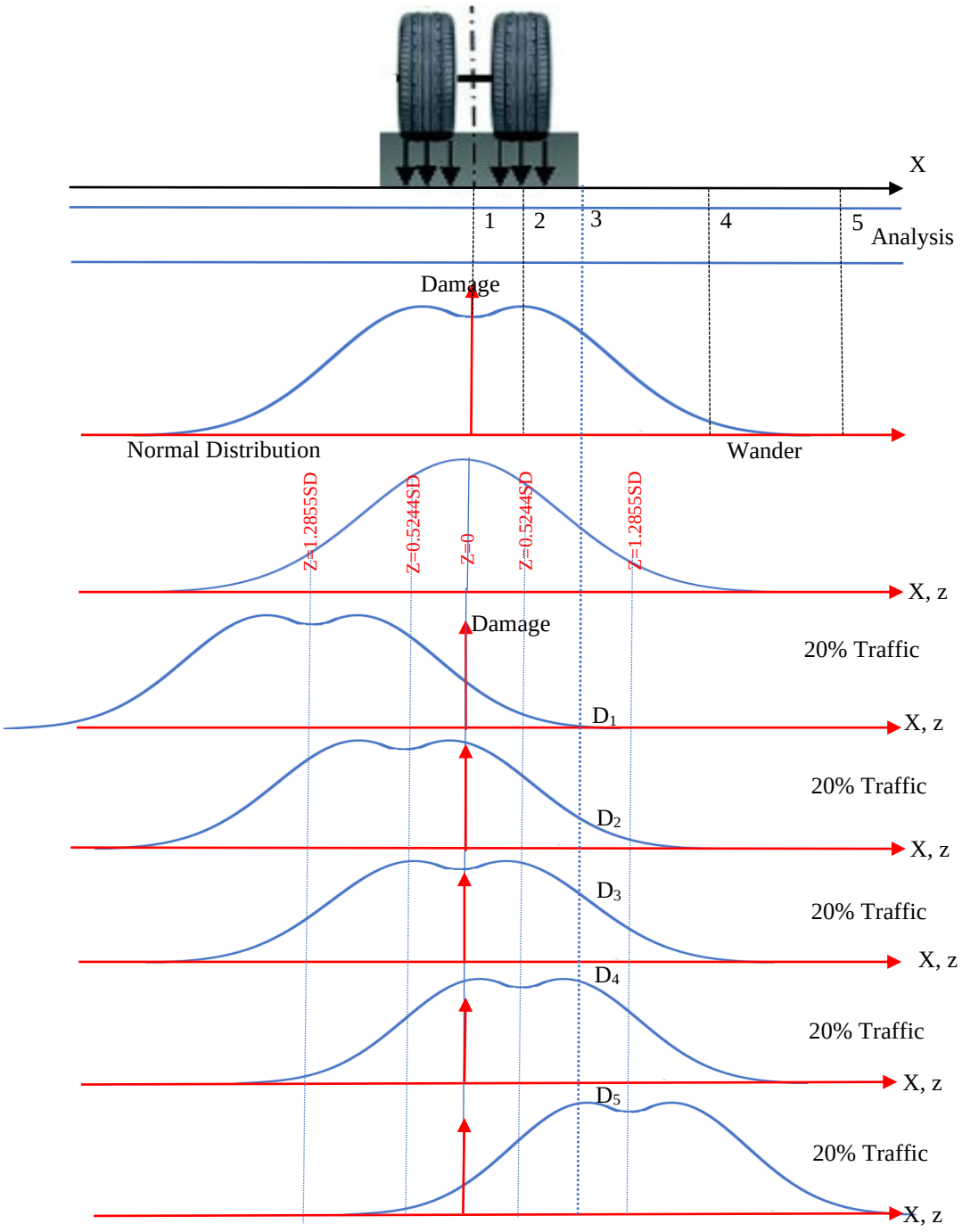

Figure 2.7 MEPDG analytical approach for wheel wander (ARA Inc., 2004)

$$D = 0.2D_1 + 0.2D_2 + 0.2D_3 + 0.2D_4 + 0.2D_5 = 0.2\sum_1^5 D_i \qquad 2.11$$

The permanent deformation of the asphalt concrete layer for roads (PEDRO) model is a linear viscoelastic program. Said et al. developed the PEDRO model based on the results of the shear box test of the AC mixture. This model is particularly used to evaluate the rutting of AC layers (Said et al., 2011, 2013). The accumulated rutting in AC pavement from the PEDRO model and field observations for different wheel wanders are in good agreement (Jelagin et al., 2018).

2.9.3 Pavement Distresses and CAT

Many researchers reported that the structural performance of pavement is significantly affected by the movement of heavy vehicles resulting in the reduction of pavement life (Almeida et al., 2019; Pais et al., 2019). The channelized AT traffic as heavy traffic increases the loading repetition on the narrower width of the lane compared to human-driven vehicles (Noorvand et al., 2017). The increased load repetitions induce the accumulation of pavement distresses (Litman, 2020). In-situ pavement tests showed significantly higher responses for the reduction of wheel wandering on the pavement lane (Shafiee et al., 2014). Said and Hakim found that rutting reduced about 38% for increasing wheel wander from zero to 0.125 m. Multi-linear elastic analysis of a typical pavement section showed similar rutting and fatigue cracking for 2.1 and 1.1 times lower load repetitions, respectively, for zero wander vehicles compared to human-driven (Noorvand et al., 2017). Wu and Harvey (2008) conducted heavy vehicle simulator tests and modeled a testing system to estimate the effect of traffic wander on rutting. Traffic wander induced 56% more rutting in the pavement section than non-wander traffic. Zhou et al. (2019) performed field tests to evaluate the impact of AT on fatigue and rutting of AC pavement.

Predicted data showed that AT reduces fatigue and rutting life of AC pavement by 20% and 32%, respectively, compared to the human-driven truck. The substantial increment in rutting and fatigue crack is also observed from the simulation of AC pavement by Chen et al. (Chen et al., 2019).

The number of connected trucks driving in the close distance is said to be truck platooning. The trucks in a platoon can be connected in any of (i) longitudinal directions, (ii) both longitudinal and transverse directions, (iii) coupled in longitudinal and transverse direction using cruise control. The CACC is incorporated in the third scenario use and all trucks follow the same track. Platooning in freight transport is gaining feasibility with the introduction of connected and autonomous trucks (CAT). Despite increasing safety, fuel savings, and emission control, truck platooning has a significant negative impact on pavement performance (Ahmed & Yang, 2019; Gungor et al., 2020; Gungor & Al-Qadi, 2020a). The reduced healing time of asphalt concrete from the close inter-truck distance and channelization of truck loading causes asphalt pavement deterioration for truck platooning (Bouchihati, 2020; Gungor & Al-Qadi, 2020a). Bouchihati (2020) found that rutting and fatigue cracking of AC pavement reaches to the limiting value for 50% of the truck passing in a platoon.

2.9.4 Optimization of Autonomous Vehicle Movements and Distresses

Few researchers have recently developed strategies to optimize the additional pavement distresses accumulated for the movement of AT. Researchers mainly focused on controlling the wheel loading distribution and vehicle positioning on the pavement lane

explicitly. Noorvand et al. (2017) modified the traffic input in the Mechanistic-Empirical Pavement Design Guide (MEPDG) software to incorporate AT in pavement design. Load equivalency factors (LEF) for wheel loading distribution on a traffic lane and vehicle positioning (combination of AT and non-AT in same lane) on different lanes of road sections were calculated. LEF was evaluated for zero wander and uniform distribution of wheel loading (shown in Figure 2.8) on the lane comparing with human-driven vehicles. Analyzed data showed significantly reduced fatigue and rutting for uniform distribution of wheel load covering the entire width of the lane. Zhou et al. (2019) also found improved pavement performance for uniform wheel loading distribution on the pavement lane. The authors observed from the field testing that the standard deviation for wheel loading distribution of AT along the lane width is three times narrower than human-driven vehicles.

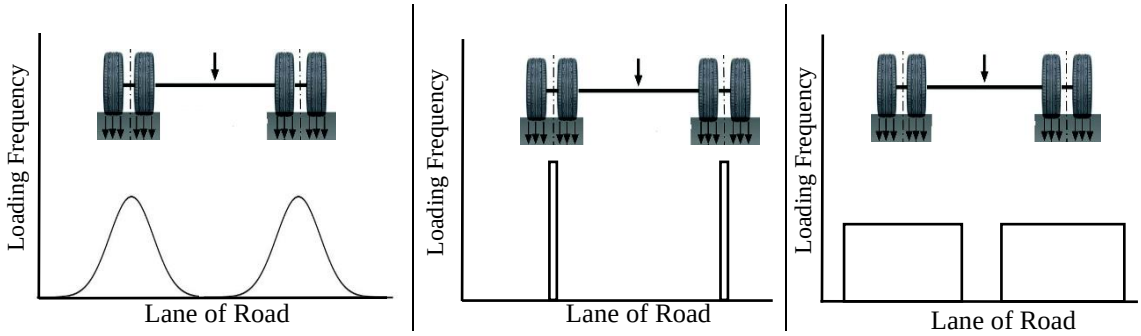

Figure 2.8 Loading Distribution of a) human-driven b) autonomous and c) uniform distributed vehicles (Regenerated from Noorvand et al., 2017)

Chen et al. (2019) predicted fatigue and rutting for zero-wander, uniform, double peak Gaussian, and two-section uniform mode distribution of wheel load (distributions shown in Figure 2.9) on the lane of pavement. The finite element analysis was deployed to observe the effects of autonomous trucks' lateral distribution within the lane. The authors

found that two-section uniform mode distribution of wheel loading distribution significantly reduced rutting and fatigue of AC pavement.

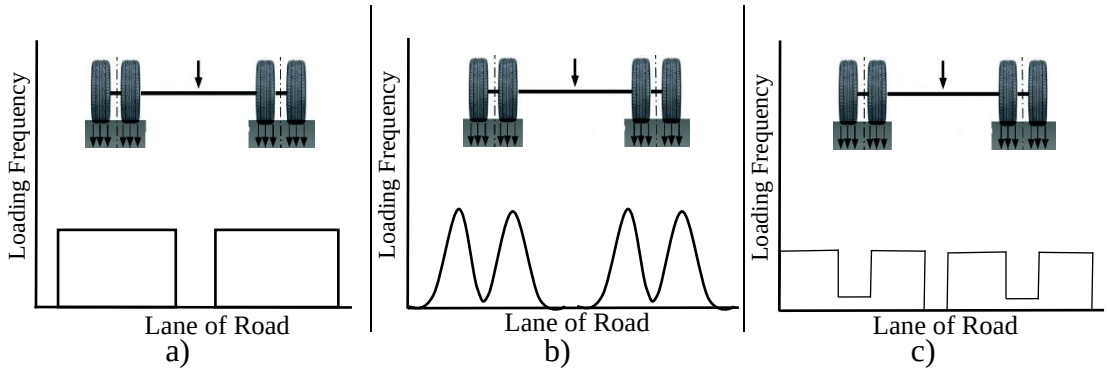

Figure 2.9 Modes of a) uniform b) double peak Gaussian c) two-section uniform loading distribution (Regenerated from Chen et al., 2019)

In another study, Chen et al. proved fatigue growth mode as an efficient approach to control AT laterally on the pavement lane. In this mode, the ATs are directed to move in the different lateral positions of the road based on the fatigue damage. The sensors placed on the pavement ensures the effect of ATs on the pavement and their position accordingly. This lateral control mode minimizes fatigue damage growth by 28% for 100% of autonomous vehicles (Chen et al., 2020).

Gungor and Al-Qadi (2020) introduced a centralized control strategy to control the positioning of AT platoon on the pavement lane. This strategy explicitly controls the positioning of the platoon using V2I communication (Figure 2.10) for the increase in the wander of AC pavement. The authors found a significant minimization in pavement damage and an increase in pavement life from the application of this strategy. The application of this strategy showed a 50% reduction in life cycle cost in a case study. Bouchihati (2020) suggested smart lanes equipped with sensors for distress optimization

and these sensors will explicitly control the positioning of the platoon for improving pavement performance. Marsac et al. performed a numerical study to increase the wheel wander of truck platooning. Each truck in a platoon was placed in the different transverse directions of a lane. The placement in that way increases the pavement performance (Marsac et al., 2020). The authors Gungor and Al-Qadi (2020) did not provide any performance improvement solution by increasing the resting period. Gungor et al. (2020) introduced the platooning-control strategy to obtain the benefits of the increased resting periods (i.e.improvement in self-healing capability) along with wander. This strategy controls the position of the truck platoon (Figure 2.11) for distribution of load on the wider lane and inter-vehicle positioning in each platoon to improve the healing period. This strategy was found to reduce the total cost by 9%.

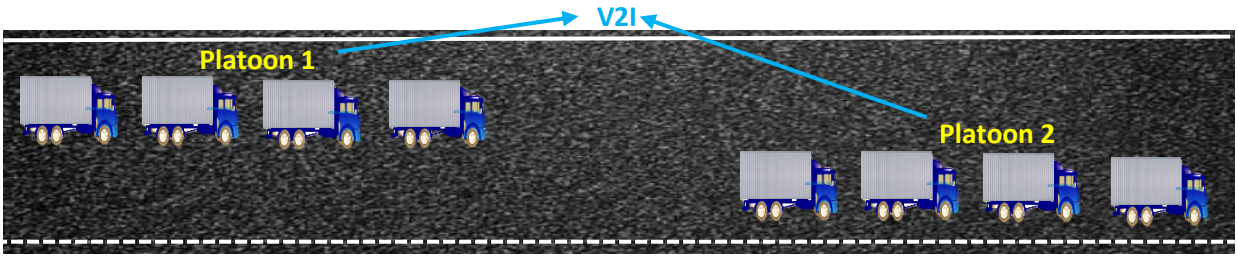

Figure 2.10 Optimization of the lateral position of truck platoons (Gungor and Al-Qadi, 2020)

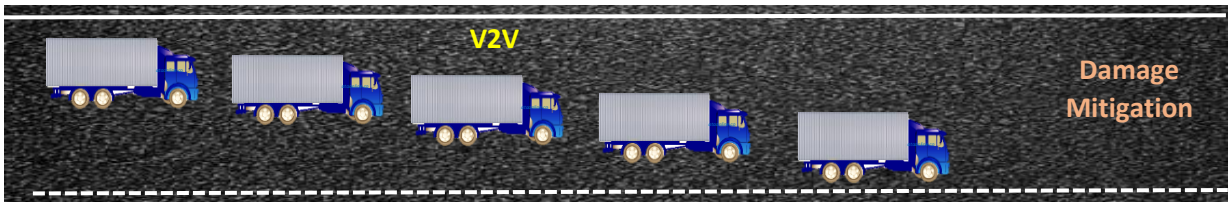

Figure 2.11 Decentralized optimization of trucks in a platoon (Gungor et al., 2020)

2.10 Future Study

The CAVs are in the development stage till now. The behavior of CAVs will depend on how CAVs will mimic human drivers. Different countries are conducting road tests to observe the applicability of the commercialization of CAVs. When the AVs commercially move on the road, the performance issues associated with automation will be obvious. Zhou et al. (2019) performed a field test and found the standard deviation ranging from 1 inch to 3 inches. The improvement in pavement performance can be studied by applying field wheel wander. The CAVs significantly affect the geometric elements of the highway (Welde & Qiao, 2020). It might be a good option for researchers to investigate the effects and optimization of the changing geometric elements on pavement distress.

The movement of the CAVs on a narrower lane will increase the pavement rutting. The water is accumulated in the rutted pavement portion in the rainy season. The accumulated water causes the hydroplaning risk for various vehicles, especially for passenger cars. The hydroplaning risk may interrupt to gain probable road safety in the wet road, one of the major considerations for CAV deployment. The inter-connected study of road safety and pavement design might provide a well-accepted solution for this contradictory situation.

Full autonomous driving can run on the road without any human intervention. Human fatigue, major causes of road accidents, will no more issue in the future. The movement of AT at night time might be beneficial for pavement performance. The additional asphalt pavement distress for CAVs can be minimized, allowing AT at night time because asphalt pavement can perform better at the low temperature of the night time.

In that case, there is a possibility of fatigue cracking and asphalt rutting to be contradictory. The asphalt pavement performance can be studied to establish optimization for the movement of vehicles at night time.

2.11 Concluding Remarks

The continuous technological developments are accelerating the commercial initialization of connected and autonomous vehicles (CAVs) on the highway. The deployment of CAVs will provide more benefits to the transportation sectors. A lot of uncertainties about the benefits of CAVs and the potential impacts on pavement infrastructures are remarkable. The summary from this review is presented below:

- The introduction of the different advanced driver-assist systems (ADAS) is transforming human-driving features to full automation.
- The full automation of passenger cars along with freight transport are proved to be advantageous for transportation sectors. The connectivity has added a new dimension to the automation and also induces more benefits by truck platooning. There are uncertainties about the gaining of benefits considered for CAVs.
- The connected and automated driving has several adverse effects on pavement infrastructures (digital and physical). The excessive studies on digital infrastructures provided different logical solutions and advancing for more advanced options.
- The geometric elements (stopping sight distance, length of sag curve, length of crest curve) for CAVs are beneficial economically due to reduction in earth work.

- The significant pavement distresses are associated with reduced wheel wander for excessive load repetition on the narrower width of the lane. The control of truck movement in the transverse direction of the lane to induce uniform loading has been proposed as a suitable solution for distress optimization. In addition, double peak uniform distribution, loading distribution at field wander, etc., might improve the pavement performance.
- The more load repetition on reduced lane width and decreased self-healing capacity of asphalt pavement due to close inter-truck distance accelerates the pavement distress for truck platooning. Researchers proposed strategies to control truck platooning explicitly for transforming disadvantages into opportunities. The explicit control by placing the truck platoons at the different transverse location or truck in a platoon at a different location or combination of both can be beneficial for pavement distress optimization.
- Extensive studies on pavement performance are required to be harmonious with technological advancements.

2.12 References

Adanu, E. K., & Jones, S. (2017). Effects of human-centered factors on crash injury severities. *Journal of Advanced Transportation*, *2017*.

Ahmed, M., & Yang, G. (2019). *Impacts of cooperative automated transportation on wyoming highway infrastructure*. Department of Civil and Architectural Engineering, University of Wyoming.

Almeida, A., Moreira, J. J. M., Silva, J. P., & Viteri, C. G. V. (2019). Impact of traffic loads on flexible pavements considering Ecuador's traffic and pavement condition. *International Journal of Pavement Engineering*, 0(0), 1–8.

American Automobile Association. (2019). *Advanced Driver Assistance Technology Names* (Issue January). https://www.aaa.com/AAA/common/AAR/files/ADAS-Technology-Names-Research-Report.pdf

Andersson, P., & Ivehammar, P. (2019). Benefits and costs of autonomous trucks and cars. *Journal of Transportation Technologies*, *09*(02), 121–145.

ARA Inc. (2004). *Guide for Mechanistic–Empirical design of new and rehabilitated pavement structures*. Final Rep., NCHRP Project 1-37A.

Aripin, M. K., Sam, Y. M., Kumeresan, A. D., Ismail, M. F., & Kemao, P. (2014). A Review on integrated active steering and braking control for vehicle yaw stability system. *Jurnal Teknologi (Sciences & Engineering)*, *71*(2), 105–111.

Associated Press. (2020). *US agency posts online map to track autonomous vehicle tests*. https://www.usnews.com/news/us/articles/2020-09-02/us-agency-posts-online-map-to-track-autonomous-vehicle-tests

Atkins. (2017). *Analysis of geospatial data requirement to support the operation of autonomous cars*. SDFE - Danish Ministry of Energy, Utilities and Climate (Issue December).

Baidu. (2020). *How coronavirus is accelerating a future with autonomous vehicles*. https://www.technologyreview.com/2020/05/18/1001760/how-coronavirus-is-accelerating-autonomous-vehicles/

Bell, S. (2017). *The connected car taxonomy decoded : An overview of connected autonomous vehicles & intelligent transportation systems*. Heavy Reading.

Belmonte, F. J., Martin, S., Sancristobal, E., Ruiperez-Valiente, J. A., & Castro, M. (2020). Overview of Embedded Systems to Build Reliable and Safe ADAS and AD Systems. *IEEE Intelligent Transportation Systems Magazine*. https://doi.org/10.1109-/MITS.2019.2953543

Bennett, R., Vijaygopal, R., & Kottasz, R. (2019). Attitudes towards autonomous vehicles among people with physical disabilities. *Transportation Research Part A: Policy and Practice*, *127*(July 2018), 1–17. https://doi.org/10.1016/j.tra.2019.07.002

Binshuang, Z., Jiaying, C., Runmin, Z., & Xiaoming, H. (2019). Skid resistance demands of asphalt pavement during the braking process of autonomous vehicles. *MATEC Web of Conferences*, *275*(201 9), 04002. https://doi.org/10.1051/matecconf/20192750402

Blab, R., & Litzka, J. (1995). Measurements of the lateral distribution of heavy vehicles and its effects on the design of road pavements. *Proceedings of the International Symposium on Heavy Vehicle Weights and Dimensions*, 389–395.

Boateng, R., Park, H., Smith, B. L., & Zhang, X. (2019). *Providing traffic control device information in a connected and automated vehicle environment*. http://www.virginia-dot.org/vtrc/main/online_reports/pdf/19-r19.pdf

Bouchihati, M. E. (2020). *The impact of truck platooning on the pavement structure of Dutch Motorways The link between truck platooning and road surface wear*. Delft University of Technology.

Buiter, R., Cortenraad, W. M. H., van Eck, A. C., & van Rij, H. (1989). Effects of

transverse distribution of heavy vehicles on thickness design of full-depth asphalt pavements. *Transportation Research Record*, *1227*, 66–74.

Calvert, S. C., Schakel, W. J., & van Lint, J. W. C. (2017). Will automated vehicles negatively impact traffic flow? *Journal of Advanced Transportation*, *2017*. https://doi.org/10.1155/2017/3082781

CAVita LLC. (2017). *State CEO leadership forum on connected & autonomous vehicles and transportation infrastructure readiness in conjunction with 2017 ITSWC, Montreal, Canada* (Vol. 24, Issue 111). http://onlinepubs.trb.org/onlinepubs/-nchrp/docs/NCHRP20-24(111)_FR.pdf

Chandni, C. K., Sajith Variyar, V. V., & Guruvayurappan, K. (2017). Vision based closed loop PID controller design and implementation for autonomous car. *2017 International Conference on Advances in Computing, Communications and Informatics, ICACCI 2017*, *2017-January*, 1928–1933. https://doi.org/10.-1109/ICACCI.2017.8126127

Chen, F., Song, M., & Ma, X. (2020). A lateral control scheme of autonomous vehicles considering pavement sustainability. *Journal of Cleaner Production*, *256*, 120669. https://doi.org/10.1016/j.jclepro.2020.120669

Chen, F., Song, M., Ma, X., & Zhu, X. (2019). Assess the impacts of different autonomous trucks' lateral control modes on asphalt pavement performance. *Transportation Research Part C: Emerging Technologies*, *103*(March), 17–29.

Cheong, M., Lee, Y., Park, W., & Yeom, I. (2017). Analysis of V2V communication for ADAS. *International Conference on Ubiquitous and Future Networks, ICUFN*, 284–

286. https://doi.org/10.1109/ICUFN.2017.7993794

Chong, J. (2016). Automated and connected vehicles: Status of the technology and key policy issues for canadian governments. In *Library of Parliament Background Papers*.

Chu, L. J., & Fwa, T. F. (2018). Pavement skid resistance consideration in rain-related wet-weather speed limits determination. *Road Materials and Pavement Design*, *19*(2), 334–352. https://doi.org/10.1080/14680629.2016.1261723

Dominguez, S., Ali, A., Garcia, G., & Martinet, P. (2016). Comparison of lateral controllers for autonomous vehicle : Experimental results. *IEEE Conference on Intelligent Transportation Systems, Proceedings, ITSC*, 1418–1423.

Engholm, A., Pernestål, A., & Kristoffersson, I. (2020). Cost analysis of driverless truck operations. *Transportation Research Record*, *2674*(9), 511–524.

Erlingsson, S. (2012). Rutting development in a flexible pavement structure. *Road Materials and Pavement Design*, *13*(2), 218–234.

European Commission. (2018). *Autonomous vehicles & traffic safety 2018*. https://ec.europa.eu/transport/road_safety/sites/roadsafety/files/pdf/ersosynthesis2018-autonomoussafety.pdf

Faber, T., Sharma, S., Snelder, M., Klunder, G., Tavasszy, L., & van Lint, H. (2020). Evaluating traffic efficiency and safety by varying truck platoon characteristics in a critical traffic situation. *Transportation Research Record: Journal of the Transportation Research Board*, *2674*(10), 525–547.

Fagnant, D. J., & Kockelman, K. (2015). Preparing a nation for autonomous vehicles:

Opportunities, barriers and policy recommendations. *Transportation Research Part A: Policy and Practice*, *77*, 167–181. https://doi.org/10.1016/j.tra.2015.04.003

Farah, H. (2016). *State of art on infrastructure for automated vehicles*. Delft University of Technology. https://repository.tudelft.nl/islandora/object/uuid%3A27b22b96-159b-4c45-bcca-b0fefc9969be

Fee, G. (2020). Preparing for autonomous vehicles. *Asphalt Magazine*. http://asphaltmagazine.com/autonomous-vehicles/

Filho, C. M., Wolf, D. F., Grassi, V., & Osorio, F. S. (2014). Longitudinal and lateral control for autonomous ground vehicles. *IEEE Intelligent Vehicles Symposium, Proceedings*, *Iv*, 588–593. https://doi.org/10.1109/IVS.2014.6856431

Future Agenda. (2020). *The future of autonomous vehicles: Global insights gained from multiple expert discussions*.

Garcia, A., & Camacho-Torregrosa, F. J. (2020). Influence of lane width on semi-autonomous vehicle performance. *Transportation Research Record*, *2674*(9), 279–286. https://doi.org/10.1177/0361198120928351

Greenwald, J. M., & Kornhauser, A. (2019). It's up to us: Policies to improve climate outcomes from automated vehicles. *Energy Policy*, *127*(September 2018), 445–451. https://doi.org/10.1016/j.enpol.2018.12.017

Gungor, O. E. (2018). *Final report: A literature review on wheel wander*.

Gungor, O. E., & Al-Qadi, I. L. (2020a). All for one: Centralized optimization of truck platoons to improve roadway infrastructure sustainability. *Transportation Research Part C: Emerging Technologies*, *114*(January), 84–98.

Gungor, O. E., & Al-Qadi, I. L. (2020b). Wander 2D: a flexible pavement design framework for autonomous and connected trucks. *International Journal of Pavement Engineering*, *0*(0), 1–16. https://doi.org/10.1080/10298436.2020.1735636

Gungor, O. E., She, R., Al-Qadi, I. L., & Ouyang, Y. (2020). One for all: Decentralized optimization of lateral position of autonomous trucks in a platoon to improve roadway infrastructure sustainability. *Transportation Research Part C: Emerging Technologies*, *120*(May), 102783. https://doi.org/10.1016/j.trc.2020.102783

Gurumurthy, K. M., & Kockelman, K. M. (2020). Modeling Americans' autonomous vehicle preferences: A focus on dynamic ride-sharing, privacy & long-distance mode choices. *Technological Forecasting and Social Change*, *150*(October 2019), 119792. https://doi.org/10.1016/j.techfore.2019.119792

Hagl, M., & Kouabenan, D. R. (2020). Safe on the road – Does advanced driver-assistance systems use affect road risk perception? *Transportation Research Part F: Traffic Psychology and Behaviour*, *73*, 488–498. https://doi.org/10.1016/j.trf.2020.07.011

Hallmark, S. (2019). *Preparing Local Agencies for the Future of Connected and Autonomous Vehicles* (Issue May). http://mndot.gov/research/reports/2019/2019-18.pdf

Hancock, M. W., & Wright, B. (2018). *A policy on geometric design of highways and streets*. American Association of State Highway and Transportation Officials (AASHTO), Washington, DC, USA. https://doi.org/10.1016/b978-1-85617-198-4.50009-6

Heaslip, K., Goodall, N., Kim, B., & Abi Aad, M. (2020). Assessment of capacity changes due to automated vehicles on interstate corridors. Final Report VTRC 21-R1. In

Federal Highway Administration. http://www.virginiadot.org/vtrc/main/online_reports/pdf/21-r1.pdf

Hexagon. (2020). *Automotive: Driving towards autonomy*. https://novatel.com/industries/autonomous-vehicles.

Hoogendoorn, R., Van Arem, B., & Hoogendoorn, S. (2014). Automated driving, traffic flow efficiency, and human factors. *Transportation Research Record*, *2422*(2422), 113–120. https://doi.org/10.3141/2422-13

Jelagin, D., Ahmed, A., Lu, X., & Said, S. (2018). *Asphalt layer rutting performance prediction tools. VTI rapport 968A* (Issue September).

Khoury, J., Amine, K., & Saad, R. A. (2019). An initial investigation of the effects of a fully automated vehicle fleet on geometric design. *Journal of Advanced Transportation*, *2019*. https://doi.org/10.1155/2019/6126408

Kopelias, P., Demiridi, E., Vogiatzis, K., Skabardonis, A., & Zafiropoulou, V. (2020). Connected & autonomous vehicles – Environmental impacts – A review. *Science of the Total Environment*, *712*, 135237. https://doi.org/10.1016/j.scitotenv.2019.135237

Lengyel, H., Tettamanti, T., & Szalay, Z. (2020). Conflicts of automated driving with conventional traffic infrastructure. *IEEE Access*, *8*, 163280–163297.

Lim, H. S. M., & Taeihagh, A. (2018). Autonomous vehicles for smart and sustainable cities: An in-depth exploration of privacy and cybersecurity implications. *Energies*, *11*(5). https://doi.org/10.3390/en11051062

Linder, C. (2020). Self driving freight trucks - Autonomous trucks. *Popular Mechanics*. https://doi.org/https://www.popularmechanics.com/technology/infrastructure/a30196

644/self-driving-truck-cross-country/

Litman, T. (2020). Autonomous Vehicle implementation predictions: Implications for transport planning. In *Victoria Transport Policy Institute*. https://doi.org/10.1613-/jair.301

Liu, F., Zhao, F., Liu, Z., & Hao, H. (2019). Can autonomous vehicle reduce greenhouse gas emissions? A country-level evaluation. *Energy Policy*, *132*(June), 462–473. https://doi.org/10.1016/j.enpol.2019.06.013

Liu, Yi, Wang, W., Hua, X., & Wang, S. (2020). Safety analysis of a modified cooperative adaptive cruise control algorithm accounting for communication delay. *Sustainability (Switzerland)*, *12*(18). https://doi.org/10.3390/su12187568

Liu, Yuyan, Tight, M., Sun, Q., & Kang, R. (2019). A systematic review: Road infrastructure requirement for Connected and Autonomous Vehicles (CAVs). *Journal of Physics: Conference Series*, *1187*(4). https://doi.org/10.1088/1742-6596/1187/4/-042073

Mahdinia, I., Arvin, R., Khattak, A. J., & Ghiasi, A. (2020). Safety, energy, and emissions impacts of adaptive cruise control and cooperative adaptive cruise control. *Transportation Research Record*, *2674*(6), 253–267. https://doi.org/10.1177-/0361198120918572

Marsac, P., Blanc, J., Chupin, O., Gabet, T., Hammoum, F., Garg, N., & Nguyen, M. L. (2020). Optimization of truck platoon wander patterns based on thermo-viscoelastic simulations to mitigate the damage effects on road structures. *Proceedings of 6th International Conference on Accelerated Pavement Testing, France*.

Maurer, M., Gerdes, J. C., Lenz, B., & Winner, H. (2015). Autonomous driving. In *Springer* (Vol. 57, Issue 4). https://doi.org/10.1515/itit-2015-0027

Meyer, G., & Beiker, S. (2019). *Road vehicle automation 5*. Springer International Publishing. https://doi.org/https://doi.org/10.1007/978-3-319-94896-6_12

Milakis, D., Van Arem, B., & Van Wee, B. (2017). Policy and society related implications of automated driving: A review of literature and directions for future research. *Journal of Intelligent Transportation Systems: Technology, Planning, and Operations*, *21*(4), 324–348. https://doi.org/10.1080/15472450.2017.1291351

Mitchell 1. (2019). *All About ADAS*. https://mitchell1.com/shopconnection/all-about-adas/

Narayanan, S., Chaniotakis, E., & Antoniou, C. (2020). Shared autonomous vehicle services: A comprehensive review. *Transportation Research Part C: Emerging Technologies*, *111*(January), 255–293. https://doi.org/10.1016/j.trc.2019.12.008

National Academies of Sciences, Engineering, and Medicines (2009). *Guide for pavement friction*. American Association of State Highway and Transportation Officials, Report no. NCHRP 1-43. https://doi.org/10.17226/23038

National Academies of Sciences, Engineering, and Medicines (2015). *Towards road transport automation: opportunities in public-private collaboration*. The National Academies Press, Washington, DC, USA. https://doi.org/10.17226/22087

National Science and Technology Council, & US DOT. (2020). *Ensuring American leadership in automated vehicle technologies, Automated vehicles 4.0* (Issue January). https://www.transportation.gov/av/4

Neumeister, D., & Pape, D. (2019). *Automated vehicles and adverse weather*. Federal

Highway Administration, Report no. FHWA-JPO-19-755.

Noorvand, H., Karnati, G., & Underwood, B. S. (2017). Autonomous vehicles: Assessment of the implications of truck positioning on flexible pavement performance and design. *Transportation Research Record*, *2640*(January), 21–28. https://doi.org/-10.3141/2640-03

Norouzi, A., Masoumi, M., Barari, A., & Farrokhpour Sani, S. (2019). Lateral control of an autonomous vehicle using integrated backstepping and sliding mode controller. *Proceedings of the Institution of Mechanical Engineers, Part K: Journal of Multi-Body Dynamics*, *233*(1), 141–151. https://doi.org/10.1177/1464419318797051

Pais, J. C., Figueiras, H., Pereira, P., & Kaloush, K. (2019). The pavements cost due to traffic overloads. *International Journal of Pavement Engineering*, 20(12), 1463–1473. https://doi.org/10.1080/10298436.2018.1435876

Pakusch, C., Stevens, G., Boden, A., & Bossauer, P. (2018). Unintended effects of autonomous driving: A study on mobility preferences in the future. *Sustainability (Switzerland)*, *10*(7), 1–22. https://doi.org/10.3390/su10072404

Patella, S. M., Aletta, F., & Mannini, L. (2019). Assessing the impact of Autonomous Vehicles on urban noise pollution. *Noise Mapping*, *6*(1), 72–82.

Poe, C. M. (2020). *Connected roadway classification system development*. National Cooperative Highway Research Program, Transportation Research Board, Report No. NCHRP 20-24(112).

SAE International. (2014). *SAE J3016: Taxonomy and definitions for terms related to on-road motor vehicle automated driving systems*.

Said, S. F., Hakim, H., & Eriksson, O. (2013). Rheological characterization of asphalt concrete using a shear box. *Journal of Testing and Evaluation*, *41*(4), 602–610. https://doi.org/10.1520/JTE20120177

Said, S. F., Hakim, H., Oscarsson, E., & Hjort, M. (2011). Prediction of flow rutting in asphalt concrete layers. *International Journal of Pavement Engineering*, *12*(6), 519–532. https://doi.org/10.1080/10298436.2011.559549

Shafiee, M. H., Nassiri, S., & Bayat, A. (2014). Field investigation of the effect of operational speed and lateral wheel wander on flexible pavement mechanistic responses. *2014 Transportation Association of Canada Conference and Exhibition: Past, Present, Future, ATC 2014*, *5112*.

Shladover, S. E. (2018). Connected and automated vehicle systems: Introduction and overview. *Journal of Intelligent Transportation Systems: Technology, Planning, and Operations*, *22*(3), 190–200. https://doi.org/10.1080/15472450.2017.1336053

Shladover, S. E., Su, D., & Lu, X. Y. (2012). Impacts of cooperative adaptive cruise control on freeway traffic flow. *Transportation Research Record*, *2324*(January), 63–70. https://doi.org/10.3141/2324-08

Siddharthan, R. V., Nasimifar, M., Tan, X., & Hajj, E. Y. (2017). Investigation of impact of wheel wander on pavement performance. *Road Materials and Pavement Design*, *18*(2), 390–407. https://doi.org/10.1080/14680629.2016.1162730

Simko, D. J. (2016). Increasing road infrastructure capacity through the use of autonomous vehicles. In *Naval Postgraduate School, Monterey, California* (Issue September). https://doi.org/July 01, 2016

Skarbek-Zabkin, A., & Szczepanek, M. (2018). Autonomous vehicles and their impact on road infrastructure and user safety. *11th International Science and Technical Conference Automotive Safety*, 1–4. https://doi.org/10.1109/AUTOSAFE.2018.-8373343

Stern, R. E., Chen, Y., Churchill, M., Wu, F., Delle Monache, M. L., Piccoli, B., Seibold, B., Sprinkle, J., & Work, D. B. (2019). Quantifying air quality benefits resulting from few autonomous vehicles stabilizing traffic. *Transportation Research Part D: Transport and Environment*, *67*(December 2018), 351–365. https://doi.org/-10.1016/j.trd.2018.12.008

Taeihagh, A., & Lim, H. S. M. (2018). Governing autonomous vehicles: Emerging responses for safety, liability, privacy, cybersecurity, and industry risks. *Transport Reviews*, *39*(1), 103–128.

Thomas, M. (2018). Reinventing Carsharing As a Modern (and Profitable) Service. In *2018 ITS America Annual Meeting Detroit.*

Tientrakool, P., Ho, Y. C., & Maxemchuk, N. F. (2011). Highway capacity benefits from using vehicle-to-vehicle communication and sensors for collision avoidance. *IEEE Vehicular Technology Conference*, 0–4. https://doi.org/10.1109/VETECF.2011-.6093130

National Highway Traffic Safety Administration (2015). *Critical reasons for crashes investigated in the national motor vehicle crash causation survey*. National Center for Statistics and Analysis, Washington DC, USA.

Urmson, C. (2006). Driving beyond stopping distance constraints. *IEEE International*

Conference on Intelligent Robots and Systems, 1189–1194. https://doi.org/-10.1109/IROS.2006.281852

Velodyne LiDAR Inc. (2019). *User's manual and programming guide: High definition LiDAR sensor*.

Wanek-Libman, M. (2020). *CTDOT scheduled to deploy first full-size automated transit bus in North America*. https://www.masstransitmag.com/alt-mobility/autonomous-vehicles/article/21143509/ctdot-scheduled-to-deploy-first-fullsize-automated-transit-bus-in-north-america

Wang, J., Zhang, L., Huang, Y., & Zhao, J. (2020). Safety of autonomous vehicles. *Journal of Advanced Transportation*, *2020*(i). https://doi.org/10.1155/2020/8867757

Wang, L., Sun, P., Xie, M., Ma, S., Li, B., Shi, Y., & Su, Q. (2020). Advanced Driver-Assistance System (ADAS) for intelligent transportation based on the recognition of traffic cones. *Advances in Civil Engineering*, *2020*. https://doi.org/10.1155-/2020/8883639

Washburn, S. S., & Washburn, L. D. (2018). *Future highways - Automated vehicles*. https://s3.amazonaws.com/suncam/docs/208.pdf

Welde, Y., & Qiao, F. (2020). Effects of autonomous and automated vehicles on stopping sight distance and vertical curves in geometric design. *Resilience and Sustainable Transportation Systems*, *3*(1986), 148–156.

Wevolver. (2020). *Autonomous vehicle technology report*. https://www.wevolver.com-/article/2020.autonomous.vehicle.technology.report

Winston, C., & Karpilow, Q. (2020). Autonomous vehicles: The road to economic growth?

Brookings Institution Press.

Wu, R., & Harvey, J. T. (2008). Evaluation of the effect of wander on rutting performance in HVS tests. *Third International Conference on Accelerated Pavement Testing October 2008, Madrid, Spain, August*.

Yoneda, K., Suganuma, N., Yanase, R., & Aldibaja, M. (2019). Automated driving recognition technologies for adverse weather conditions. *International Association of Traffic and Safety Sciences*, *43*, 253–262.

Zhang, L., Chen, F., Ma, X., & Pan, X. (2020). Fuel economy in truck platooning: A literature overview and directions for future research. *Journal of Advanced Transportation*, *2020*. https://doi.org/10.1155/2020/2604012

Zhou, F., Hu, S., Chrysler, S. T., Kim, Y., Damnjanovic, I., Talebpour, A., & Espejo, A. (2019). Optimization of lateral wandering of automated vehicles to reduce hydroplaning potential and to improve pavement life. *Transportation Research Record*, 1–9. https://doi.org/10.1177/0361198119853560

Chapter 3 Simulation of Autonomous Truck for Optimization of Asphalt Pavement Distresses

Md Masud Rana[a]* and Kamal Hossain[a]

[a]Department of Civil Engineering, Memorial University of Newfoundland, St. John's, Newfoundland, CANADA

Abstract

In recent years progressive development in automation technology is accelerating the commercial implementation of this technology in transportation sectors. This implementation of automation technology is not only bounded to passenger cars but also this technology has reached out to the trucking sector. Despite having more advantages, automation in trucking technology has some detrimental effects on the performance of asphalt pavement. Researchers are now studying to improve pavement performance by different means for the smooth movement of autonomous trucks (AT). This study also focuses on the optimization of pavement distresses by controlling vehicular loading distribution patterns, traffic distribution on lanes of a road and limiting the running duration of AT to low-temperature time only. Mechanistic-Empirical Pavement Design Software, AASHTOWare was incorporated in this research to analyze and then optimize the generation of asphalt pavement distresses from autonomous truck loading. Autonomous trucks with loading patterns and traffic distribution on lanes have been devised to input in

Rana, M., Hossain, K. (2020). Simulation of Autonomous Truck for Optimization of Asphalt Pavement Distresses. Submitted to Road Materials and Pavement Design.

AASHTOWare by evaluating equivalency factor (EF) respective to the number of traffic repetitions, and varying lane distribution factors. Using multi-layer elastic theory EFs were calculated for fatigue cracking and rutting separately. The obtained EFs along with lane distribution factors were inputted in AASHTOWare to evaluate pavement performance for different loading distribution patterns and traffic distribution on travel lanes. The acquired performances clearly showed significant improvement in pavement distresses for a small increase of standard deviation of wheel wander and uniform distribution of traffic loading and for equally distributed traffic on the road lanes. Besides, an attempt has been made to decrease pavement distresses in putting all AT in low-temperature duration of a day. Placing all ATs in a certain period of a day might be beneficial for reducing asphalt pavement distresses and may bring a fruitful solution to prevent the early deterioration of the pavement.

Keywords: Autonomous Trucks, Pavement Distresses, Traffic Load Distribution, Uniform Distribution, Low-Temperature Period, Improvement of Pavement Performance.

Rana, M., Hossain, K. (2020). Simulation of Autonomous Truck for Optimization of Asphalt Pavement Distresses. Submitted to Road Materials and Pavement Design.

3.1 Introduction

Rapidly growing technological advancement in the field of automation industry are about to launch connected and autonomous vehicle in road transport system commercially. Over the last decades this technology has been progressively implemented for vehicles in different stages from zero level to fully autonomous conditions. In the recent crisis of COVID-19, fully autonomous vehicles are being used for supplying medical necessities in some places in the U.S. and China (Donelson, 2020). It is predicted that autonomous vehicles will occupy 25% of all miles driven in the U.S. by 2030. Estimation of the Center for Automotive Research proclaims that new vehicle sales might get increased by up to 55 percent by 2040 (Fee, 2020). In early December 2019, Technology company, Waymo led one pilot program for autonomous taxi service in Arizona. The number of rides in this program reaches 100,000 (When Will Self-Driving Cars Be Available 2020?, 2020).

The application of automation techniques is not restrained to passenger cars only (Noorvand et al., 2017). It has been initiated to bring trucks under automation technology to increase efficiency in the shipment of goods (Andersson & Ivehammar, 2019). In December 2019, an autonomous freight truck made a cross country trip of 2800 miles in California to deliver butter commercially (Linder, 2020). The reasons behind the initialization of autonomous vehicles including truck are a significant reduction in crash rate occurs due to human error, relieving drivers stress, improved productivity and mobility being used as mobile office and bedrooms, minimizing traffic congestion, parking costs, and pollution emissions, etc. (Litman, 2020). The freight transportation system might get more benefitted by autonomous trucks (AT) from improved operational efficiency in

moving goods and overcoming shortages in the truck driver (Gungor & Al-Qadi, 2020a). Despite having a lot of advantages, decision-makers and practitioners are concerned about planning implications of AT associated with roadway design, transportation pricing, curb management, parking planning, public transit needs and so on (Litman, 2020). With the introduction of AT, pavement engineers are giving attention to the structural performance of the pavement. The reason to get more attention is the effect of AT traffic on the long term performance of asphalt concrete (AC) pavement. Implementation of AT will affect the performance of AC pavement induced from channelized or less wander traffic loading, reduced inter-vehicle distances and constant speeds and less stop/start actions (Steyn & Maina, 2019).

3.2 Wheel Wander and Pavement Distresses

The wheel wander refers to the lateral positioning of the wheel at the time of vehicular movement on the road section. Influencing factors for lateral wander are drivers' habit, wind effect, and mechanical alignment (Buiter et al., 1989). Lateral positioning of the wheel for human-driven vehicles follows probabilistic distribution along the cross-section of the lane (Gungor & Al-Qadi, 2020b; Siddharthan et al., 2017).

Researchers found wheel positioning as normally distributed within a lane (ARA Inc., 2004b; Wu, 2014). This distribution is statistically modeled with zero mean and known standard deviation following Equation 3.1 (Gungor, 2018). In the case of human driving vehicles, Mechanistic-Empirical (ME) pavement design considers wheel load on the pavement lane with a standard deviation of 10 inches and zero mean (ARA Inc., 2004b).

$$f(x) = \frac{1}{\sqrt{2\pi\sigma^2}} e^{-\frac{(x-\mu)^2}{2\sigma^2}} \quad 3.1$$

Where,

μ=mean of wheel wander distribution

σ=standard deviation of wander effect

The major difference between human-driven vehicles from autonomous vehicles and the semi-autonomous vehicle comes from the distribution of wheel load in a pavement lane. Dynamic control systems in autonomous vehicle and semi-autonomous vehicle controls them to drive along the centerline of the lane (Hills and Lee, 2012). This lane-centering tendency of AT distributes wheel load as a single point distribution, resulting in channelized traffic. This type of channelization is also known as zero wander or less wander distribution. Channelized or less wander traffic increases the repetition of load on the narrower width of the lane (Noorvand et al., 2017) and eventually leads to pavement damage in a faster rate (Litman, 2020). Shafiee et al. installed strain gauges and pressure cells on the University of Alberta's Integrated Road Research Facility (IRRF)'s test road to evaluate the effects of wheel wander (Shafiee et al., 2014). Pavement responses were measured for moving trucks. Due to insufficient truck load, this study determined the effect of wander on induced stress instead of strain. This experiment concluded that zero wander can significantly affect pavement responses. The effect of the wheel wander on rutting on pavement structure was measured by Wu and Harvey (2008). This study used heavy vehicles simulator at the University of California Pavement Research Center for two scenarios: with wander and without wander. This field observation concluded that wheel

significantly decreased magnitude of rutting and change the position of maximum rutting (Wu, 2014).

3.3 Current Knowledge on Pavement Damage

Different authors recently developed various strategies to control the distribution of wheel wander explicitly to reduce pavement distress for ATs. Most of the modifications have been introduced considering the MEPDG approach as a basis. The approach followed for fatigue cracking in MEPDG is dividing lane into equal five areas, each address 20% of truck traffic positioning. The center positioning of truck traffic is fixed and calculated by multiplying standard deviation with standard deviates (0, ±0.5244, ±1.28155). Total damage at any location 3 is computed by adding contributions from each positioning of the truck, following Equation 3.2. Damage accumulations are represented as D1, D2, D3, D4, and D5 due to positioning of the truck at five different locations, respectively. No explanation of modified rutting determination procedures is given in the MEPDG guide (Gungor, 2018).

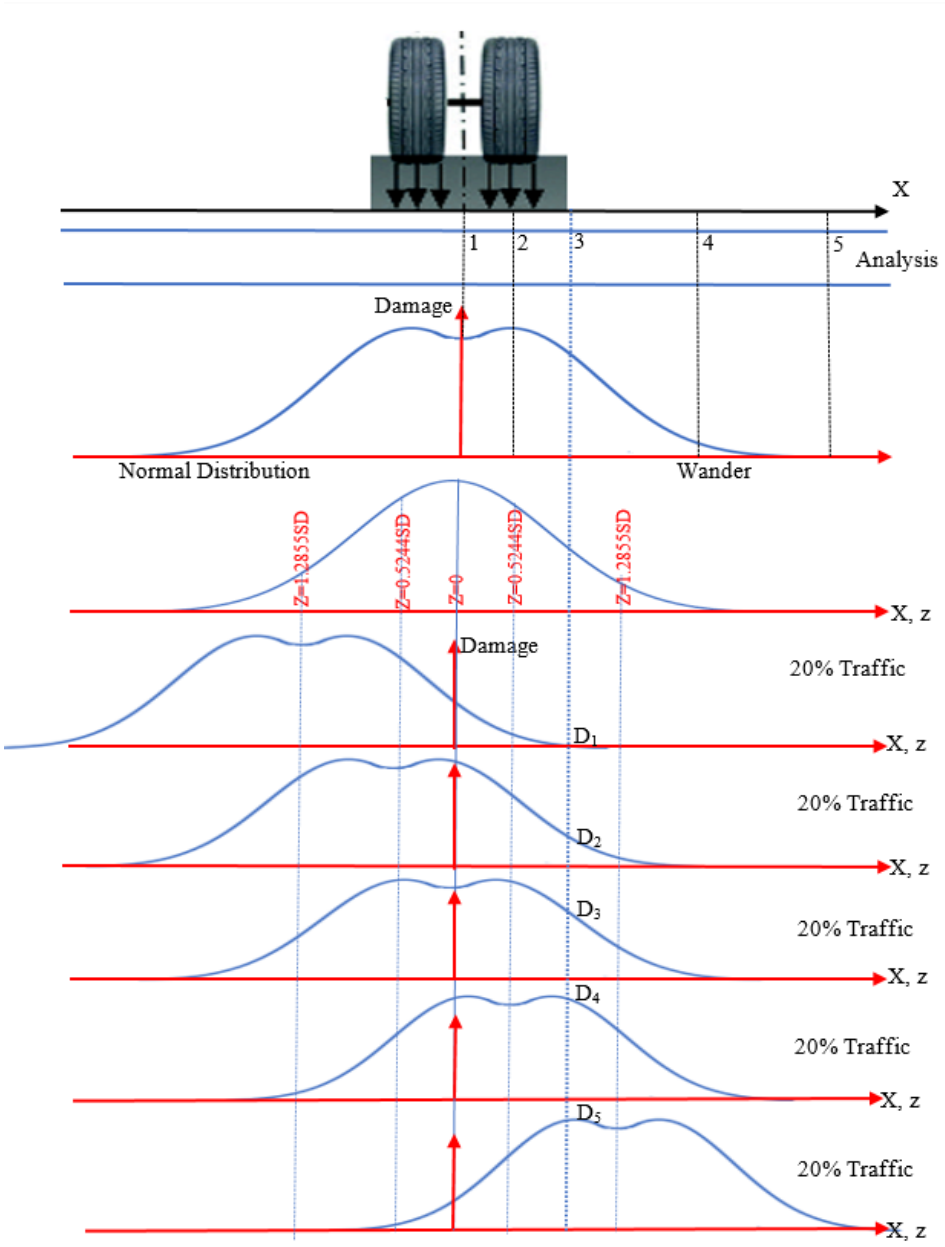

Figure 3.1 MEPDG analytical approach for wheel wander (ARA Inc., 2004)

$$D = 0.2D_1 + 0.2D_2 + 0.2D_3 + 0.2D_4 + 0.2D_5 = 0.2\sum_1^5 D_i \quad 3.2$$

Noorvand et al. systematically devised vehicle positioning in a lane of road section to control wheel wander. AASHTOware was used in this study with proper modifications

of traffic input to control vehicle positioning. The thickness for different positioning was evaluated for three lanes highway (Noorvand et al., 2017). The authors assigned a dedicated lane for more than 50% of AT volume. The observation from the analysis showed reduced thickness in the asphalt concrete layer (AC) accounting for the uniform distribution of traffic loading, covering the entire width. Gungor and Al-Qadi proposed the Wander 2D approach for controlling the lateral position of ATs and evaluate cumulative fatigue and rutting in asphalt pavement (Gungor & Al-Qadi, 2020b). This approach is an entirely analytical solution. The authors recommend using the truncated normal distribution for wheel wander modeling. Truncated normal distribution accounts for lane width, and axle width for pavement performance. The mapping technique was incorporated to transfer pavement damage of ATs for zero wander to wander of human-driven vehicles.

The centralized control strategy was introduced by Gungor and Al-Qadi in another study (Gungor & Al-Qadi, 2020a). This strategy turns challenges of traffic platooning, induced from the introduction of ATs, into opportunities. In this strategy, optimization of the lateral position of the traffic platoon is employed to reduce pavement distresses. The application of this strategy, in a case study by authors, significantly reduced the pavement life cycle cost up to approximately 50%. Chen et al. performed a finite element analysis to observe the effects of autonomous trucks' lateral distribution within the lane. The effects were analyzed concerning rutting depth and fatigue damage (Chen et al., 2019). Authors considered vehicles with zero-wander, uniform, double peak Gaussian, and two-section uniform mode. Five proportions of AT to non-AT were taken for every distribution mode.

The authors observed two-section uniform distribution appeared to have a significant decrease in rutting and fatigue damage.

Chen et al. proposed the techniques for the maximization of pavement fatigue performance by different lateral control modes (Chen et al., 2020). Finite element analysis was performed for normal distribution, uniform distribution, lane centering, and the fatigue damage-oriented mode. Comparative analyses were performed for fatigue growth among the lateral control modes of AVs. The fatigue damage-oriented study minimizes fatigue damage growth by 28% for 100% of autonomous vehicles. Zhou et al. performed field tests to quantify wheel wandering of AVs. These field tests were performed on the Texas A&M RELLIS campus which was a World War II base (Zhou et al., 2019). The obtained results concluded that AV could be modeled with normal distribution having narrower lateral wandering than human-driven vehicles. It concluded three times narrower standard deviation 3.0 (cm) to 7.5 (cm) (1.2" to 3.0") for AVs. The narrower wandering of AVs significantly shortens pavement fatigue life and increases pavement rutting when compared with human-operated traffic.

In this study, pavement performance was simulated for separated scenario (SS) and integrated scenario (IS) based on the distribution of ATs on the traveling lane of a road section. Integrated scenarios were classified as equally distributed (ED) and disproportionately distributed (DD) based on the nature of AT distribution on the lane. Both scenarios were replicated for vehicular loading distribution patterns of zero wander, wander with 7.5 (cm) standard deviation, and uniform distribution. Besides, the simulation

was run by putting all ATs on the low-temperature span of a day. Optimization of pavement distresses was adopted based on AC rutting and BU cracking in the following ways.

- The ratio of AT to non-AT was evaluated based on pavement distresses in the SS scenario. This was done to assign a dedicated lane for ATs, ensuring equivalent distresses on both lanes at the end of service life.
- Pavement performance was compared among simulations of different loading distribution patterns. Improvement of performance with the incorporation of different wanders was observed.
- A comparison was made between the distresses of ED and DD scenario to obtain the optimized condition.
- Percentage change in pavement performance was comprehended by fabricating climate input to put all ATs on the low-temperature span of a day.

3.4 Study Objective and Contribution

The objective of this study is to simulate autonomous trucks based on traffic distribution in the lanes of a road section and loading distribution pattern of the truck and, then to select the optimized simulation based on the least pavement distresses. AC rutting and bottom-up fatigue (BU) cracking were considered as a basis for pavement distresses. Traffic distribution on the lane along with the loading distribution pattern of AT was replicated for 24 simulations. Simulations were devised by equivalency factors obtained using multilayer elastic theory. Adjusted traffic volume from EFs was inputted in AASHTOware-a robust pavement analysis software. The equivalent percentage of non-AT to AT was estimated

based on pavement distresses in this study. Loading distribution patterns were compared to zero wander based on AC rutting and BU fatigue cracking. Pavement distresses were compared between two scenarios, fabricated from traffic distribution on traveling lane. Comparative studies were performed to obtain an optimized scenario based on performance perspectives. Also, an attempt has been made to minimize AT impacts on AC pavement by scheduling AT traffic in the low-temperature period of the day.

3.5 Methodology

The goal of this research is to simulate the implementation of AT in mechanistic-empirical pavement design and its impacts on induced pavement performance. Based on traffic distribution on the lane, AT was characterized as the baseline, separated and integrated scenarios. Each scenario was simulated for different loading distribution patterns to obtain optimized simulation for the movement of autonomous trucks. An attempt was made to minimize pavement distresses by limiting the running duration of ATs also. The methodology in this research mainly consists of four main phases. In the first phase, the traffic details, material properties, structural design and climate inputs were collected from different sources. In the second phase, load equivalency factors for a different distribution of loadings were calculated using multi-layered elastic theory for fatigue and rutting separately. In the third phase, traffic volume was adjusted using equivalency and lane distribution factors for different simulations considered in this analysis. In the fourth phase, the performance was predicted using AASHTOware for all simulations and compared to select an optimized option. The general framework of the current study is presented in Figure 3.2.

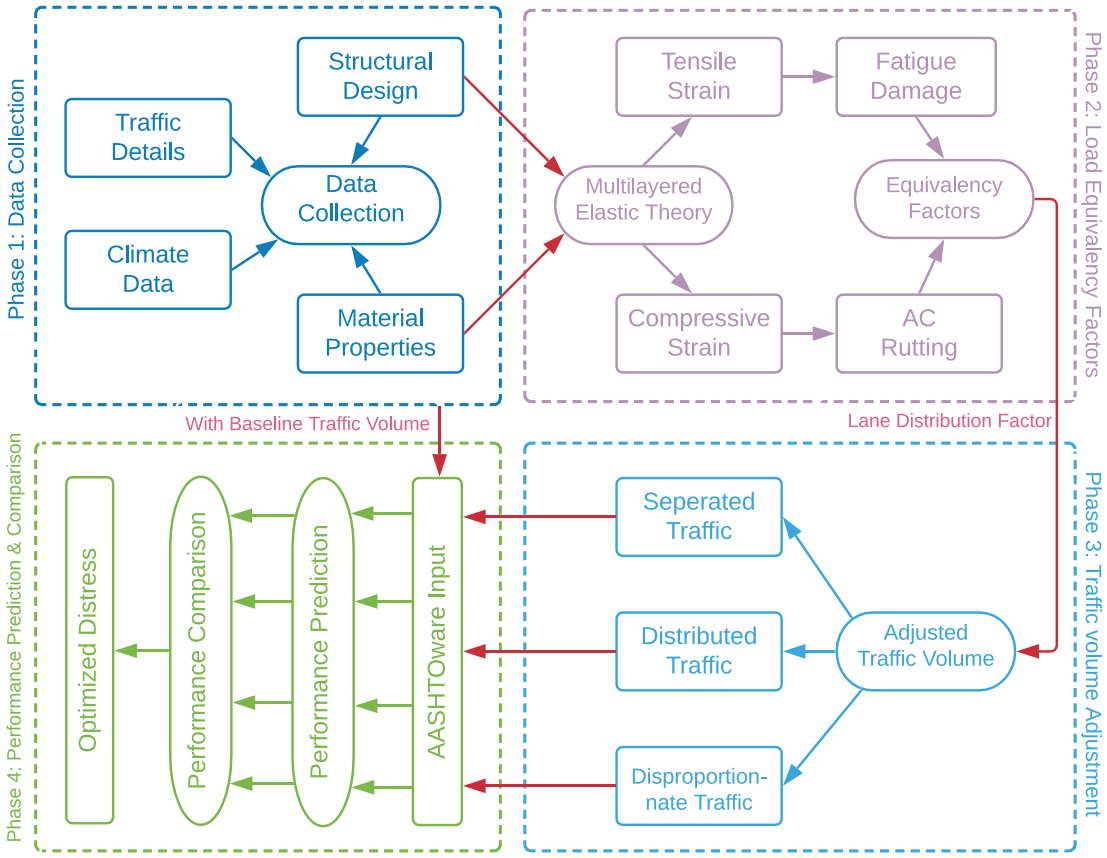

Figure 3.2 Framework for performance evaluation to obtain an optimized scenario

3.5.1 Data Collection

In the first phase, the traffic details, material properties, and structural design were collected from the Long Term Pavement Performance (LTPP) database for one road section in Ontario, Canada. Collected data showed the road section as two-way with two-lane per direction road section. This road section comprises asphalt, sub-base, base, and subgrade layers. The asphalt layer thickness was considered as 16.50 cm (6.6 in). The obtained AADTT was 1890 for the studied road section. But AADTT was taken as 2000 for the baseline scenario in this analysis. Climate data was selected from the AASHTOware database for the co-ordinates of the road section. Local calibration factors used in this study

were obtained from Ontario's Default Parameters for AASHTOWare Pavement ME Design Interim Report – 2019 (MTO, 2019).

3.5.2 Equivalency Factors for Autonomous Trucks

Asphalt pavement performance was predicted in this analysis for four types of loading distribution patterns. These distributions are loading distribution with zero wander, normal distribution with a standard deviation of 7.5 cm (3") and 25.0 cm (10"), and uniform distribution. These distributions were designated as W0, W3, W10, and WU respectively. Default loading distribution with 25 cm (10") standard deviation incorporated in MEPDG is regarded as baseline distribution. Zero wander demonstrates fully autonomous vehicles for analysis. Field observation by Zhou et al. (Zhou et al., 2019) obtained AT loading distribution as normally distributed with standard deviation ranging from 3.0 cm (1.2") to 7.5 cm (3.0"). Few researchers (Noorvand et al., 2017; Zhou et al., 2019) suggested uniform distribution of traffic load to reduce the effects of ATs on pavement distresses. The fatigue and rutting being key distresses, influenced by vehicle distribution, are implemented in this study for EFs evaluation separately. To instrument these distributions in AASHTOware, equivalency factors of ATs for different distributions were evaluated compared to baseline distribution. Application of load equivalency factor is a very common practice in the field of pavement design. Kawa et al. described LEF for vehicle loading, the number of load repetitions and so on (Kawa et al., 1998). This study incorporates LEF for the number of load repetitions following Equation 3.3.

$$LEF = \frac{N_{18}}{N_L} \quad 3.3$$

Where,

N_{18} = Number of load repetition of standard axle load at specific pavement distress

N_L = Number of load repetition of any load at specific pavement distress

Equivalency factors were evaluated by the application of multilayered elastic theory for the studied road section. A standard single axle load (80 kN or 18000 lb) was applied for these analyses. Vertical compressive strain at the middle point of every sublayer and tensile strain at bottom of the AC layer for different horizontal locations were obtained from MLET. Horizontal positions and sub layering of the AC layers were implemented following the MEPDG guide. The middle points of sub-layers within AC layer were 0.25 in. (0.625 cm), 0.75 in. (1.25 cm), 1.5 in. (3.75 cm), 2.5 in. (6.25 cm), 3.5 in. (8.75 cm) and 5.3 in. (13.25 cm). Tensile strain at bottom of the AC layer and compressive strain at the middle of the sixth sub-layer for single load repetition are presented in Figure 3.3.

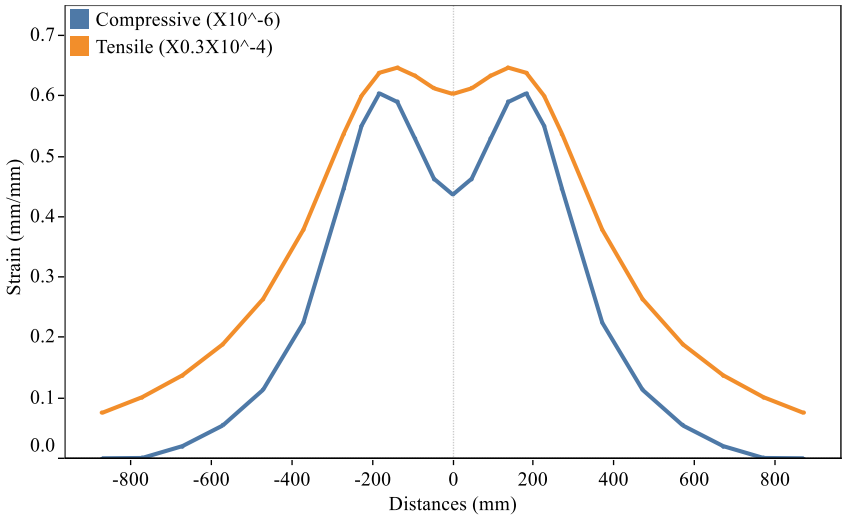

Figure 3.3 Tensile strain at bottom of AC layer and compressive strain at middle of sixth sublayer

The compressive strain and tensile strain presented in Figure 2 represents the strain distribution for zero wander. Estimated horizontal and vertical strain were used in transfer functions of mechanistic-empirical pavement design to obtain fatigue damage and permanent plastic strain in each sub-layer of AC layer. The obtained fatigue and rutting values represent distress for zero wander case. Fatigue damage evaluation, described in the MEPDG approach, was applied to obtain fatigue damage for normal distribution of truck loading with a standard deviation of 7.5 cm and 25.0 cm. This approach evaluated fatigue damage for truck positioning in five places shown in Figure 2.1. The considerable quintile positions for uniform distribution of autonomous vehicles were 0, ±21.3 cm (8.5 in), and ±42.6 cm (17.0 in), covering the whole width of the lane (Chen et al., 2020; Noorvand et al., 2017). It is noticed that maximum fatigue damage occurs under wheel load for zero and 7.5 cm standard distribution of loading and at the middle point of two-wheel loads for baseline and uniform distribution. Fatigue damage of different loading distribution concerning the different number of load repetitions is presented in Figure 3.4.

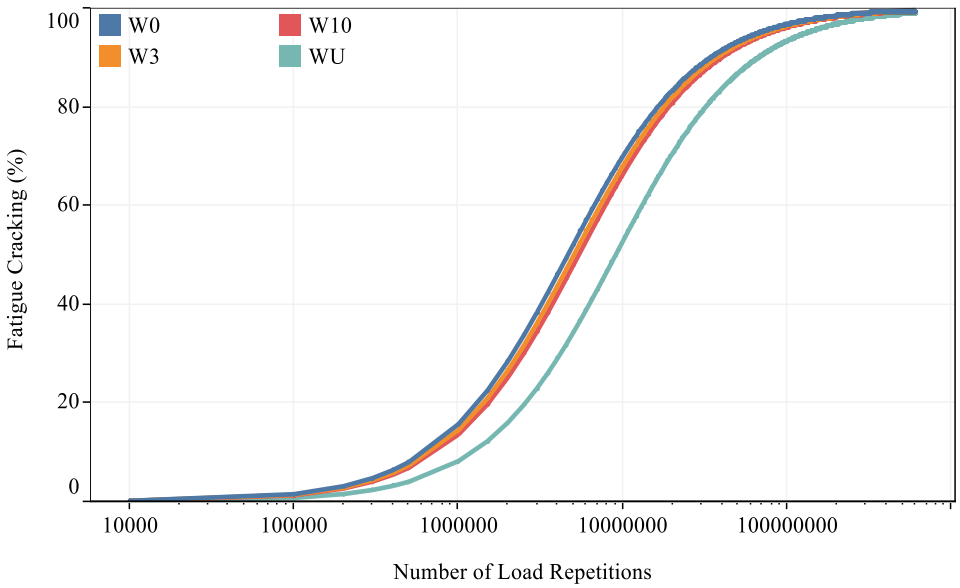

Figure 3.4 Fatigue cracking for different loading distribution pattern

From fatigue cracking of asphalt pavement, the number of load repetitions at 20% fatigue cracking are evaluated for W0, W3, W10, and WU cases. Equivalency factors for ATs are determined from Equation 3.3, comparing to baseline distribution, W10. The obtained EF for truck traffic are 1.17, 1.07, and 0.80 for W0, W3, and WU, respectively.

Erlingsson determined rutting in AC pavement from induced permanent plastic strain for different loading distribution pattern, expressed as normal distribution with different standard deviation. The following equation was developed by the author (Erlingsson, 2012).

$$R_D(N) = \int f(y)\left[\sum_{i=1}^{n}\sum_{j=1}^{m}\varepsilon_p(y,N).\Delta z_{ij}\right]dy \qquad 3.4$$

Where,

ε_p= accumulated plastic strain at wander location y

$f(y)$=frequency of applied traffic load at y

Δz= thickness of sublayer

i = number of layers

j = number of sublayers in each layer

AC rutting was determined for W3, W10, and WU for placement of a group of load on five locations. For the WU case, group load was applied at five quintiles of uniform distribution. AC rutting for all the cases is presented in Figure 3.5.

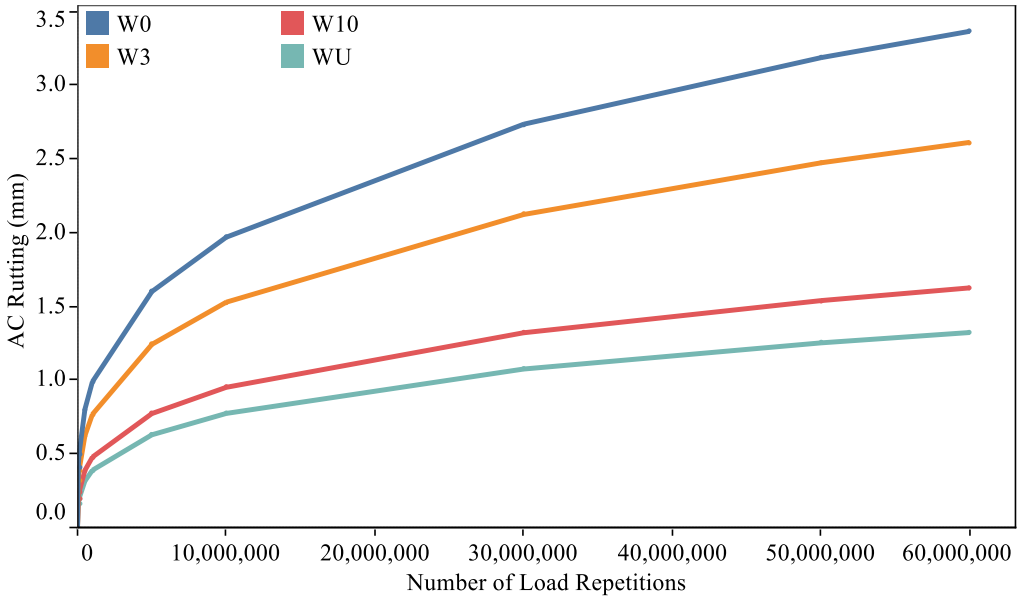

Figure 3.5 AC rutting for a different distribution of loading

LEFs for rutting was determined from Equation 3 to observe the effect of the same load in different loading distribution. LEFs of rutting are 2.3, 2.1, and 0.60 for W0, W3, and WU, respectively concerning W10. LEFs from fatigue and AC rutting was used in traffic volume adjustment.

3.5.3 Traffic Volume Adjustment

The autonomous truck is now in the implementation stage. Commercial usage is not started yet. It is not a feasible plan to provide a dedicated road section for AT in present or near future. The current analysis investigates the performance of AC pavement for three scenarios based on the dedicated lane for AT and sharing the same lane by AT and NAT. Three scenarios were- Baseline, Separated, and Integrated scenario. The scenario when only NAT will move on the road section will be regarded as the baseline scenario. Separated scenario (SS) will refer to observed pavement distresses in case of placing ATs in a dedicated lane. An integrated scenario (IS) will refer to the scenarios when a single lane of a road section is shared by AT and NATs. The integrated scenario was divided into two types based on distribution pattern- equally distributed (ED) and disproportionately distributed (DD) over lanes. AT was considered as equally distributed over two lanes in a distributed scenario. The non-distributed scenario demonstrated the disproportional distribution of AT with NAT in one lane. AADTT input was modified to incorporate the mentioned scenarios in ME pavement design. AADTT input was adjusted for SS scenario with the following Equations 3.6 and 3.7 for autonomous and non-autonomous vehicles. The same LD rules of (100%) were applied to calculate adjusted traffic volume for both cases. Design traffic volume in a road section is estimated using Equation 3.5. This estimation is based on the lane and directional distribution factors.

$$AADTT_D = AADTT_{input} \times DD \times LD \quad 3.5$$

Where,

$AADTT_D$= Annual average truck traffic used in pavement design

$AADTT_{input}$= Two-way annual average daily truck traffic

DD=Directional distribution factor usually ranges from 0.5 to 0.6.

LD= Lane distribution factor

Lane distribution factor is used as a criterion to position vehicles in a road section. Asphalt pavement performance is greatly influenced by the positioning of vehicles. MEPDG recommended values of lane distribution factor (LD) for a single lane, two-lane and three-lane roadways per direction are 1.00, 0.90, and 0.60, respectively (ARA Inc., 2004b). Load equivalency and lane distribution factors are the key components in evaluating adjusted AADTT. Adjusted AADTT values of these scenarios were implemented for the three lanes road section by the researcher (Noorvand et al., 2017). A similar concept was modified for a two-lane road in this analysis. AADTT input was adjusted for SS scenario with the following Equations 3.6 and 3.7 for autonomous and non-autonomous vehicles. The same LD rules of (100%) were applied to calculate adjusted traffic volume.

$$(AADTT_{adjusted})_{AT-S} = AADTT_{input} \times P_{AT} \times LEF \quad 3.6$$

$$(AADTT_{adjusted})_{NAT-S} = AADTT_{input} \times P_{NAT} \quad 3.7$$

Where,

P_{AT}= Percentage of autonomous truck

P_{NAT}= Percentage of non-autonomous truck

LEF= Load-equivalency factors for different distribution

As both AT and NAT distributed over the lane, a single AADTTT value was used as input for distributed and non-distributed scenarios. Both scenarios were devised using Equation 3.8.

$$(AADTT_{adjusted})_{\frac{ED}{DD}} = (AADTT_{adjusted})_{NAT} + \frac{LD_{AT}}{LD_{NAT}} \times \ AADTT_{input} \times P_{AT} \times LEF \quad 3.8$$

Where,

LD_{AT}=Lane distribution factors of autonomous truck

LD_{NAT}= Lane distribution factors of non-autonomous vehicle

In the case of disproportionately arranged AT, LEF values for AT and NAT were considered as 0.90 for both conditions. In a distributed scenario, AT was distributed equally over two lanes using LDF value as 0.5 for AT.

3.5.4 Performance Prediction and Comparison

The widely accepted Pavement ME software, AASHTOWare, was used for predicting the pavement performance for baseline, separated, and integrated scenarios with different loading distribution patterns. The traffic details including adjusted traffic, material properties, structural design, and climate data, collected from different sources, were given as input in MEPDG. Material properties, structural design, and climate data were kept constant to evaluate the effect of AT's implementation on the AC pavement performance. Pavement performance data for separated and integrated scenarios with different loading distributions patterns were compared with the baseline scenario. Performance of different loading distribution was compared with each other within each scenario. AC rutting and BU cracking values were compared between DD and ED. The aim of comparing

performance was to select the optimized scenario with specific loading distribution for the implementation of ATs.

3.6 Results and Discussion

Three scenarios were considered in this analysis for attaining optimized pavement distresses for the movement of autonomous trucks in the two-lane road section. The scenarios were- baseline, separated, and integrated scenario. These scenarios were characterized based on traffic distribution on lanes of the road section. Based on the nature of the traffic distribution pattern, the integrated scenario was divided into two categories- equally distributed and disproportionately distributed. All of the scenarios were simulated for four different loading distributions patterns for fatigue and rutting separately. These loading distribution patterns were- zero wander, normal distribution with a standard deviation of 7.5 cm (3.0") and 25 cm (10.0"), and uniform distribution. Simulations of fatigue criteria explored in this analysis are presented in Table 3.1 with nomenclature. Simulations were designated by purpose to short the name for explaining efficiently in the next sections. The first letter of the designated name indicates scenario, the second one for distress, and the last portion for loading distribution. A similar pattern of designation has been used for rutting in the description of the performance data.

Table 3.1 Nomenclature of the scenarios for fatigue distress used in the analysis

Scenario	Distress	Loading Distribution	Designation
Baseline	Fatigue/AC Rutting	Normal distribution with 25 cm standard deviation (W10)	Baseline
Separated	Fatigue	Zero wander (W0)	SFW0
		Normal distribution with 7.5 cm standard deviation (W3)	SFW3
		Uniform distribution (WU)	SFWU
Equally distributed	Fatigue	Zero wander (W0)	EFW0
		Normal distribution with 7.5 cm standard deviation (W3)	EFW3
		Uniform distribution (WU)	EFWU
Disproport-ionately distributed	Fatigue	Zero wander (W0)	DFW0
		Normal distribution with 7.5 cm standard deviation (W3)	DFW3
		Uniform distribution (WU)	DFWU

3.6.1 Adjusted Traffic Volume

Traffic volume was adjusted for separated and integrated scenarios from the baseline traffic volume. This adjustment was made based on EFs, obtained from the calculation, and lane distribution factors. Traffic volume was adjusted for load-related key distresses fatigue and cracking individually. The number of simulations for fatigue distress was counted to be as 12 presented in Table 3.1. Presented data showed four simulations for each of SS, ED, and DD scenario. The same number of simulations were fabricated for AC rutting also. Baseline traffic volume considered to be as 2000 was adjusted for 24 simulations in this study. Scenarios were simulated for ATs ranging from 0% to 100%, having a 10% interval.

The evaluated traffic volume for all scenarios is presented in Figure 3.6. The figure represented simulations of separated scenarios as SFW0, SFW3, SFWU, SRW0, SRW3, and SRWU. AT and NAT move on the separated lane in those scenarios. LDF was used as 1.0 for AT and NAT in separated scenario (ARA Inc., 2004b). AADTT for AT and NAT was adjusted using Equation 3.5, and Equation 3.6, respectively for the SS scenario. At 0% AT, truck volume for baseline and separated scenarios is found as 0 for all simulations. When the lane is fully occupied by AT, AADTT reaches a maximum of 4600 for SRW0. AT and NAT share two lanes in integrated scenarios. Single AADTT is inputted for various simulations of ED and DD scenarios. In the figure, 10% AT indicates that 10% AT shares lanes of the road section with 90% NAT. The same LDF 0.90 was used for AT and NAT in the DD scenario. PDF for equally distributed AT was considered as 0.50. Equation 3.8 was used for the calculation of adjusted traffic for both integrated scenarios with different LDF. Traffic volume for both integrated scenarios is 2000 at initial condition, regarded as the baseline value. AADTT for DRW0 and DRW3 reaches about 4600 and 4300, respectively at the fully autonomous condition. When AT is ensured to distribute equally, AADTT decreases from 10% AT and reaches a minimum at 100% AT. Noorvand et al. also observed a similar trend of truck traffic volume (Noorvand et al., 2017). Traffic volume for uniform loading distribution is found to be lowest in both scenarios.

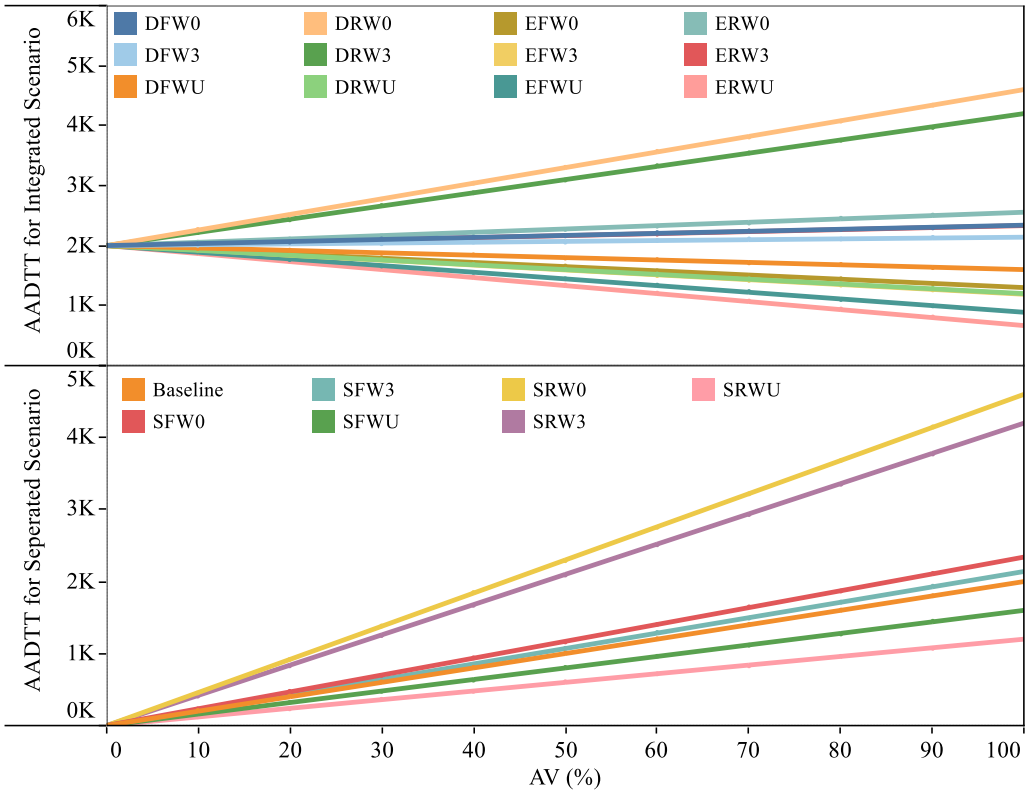

Figure 3.6 Adjusted AADTT for all simulations

3.6.2 Pavement Performance

The robust Pavement ME design software, AASHTOWare, requires fundamental input regarding the pavement section to predict the performance. In this study, the analysis period was considered as 20 years for the studied road section. The limiting value for terminal IRI, total rutting, AC rutting, BU fatigue cracking, and TD fatigue cracking were 2.7 (m/km) (172 in/mile), 18.75 (mm) (0.75 inch), 6.25 mm (0.25 inch), 25 (% lane area), and 380 (m/km) (2000 ft/mile), respectively. The distress data were targeted with a reliability of 90%. Material properties and structural design data of the section, significant for performance prediction, was collected from the LTPP database. Climate input of

AASHTOWare consists of hourly temperature, wind speed, percent sunshine, precipitation, and relative humidity. Climate data for the analyzed section was selected from the AASHTOWare database for the co-ordinates of that section.

The pavement section was analyzed with constant material properties, structural design data, climate data and traffic details, except traffic volume and lane distribution factors, for all simulations of baseline, separated, and integrated scenarios. Pavement distresses of separated scenarios for SFW0, SFW3, SFWU, SRW0, SRW3, and SRWU simulations were compared with the baseline scenario for different percentages of traffic volume. In this study, bottom-up (BU) fatigue cracking, and AC rutting was taken into consideration for pavement distresses. A comparison of BU cracking and AC rutting between baseline and separated scenarios are presented in Figure 3.7-3.8.

Predicted AC rutting of the baseline scenario and separated scenario for different simulations of AT at the end of the pavement life is illustrated in Figure 3.7. The AC rutting for all simulations is gradually increasing with the increment of AT. Based on induced AC rutting, the simulations can be presented from highest to lowest order as: SRW0>SRW3>SFW0>SFW3>SFWU>SRWU. AC rutting of NAT or baseline scenario is presented in reverse order to obtain an equivalent percentage of AT to NAT. At equal rutting point, NAT:AT for SRW0, SRW3, SRWU, SFW0, SFW3 and SFWU is 70%:30%, 67%:35%, 36%:64%, 54%:46%, 52%:48%, and 44%:56% respectively. AC rutting at equivalent point of SRW0, SRW3, SRWU, SFW0, SFW3 and SFWU is 1.52 (mm), 1.50 (mm), 1.31 (mm), 1.44 (mm), 1.42 (mm), and 1.36 (mm) respectively. Simulations from

both EFs showed that the provision of uniform distribution of AT might provide significant improvement in AC rutting.

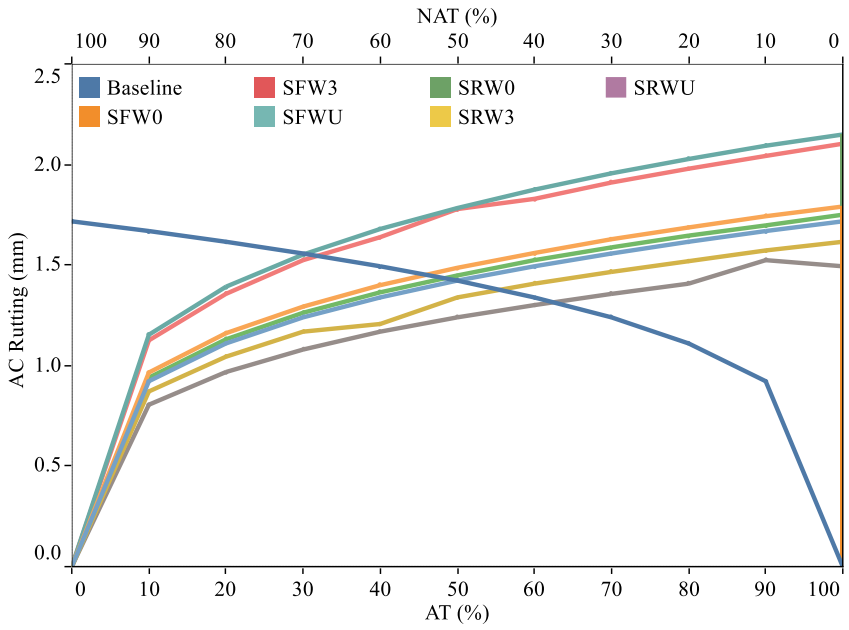

Figure 3.7 AC rutting of baseline and separated scenarios for different simulations

The representation of Figure 3.8 shows the BU cracking of baseline and separated scenarios for different simulations of AT at the end of the pavement life. A significant increase in fatigue cracking is observed for SRW0 and SRW3 from 20% AT. The highest to the lowest order of BU cracking is similar to AC rutting. NAT:AT for SRW0, SRW3, SRWU, SFW0, SFW3 and SFWU is 70%:30%, 66%:34%, 37%:63%, 55%:45%, 51%:49%, and 56%:44% respectively. BU cracking at equivalent point of SRW0, SRW3, SRWU, SFW0, SFW3 and SFWU is found to be as about14.0%, 12.5%, 2.0%, 5.0%, 3.8%, and 3.0%, respectively. From the observation of AC rutting and BU cracking, it can be concluded that explicit control of autonomous vehicle moving on the road, to ensure uniform distribution, could significantly improve the pavement performance. It is also

noticeable that the incorporation of field wander might allow a certain additional percentage of AT movement at specific pavement distresses.

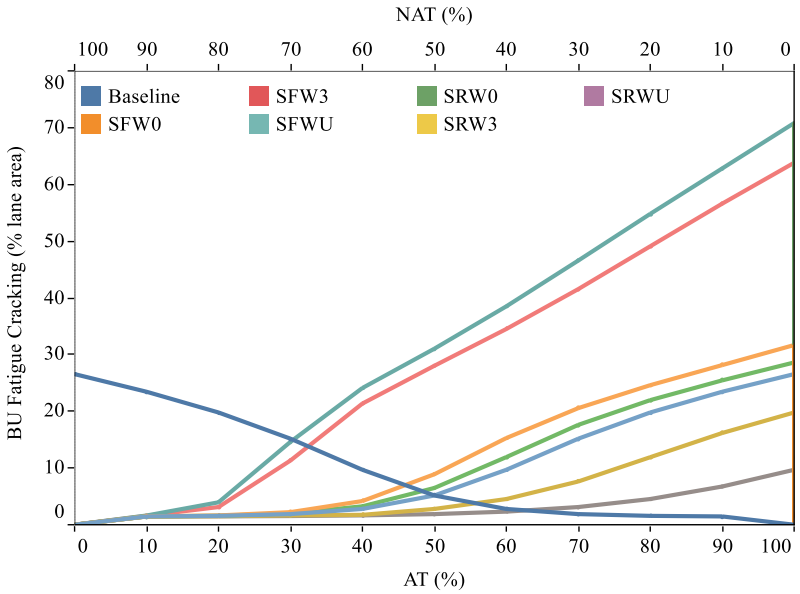

Figure 3.8 BU cracking of baseline and separated scenarios for different simulations

Figure 3.9 demonstrates the AC rutting of the disproportionately distributed scenario for different simulations of AT at the end of the pavement life. It is observed that AC rutting increases with an increased percentage of AT for DRW0, DRW3, DFW0, and DFW3. Simulations, DRWU and DFWU, accounted for uniform distribution of AT exhibited lower rutting from partial to full engagement of autonomous vehicles.

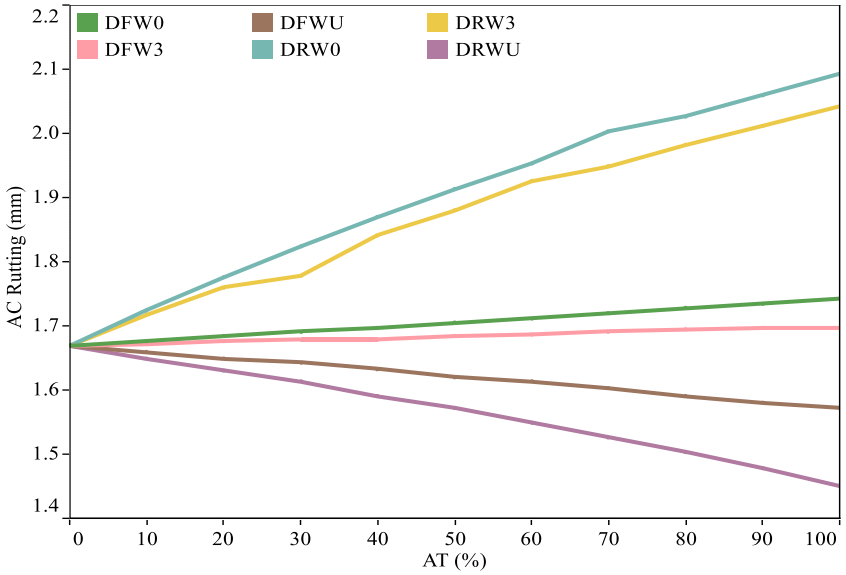

Figure 3.9 AC rutting of the disproportionately distributed scenario for different simulations

Predicted BU cracking of AC pavement of disproportionately distributed scenarios for different simulations of ATs at the end of the pavement life is illustrated in Figure 3.10. Simulations of AT for both AC rutting and BU cracking distresses showed deterioration of pavement for cracking in the case of W0 and W3 wandering. The predicted maximum and minimum BU cracking are found to be as 62.0% and 8.0% for DRW0 and DRWU simulations, respectively.

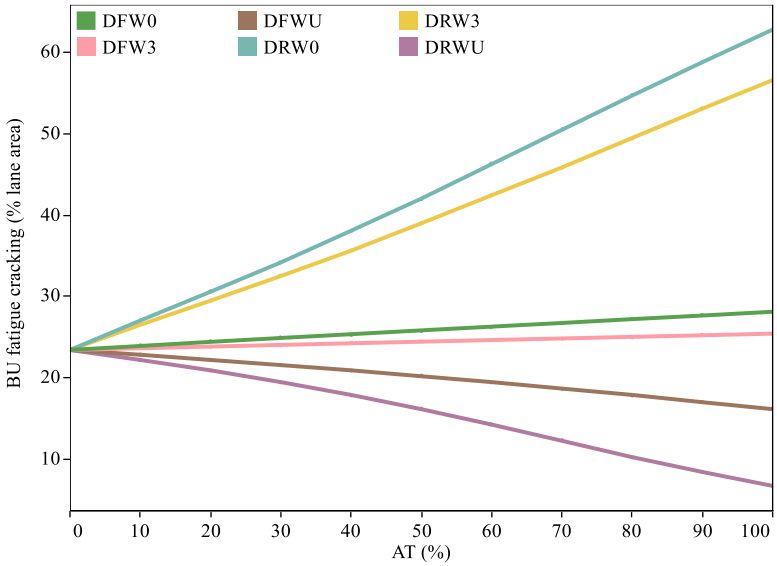

Figure 3.10 BU cracking of disproportionately distributed scenario for different simulations

Figure 3.11 demonstrates AC rutting of the equally distributed scenario for different simulations of AT at the end of design life. The obtained data exhibited a significant reduction in pavement distresses for equal distribution of AT in a lane. A comparison of predicted AC rutting concerning baseline value indicated minimal increment for ERW0 and ERW3. AC rutting significantly reduced for EFW0, EFW3, EFWU and ERWU. AC rutting for uniform distribution of loading, simulated by EFWU and EFRU, is noticed to be decreased to 1.32 (mm) and 1.23 (mm), respectively.

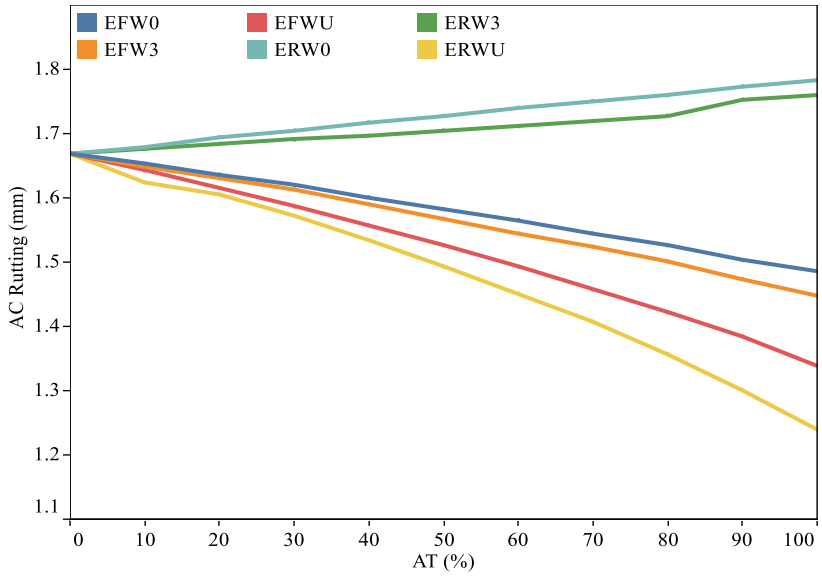

Figure 3.11 AC rutting of an equally distributed scenario for different simulations

Predicted BU cracking of AC pavement of equally distributed scenario, for different simulations of ATs, at the end of the pavement life is illustrated in Figure 3.12. BU cracking changes from 24.0% to 27.0% and 31.0% for ERW0 and ERW3, respectively. The BU cracking reduces from 24.0% to 3.0% and 4.0% for ERWU and EFWU, respectively.

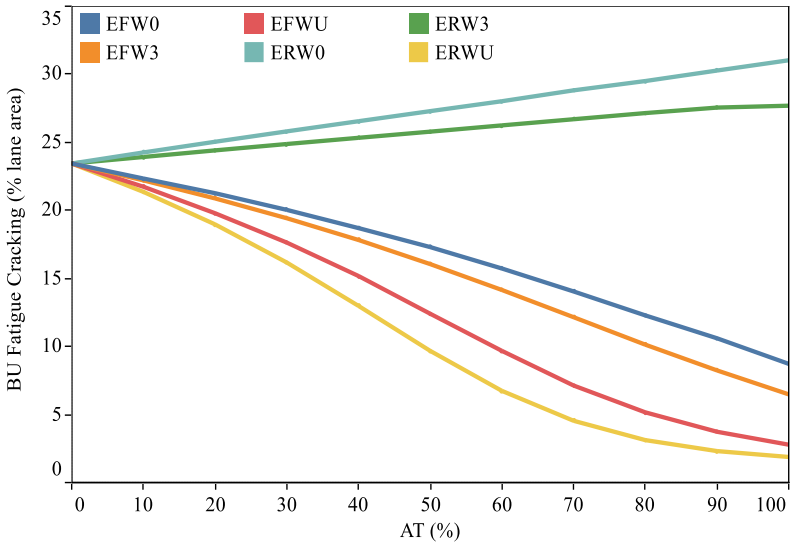

Figure 3.12 BU cracking of equally distributed scenario for different simulations

Percentage change in AC pavement distresses for different AT distribution pattern compared to zero wander are represented in Figure 3.13. Percentage change in AC rutting and BU cracking of AC pavement for both DD and ED scenarios. The percentage change in distresses of different simulations was evaluated comparing to zero wander. Significant improvement in AC rutting and BU cracking is observed for every simulation of W3 and WU. The maximum reduction of AC rutting and BU cracking for uniform distribution of ATs is found to be 30.7% and 93.9% for DRWU and ERWU. For the W3 pattern of AT distribution, the maximum change in AC rutting and BU cracking is observed for DFW3 and ERW3. The percentage change in AC rutting and BU cracking for DFW3 and ERW3 is 2.62% and 10.8% respectively. The introduction of uniform distribution of AT improves the pavement performance significantly for both ED and DD scenarios. There is the pavement improvement distresses for normal distribution with 7.5 (cm) standard deviation of AT. AADTT input in this study is not significant to induce AC rutting. Change in AC

rutting for every scenario and loading distribution pattern changes insignificantly. The high strength of material properties might provide significant resistance to AC rutting.

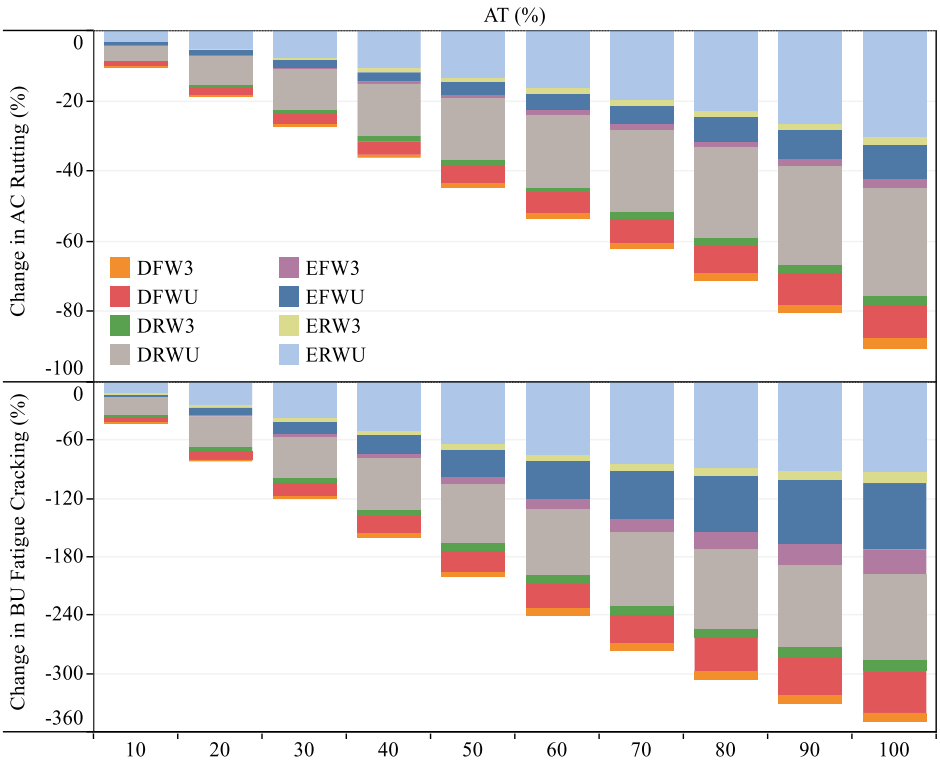

Figure 3.13 Change in pavement distresses for different wanders compared to zero wander

AC rutting and BU cracking of AC pavement for ED scenarios are compared with the DD scenario for different simulations of ATs percentage change in distresses are illustrated in Figure 3.14. The changes are evaluated for 10% to 100% of AT, shared lane with NAT in the road section. The highest improvement in AC rutting and BU cracking is noticed at 100% of AT. The change in AC rutting at the end of design life for the implementation of fully AT is found to vary from 13.8% to 14.9%. The simulation, EFWU, experienced a maximum reduction in AC rutting compared to DD scenario. Improvement

of fatigue distress was also observed for ED scenario. Predicted data showed a maximum reduction, 82%, for EFWU compared to DD scenario. It is noticeable that the movement of zero wander AT with ED scenario significantly reduced AC rutting and BU cracking by 14.7% and 69.0%. It can be summarized as explicit control of AT on the road section to distribute equally in lane might be beneficial for performance improvement in AC pavement.

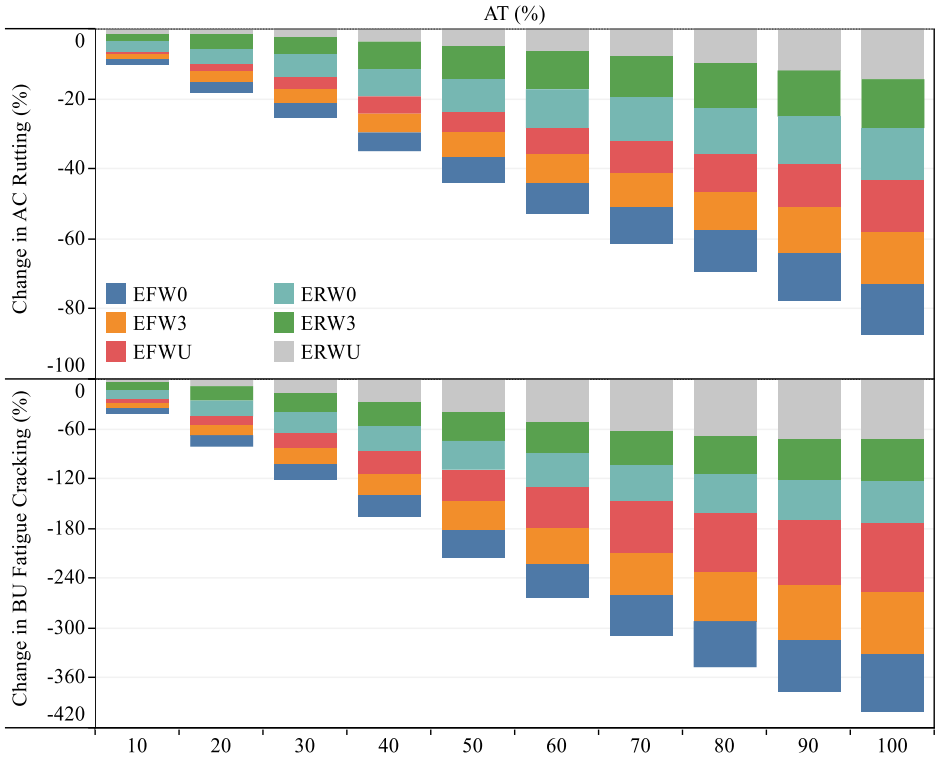

Figure 3.14 Comparing pavement distresses between two integrated scenarios

3.7 Scheduling Vehicle Movement Duration

The resilient modulus of asphalt material varies with pavement temperature and significantly affect the asphalt pavement performance. Resilient modulus is the critical variable in asphalt pavement design, increases at low temperatures (Gao et al., 2019; Zhao et al., 2020b). An attempt has been made in this study to minimize the effects of autonomous vehicles by scheduling vehicle movement in a period of the low temperature of the day. Figure 3.15 represents the hourly temperature variation of the studied road section area and the hourly distribution of traffic. Hourly temperature variation was shown for a single day of February, July, and November, selected from three different seasons. Temperature variation showed significantly reduced value from 11 AM to 7 AM of a day. At the same duration of the day, traffic flow is in the minimal stage. Fully autonomous trucks will be moving without the assistance of the driver, especially for the shipment of goods. There is no possibility of mental stress for movement at night time. So, allowing AT to move on low-temperature duration might be beneficial for the pavement performance perspectives.

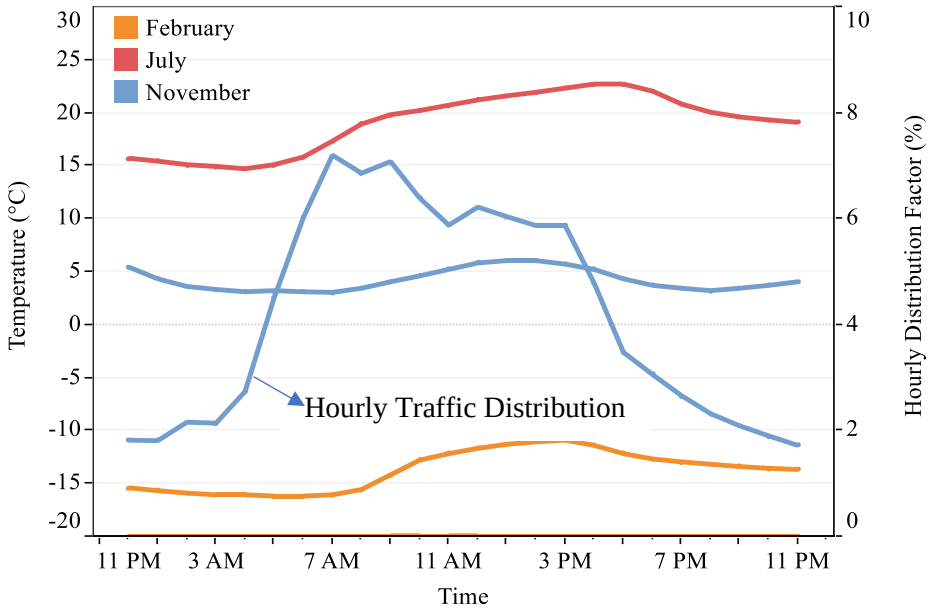

Figure 3.15 Hourly temperature variation of a day and hourly distribution factor of traffic

To simulate AT in low-temperature duration in this study, climate input in AASHTOWare was modified. The whole day was segmented into three parts of 8 hours. The temperature of 8-hour duration from 11 AM to 7 AM was replaced with the other two parts for each day. This change was made for two simulations. These simulations were DFW3 (60%AT+40%NAT) from the integrated scenario and SRW0 (100% AT) from the separated scenario. Percentage change in AC rutting and BU cracking for modifying climate input is presented in Figure 3.16. It was observed that the percentage decrease in AC rutting for the integrated and separated scenario was found to be 23.9% and 23.8%, respectively. The predicted BU cracking was significantly reduced by 30.7% and 24.1% for integrated and separated scenarios, respectively.

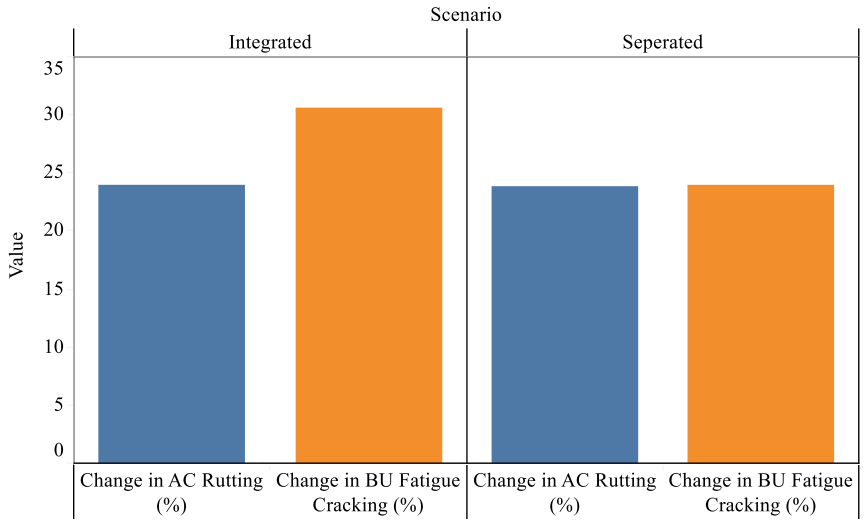

Figure 3.16 Change in pavement distress for scheduling vehicle movement duration

3.8 Concluding Remarks

This current study focuses on simulations of autonomous trucks (AT) to predict asphalt pavement distresses and select the best suitable simulation based on optimized distresses. Simulations were fabricated based on loading distribution patterns and traffic distribution on lanes of the road section. Based on traffic distribution, baseline, separated and integrated scenarios were considered in this study. The baseline scenario is designated for the movement of non-autonomous trucks (NAT). Separated scenario assigns a dedicated lane for AT and NAT separately on the pavement section. In the case of an integrated scenario, both AT and NAT share the same lane of a road. When an integrated scenario distributes AT equally on a lane of the road section is termed as equally distributed (ED) scenario and disproportionately distributed AT is known as disproportionately distributed (DD) scenario. Every traffic distribution scenario was simulated for different loading distribution patterns. These loading patterns were- zero wander, normal distribution of truck loading

with a standard deviation of 7.5 (cm) (3"), and 25.0 (cm)(10") and uniform distribution of loading. These distributions were named as W0, W3, W10, and WU. Loading pattern, W10 is incorporated in MEPDG and is considered as a baseline for all analyses in this study.

All the simulations were devised to input on Astaire by equivalency factors (EF). EF of AT was evaluated using a multi-layered elastic theory. Fatigue and rutting were evaluated for different numbers of load repetition from tensile and compressive strain obtained from multi-layered elastic theory. EF was calculated for W0, W3, and WU compared to the baseline loading pattern for the same fatigue and AC rutting. Fatigue and AC rutting, being key distresses induced from AT, EFs were estimated individually for both distresses. The number of simulations was replicated as 24 for different scenarios combined with loading distribution patterns. Traffic volume was adjusted using EFs and lane distribution factors for all the simulations. Material properties, structural design, and climate input was kept constant for prediction of pavement performance for 24 simulations. Also, the pavement section was simulated by scheduling AT in a low-temperature period of all the days of the analysis period. The predicted distresses are compared between traffic distribution scenarios and loading distribution patterns. The conclusions drawn from the comparative pavement distresses are as presented below.

- Comparison of AC rutting and BU fatigue cracking between baseline and separated scenarios showed the ratio NAT:AT to be as 36.0%:64.0% at the same distress. It is also noticeable that the incorporation of W3 wander at separated scenarios might allow a certain additional percentage of AT movement at specific pavement distresses.

- The studied section had lower traffic volume with high strength of AC materials. This might be the cause of an insignificant change in AC rutting for every traffic scenario and loading distribution pattern.
- The introduction of uniform distribution of AT improves the pavement performance significantly compared to zero wanders. Reduction of AC rutting and BU fatigue cracking, for uniform distribution of ATs is found to be by 30.7%, and 93.9%, respectively. The percentage change in AC rutting and BU cracking for W3 loading distribution is 2.62%, and 10.8%, respectively. The major limitation of the uniform distribution of loading is covering the whole width of the lane.
- A comparative study of AC rutting and BU fatigue cracking is performed between ED and DD scenarios. It is noticeable that the movement of zero wander AT with ED scenario significantly reduced AC rutting and BU cracking by 14.7%, and 69.0%., respectively.
- Significant improvement in pavement distresses is found to occur for controlling the movement of AT at the low-temperature period of each day. This control reduces AC rutting of the integrated and segregated scenario by 23.9% and 23.8%, respectively. BU cracking was significantly minimized by 30.7% and 24.1% for integrated, and separated scenarios, respectively.
- Explicit control of AT to specific loading pattern or distribution or low-temperature period might bring remarkable minimization of the detrimental effects of AT on the pavement section.

3.9 References

Andersson, P., & Ivehammar, P. (2019). Benefits and costs of autonomous trucks and cars. *Journal of Transportation Technologies*, *09*(02), 121–145.

ARA, Inc. (2004). Guide for mechanistic–empirical design of new and rehabilitated pavement structures. Final Rep., NCHRP Project 1-37A.

Buiter, R., Cortenraad, W. M. H., van Eck, A. C., & van Rij, H. (1989). Effects of transverse distribution of heavy vehicles on thickness design of full-depth asphalt pavements. *Transportation Research Record*, *1227*, 66–74.

Chen, F., Song, M., & Ma, X. (2020). A lateral control scheme of autonomous vehicles considering pavement sustainability. *Journal of Cleaner Production*, *256*, 120669. https://doi.org/10.1016/j.jclepro.2020.120669.

Chen, F., Song, M., Ma, X., & Zhu, X. (2019). Assess the impacts of different autonomous trucks' lateral control modes on asphalt pavement performance. *Transportation Research Part C: Emerging Technologies*, *103*(March), 17–29.

Donelson, B. (2020). *Coronavirus response: Real-World case for expanded autonomous vehicles testing in the U.S.* JDSupra. https://www.jdsupra.com/legalnews/-coronavirus-response-real-world-case-56295/.

Erlingsson, S. (2012). Rutting development in a flexible pavement structure. *Road Materials and Pavement Design*, *13*(2), 218–234.

Fee, G. (2020). Preparing for autonomous vehicles. *Asphalt Magazine*.

http://asphaltmagazine.com/autonomous-vehicles/.

Gao, L., Hong, F., & Ren, Y. H. (2019). Impacts of seasonal and annual weather variations on network-level pavement performance. *Infrastructures*, *4*(2), 1–13.

Gungor, O. E. (2018). *Final report: A literature review on wheel wander*. Illinois Asphalt Pavement Association. https://il-asphalt.org/files/2915/1743/1516/Erman_-Gungor_2017_UIUC.

Gungor, O. E., & Al-Qadi, I. L. (2020a). All for one: Centralized optimization of truck platoons to improve roadway infrastructure sustainability. *Transportation Research Part C: Emerging Technologies*, *114*(August 2019), 84–98.

Gungor, O. E., & Al-Qadi, I. L. (2020b). Wander 2D: A flexible pavement design framework for autonomous and connected trucks. *International Journal of Pavement Engineering*, *0*(0), 1–16. https://doi.org/10.1080/10298436.2020.1735636.

Lee, J. (2012). *Model based predictive control for automated lane centering/changing control systems* (US 8,190,330 B2). GM Global Technology Operations LLC, Detroit, MI (US).

Kawa, I., Zhang, Z., & Hudson, W. R. (1998). *Evaluation of the AASHTO 18-Kip Load Equivalency Concept*. Center for Transportation Research, The University of Texas at Austin.

Linder, C. (2019, December 11). Self Driving freight trucks - autonomous trucks. *Popular Mechanics*.https://www.popularmechanics.com/technology/infrastructure/a30196644/self-driving-truck-cross-country/.

Litman, T. (2020). Autonomous vehicle implementation predictions: Implications for transport planning. In *Victoria Transport Policy Institute*. https://doi.org/10.-1613/jair.301.

Ministry of Transport, Ontario. (2019). *Ontario's default parameters for AASHTOWare pavement ME design interim report - 2019.* https://www.library.mto.gov.on.ca/-SydneyPLUS/Sydney/Portal/default.aspx?component=AAAAIY&record=89a3febc-f471-4f73-8f3b-4a5c52068874.

Shafiee, M. H., Nassiri, S., & Bayat, A. (2014). Field investigation of the effect of operational speed and lateral wheel wander on flexible pavement mechanistic responses. *Transportation Associartion of Canada, Montreal-2014.* http://conf.tac-atc.ca/english/annualconference/tac2014/s-20/bayat.pdf.

Noorvand, H., Karnati, G., & Underwood, B. S. (2017). Autonomous vehicles: Assessment of the implications of truck positioning on flexible pavement performance and design. *Transportation Research Record, 2640*, 21–28. https://doi.org/10.3141/2640-03.

Siddharthan, R. V., Nasimifar, M., Tan, X., & Hajj, E. Y. (2017). Investigation of impact of wheel wander on pavement performance. *Road Materials and Pavement Design, 18*(2), 390–407. https://doi.org/10.1080/14680629.2016.1162730.

Steyn, W. J. v. M., & Maina, J. W. (2019). Guidelines for the use of accelerated pavement testing data in autonomous vehicle infrastructure research. *Journal of Traffic and Transportation Engineering (English Edition), 6*(3), 273–281.

The State of the Self-Driving Car Race 2020. (2020, May 15). Bloomberg.

https://www.bloomberg.com/features/2020-self-driving-car-race/.

Wu, R., & Harvey, J. T. (2008, February). Evaluation of the effect of wander on rutting performance in HVS tests. *In Proceedings of the 3rd international conference on accelerated pavement testing*.

Zhao, X., Shen, A., & Ma, B. (2020). Temperature response of asphalt pavement to low temperatures and large temperature differences. *International Journal of Pavement Engineering*, *21*(1), 49–62. https://doi.org/10.1080/10298436.2018.1435883.

Zhou, F., Hu, S., Chrysler, S. T., Kim, Y., Damnjanovic, I., Talebpour, A., & Espejo, A. (2019). Optimization of lateral wandering of automated vehicles to improve traffic safety and pavement life. *Transportation Research Record*, 1–9.

Chapter 4 Impact of Autonomous Trucks' Implementation: Rutting and Highway Safety Perspectives

Md Masud Rana[a]* and Kamal Hossain[b]

[a]Department of Civil Engineering, Memorial University of Newfoundland, St. John's, Newfoundland, CANADA

[b]Department of Civil and Environmental Engineering, Carleton University, Ottawa, CANADA

Abstract

Fast emerging information and communication technology is accelerating the implementation of automation techniques in transportation sectors. Full automation has extended to the truck and public bus sectors. The commercial application of this technology in passenger and freight transport will bring revolutionary positive changes in this sector. Despite having more advantages, automation in trucking technology has some detrimental effects on the performance of asphalt pavement and highway safety. This study focuses on quantifying the impact of the autonomous truck on asphalt concrete pavement rutting and subsequent safety factors. Hydroplaning potential and skid resistance have been investigated as safety factors in this study. Two scenarios – the baseline and autonomous scenarios – were simulated by the standard deviation of normally distributed truck traffic loading. The permanent deformation of the asphalt concrete layer for roads (PEDRO) model was incorporated in this research to predict AC pavement rutting. Asphalt properties

Rana, M., Hossain, K. (2020). Impact of Autonomous Trucks' Implementation: Rutting and Highway Safety Perspectives. Prepared for submission to *Road Materials and Pavement design (RMPD) journal.*

were processed by generating master curves for dynamic shear modulus and phase angle. Then, material properties and climate data were inputted in PEDRO to analyze a typical pavement section for different simulations with a wide range of truck loading conditions. Each truck loading was also analyzed for different variations of autonomous truck speed. The acquired performances clearly showed significant deterioration in asphalt rutting for automation of trucks, and continuous improvement in rutting was observed with increasing truck speed for each automation scenario. The obtained rutting data were implemented to determine the skid resistance and hydroplaning potential of a standard tire. A standard tire rather than a truck tire was considered due to its high susceptibility to traffic safety. Increasing truck speeds for all autonomous simulations reduces hydroplaning risk up to certain critical points. Beyond that critical point, increasing speed contributed to hydroplaning risk through the lowering of hydroplaning speed to risk level. The continuous decrease in rutting and induced hydroplaning potential with vehicle speed becomes contradictory after a certain critical point. A graphical relationship has been proposed to obtain a design threshold value for hydroplaning speed, water film depth and autonomous truck speed. Also, an attempt has been made to decrease pavement rutting by increasing the frequency of hourly traffic in the low-temperature duration of a day. Placing all ATs in a certain period of a day might be beneficial for reducing asphalt pavement rutting and may bring improvement in highway safety issues.

Keywords: Autonomous Trucks, Rutting, Skid Resistance, Hydroplaning Potential, Improvement of Pavement Performance.

Rana, M., Hossain, K. (2020). Impact of Autonomous Trucks' Implementation: Rutting and Highway Safety Perspectives. Prepared for submission to *Road Materials and Pavement design (RMPD) journal.*

4.1 Introduction

In the twenty-first century, Autonomous Vehicles (AV) are among the most exciting and promising developments. The possibility that AVs will turn science fiction into reality. Fast emerging information and communication technology is accelerating the implementation of automation techniques in transportation sectors. It is predicted that AVs will occupy 25% of all miles driven in the U.S. by 2030. Estimation of the Center for Automotive Research estimates that new vehicle sales might increase by up to 55 percent by 2040 (Fee, 2020). The application of automation techniques is not restrained to passenger cars only (Noorvand et al., 2017). The combined efforts of scientists, engineers, and practitioners to increase efficiency in the shipment of people and goods have been working to bring public transit and trucks under automation technology (Andersson & Ivehammar, 2019). The Connecticut Department of Transportation (CTDOT) announced the plan of testing the full-size driverless transit bus by 2021(Wanek-Libman, 2020). In December 2019, an autonomous freight truck made a cross country trip of 2800 miles in California to deliver butter commercially (Linder, 2019).

Researchers found the upcoming autonomous vehicles as beneficial options from road safety, environmental, social and economic perspectives (Litman, 2020). Automated public transport will assure the safe and sustainable mobility of people from one place to another. The implementation of AV will increase highway infrastructure capacity along with other advantages. This is due to the automatic braking configured in AV technologies. This technology will allow the vehicle to reduce the safe distance between vehicles and increase vehicle speed. This increased capacity may further induce an overuse of the

practical roads (Chen et al., 2016; Simko, 2016). Tientrakool et al. estimated the highway capacity for the movement of AV using assisted driving systems. An assisted driving system was incorporated using sensors alone, and a combination of sensors and vehicle-to-vehicle communication technology. Both technologies significantly increased highway capacity (Tientrakool et al., 2011). The study by Shladover et al. estimated the highway capacity for AV by equipping vehicles through adaptive cruise control and cooperative adaptive cruise control systems. Authors found 80% more highway capacity for applying the mentioned systems with increasing speed (Shladover et al., 2012). Lu et al. found that universal use of AVS increased traffic capacity by 16.01%, compared to conventional traffic (Lu et al., 2020). Transportation stakeholders might get benefit more from autonomous trucks (AT) in the freight transportation system from improved operational efficiency in moving goods. This automation will also overcome the shortage of truck drivers (Gungor & Al-Qadi, 2020a).

Despite having many advantages, researchers and practitioners are not in ultimate goals to minimize the infrastructure's problems associated with the implementation of AV technology. Researchers encountered the necessity to change the road markings, lane width, roadway capacity, pavement design and so on for AVs (Litman, 2020). Consequently, pavement engineers and researchers are working on the structural performance of AC pavement to optimize additional distresses induced by AT. The influences of AT on the performance of AC pavement are induced from channelized or less wander traffic loading, reduced inter-vehicle distances and constant speeds and fewer stop/start actions (Steyn & Maina, 2019).

4.2 Autonomous Vehicles and Wheel Wander

At the time of vehicular movement on the road, lateral positioning of the wheel spreads over a wide range of road width. This phenomenon is termed wheel wander. Drivers' habits, wind effects, and mechanical alignments are the influencing factors for wheel wander (Buiter et al., 1989). Another study showed lane width, vehicle width, speed, and rut depth are factors for quantification of the wander (Blab & Litzka, 1995). Wheel wander controls the loading distribution for human-driven vehicles along the cross-section of a road. Researchers found the wheel wander as a significant phenomenon affecting pavement performance. This wander follows a particular distribution, not being restrained to a unique location (Blab & Litzka, 1995; Wu, 2008). Lateral positioning of the wheel for human-driven vehicles follows probabilistic distribution along the cross-section of the lane (Gungor & Al-Qadi, 2020b; Siddharthan et al., 2017).

Researchers performed extensive studies and found the lateral positioning of the wheel to be normally distributed within a lane (ARA Inc., 2004; Wu, 2008). This normal distribution is modeled with zero mean and known standard deviation following Equation 4.1 (Gungor, 2018). Mechanistic-Empirical (ME) pavement design predicts the pavement distresses with a standard deviation of 25 cm (10 inches) and zero mean for the distribution of wheel load on the pavement lane (ARA Inc., 2004). A similar observation is made through the field measurements by Erlingsson et al. (Erlingsson, 2012).

$$f(x) = \frac{1}{\sqrt{2\pi\sigma^2}} e^{-\frac{(x-\mu)^2}{2\sigma^2}} \quad 4.1$$

Where,

μ=mean of wheel wander distribution

σ=standard deviation of wander effect

Wheel wander, a controlling factor of loading distribution in a pavement lane, differentiates between human-driven vehicles from autonomous and semi-autonomous vehicles. AVs and semi-AVs, along with trucks, are instructed to drive along the centerline of a lane through the dynamic control systems (Hills & Lee, 2012). This lane-centering tendency of ATs distributes the wheel load as a single point distribution, resulting in channelized traffic. This type of channelization is also known as zero wander or less wander distribution. Channelized or less wander traffic increases the repetition of the load on a narrower width of the lane (Noorvand et al., 2017).

4.3 Effect of Autonomous Vehicles on Rutting

The structural design of asphalt concrete (AC) pavement is carried out in terms of key distress criteria. These distress criteria are: AC rutting, total rutting, fatigue cracking and IRI. Traffic is one of the main components in the design of AC pavement. Mechanistic empirical (ME) design considers only heavy vehicles as traffic input to predict AC pavement distresses. FWHA signifies class 4-13 as heavy vehicles based on dimension. The range of that vehicle is termed truck traffic. The pilot program of automation of trucks is already started and going to be launched commercially very soon. The channelization of ATs has significant effects on distress criteria due to traffic loading distribution on

narrower width. Researchers conducted several studies to quantify the effects of AT on AC pavement.

Wu and Harvey performed a heavy vehicle simulator at the University of California Pavement Research Center to measure the effect of channelized traffic on AC rutting (Wu, 2008). The same scenario was modeled numerically by the authors. They found 56% reduced rutting under the non-wander condition. Erlingsson et al. measured the lateral positioning of the human-driven wheel using a VTI (The National Road and Transport Research Institute) developed system and found it to be normally distributed with a standard deviation of about 0.25 m. ME and visco-elastic approaches were employed to compare rutting between normal and channelized traffic. They concluded that rutting is about 20% faster rutting for wheel loading distribution with a standard deviation of less than 10 cm (Erlingsson, 2012). Shafiee et al. installed strain gauges and pressure cells on the University of Alberta's Integrated Road Research Facility (IRRF)'s test road to evaluate the effects of wheel wander. Pavement responses were measured for moving trucks. Due to insufficient truck load, this study determined the effect of wander on induced stress instead of strain. This experiment concluded that zero wander can significantly affect pavement responses (Shafiee et al., 2014).

Noorvand et al. investigated the effect of AT on AC pavement and presented a possible solution to nullify the effects of AT. The study concluded that, in order to produce equivalent AC rutting, the ratio of passage of non-AT to AT ranges from 2.1 to 2.3. The authors suggested devising a uniform distribution of truck movements to nullify the effects of AT on AC pavement (Noorvand et al., 2017). Zhou et al. performed field tests to quantify

wheel wandering of AVs. These field tests were performed on the Texas A&M RELLIS campus, which was a World War II base. The results on the other hand demonstrate that AVs could be modeled with normal distribution having narrower lateral wandering than human-driven vehicles. The study concluded three times narrower standard deviation 3.0 (cm) to 7.5 (cm) (1.2" to 3.0") for AV. The narrower wandering of AV significantly shortens pavement fatigue life and increases pavement rutting when compared with human-operated traffic (Zhou et al., 2019). Chen et al. performed a finite element analysis of pavement structure to evaluate the impact of the lateral position of ATs on fatigue and AC rutting. The incorporation of different percentages of AT has a potential influence in deteriorating the AC pavement in terms of fatigue and AC rutting. The authors explored through uniform, double peak Gaussian, and two-section uniform mode of loading distribution to improve AC pavement performance (Chen et al., 2019).

4.4 Skid Resistance and Hydroplaning Potential

Statistics reveal that approximately 20% of road accident occurs in wet weather conditions. Researchers believe that low skid resistance and hydroplaning (also known as aquaplaning) potential are the major cause of these accidents (Chu & Ong, 2015; Ong & Fwa, 2010). Skid resistance prevents vehicle tires from sliding on the surface of pavement in wet weather conditions. Skid resistance decreases with the increment of Water Film Depth (WFD) and increases with wheel load (Ong et al., 2005; Peng et al., 2020). Ong and Fwa observed the significant influence of WFD, tire inflation pressure, truck load, and vehicle speed on the skid resistance of trucks (Ong & Fwa, 2010). Fwa and Chu explained skid

resistance as mechanistic interaction of tires, pavement surface and WFD on the pavement surface.

Rutting on the pavement surface allows rainwater to be ponded on the rutted channel. Accumulated water forms a water film between the wheel of the moving vehicle and the pavement surface. This water film leads to a loss of traction force leading to a loss of control in driving. This phenomenon is known as hydroplaning. Viscous, dynamic, and reverted rubber are three kinds of hydroplaning found in highway pavement. Highway agencies are especially concerned about viscous and dynamic hydroplaning. Viscous hydroplaning originated for the low-speed vehicle with a very thin film of fluid (Gallaway et al., 1979; Mounce & Bartoskewitz, 1993). Researchers focused mainly on dynamic hydroplaning due to its high-risk factor. It happens when hydrodynamic pressure generated from flooded AC pavement destroys the balance between the total downward force of the tires and the bearing capacity of the pavement. Under the imbalanced condition, the vehicle at critical speed becomes unstable when the tires completely float on the water. The vehicle in this scenario is said to hydroplane and the critical speed of the vehicle is termed hydroplaning speed (Agrawal & Henry, 1977; Mounce & Bartoskewitz, 1993; Ong & Fwa, 2007; S. Zhu et al., 2017). Hydroplaning speed (HPS) is the measuring factor of hydroplaning potential. Hydroplaned vehicles face reduced traction force between tire and pavement surface. Hydroplaning potential prevents the power of vehicles to control steering, braking and acceleration (Sillem, 2008).

Gallaway et al extensively studied hydroplaning potential and introduced water film depth (WFD) as a crucial factor for HPS (Gallaway et al., 1979). Ong and Fwa

simulated hydroplaning potential on wet pavement, developing a finite volume model. Computational fluid dynamics was used in the simulation to estimate the effect of micro-texture and tire pressure on hydroplaning potential. It was observed that materials with good micro-texture might reduce HPS significantly (Ong et al., 2005). Chu et al. found the WFD, tire properties and pavement surface properties to be influencing factors for hydroplaning speed. The authors conducted a finite element analysis to evaluate the hydroplaning potential of rutted pavement. The analysis was performed at hydroplaning speed and revealed that rutted AC pavement significantly influences hydroplaning potential (Chu et al., 2015). Zhu et al. also showed that thicker WFD accelerates HPS on AC pavement (Zhu et al., 2017). Most of the researchers evaluated HPS based on the assumed rut depth (Chu et al., 2015; Chu & Fwa, 2016; Chu & Ong, 2015; Ong & Fwa, 2006, 2010; Peng et al., 2020). Rutting developed due to the movement of the vehicle might be a crucial factor in a road accident under wet weather conditions. The implementation of AT will significantly increase rutting in AC pavement. An increment of rutting might lead the vehicle to hydroplane and tend to low skid resistance. This will contradict with AV implementation in the reduction of road accidents.

4.5 Permanent Deformation of Asphalt Concrete Layer for Roads (PEDRO)

The permanent deformation of the asphalt concrete layer for roads (PEDRO) model is a linear viscoelastic program used to evaluate the rutting of AC layers. Said et al. first introduced a linear viscoelastic model based on the shear box test and developed the PEDRO model (Said et al., 2011, 2013). The analytical approach to shear distortion enables a linear viscoelastic model to predict upheaval and depression in the wheel moving path

and this is the main advantage. The PEDRO model predicts permanent deformation in AC pavement due to volume change and shear flow in AC mixtures (Jelagin et al., 2018). This model predicts vertical permanent strain due to the movement of traffic using Equation 4.2, as presented by Björklund (Ahmed et al., 2012; Andersson, 2017; Said et al., 2020).

$$\mathcal{E}_p = \frac{\sigma_0(1-2\upsilon)}{V\eta_p} R_e\left[\sqrt{(z+ix)^2+a^2} - (z+ix)\right] + \frac{\sigma_0 z}{V\eta_p} R_e\left[1 - \frac{z+ix}{(z+ix)^2+a^2}\right] \quad 4.2$$

Where,

$\mathcal{E}_p$= permanent vertical strain (m/m)

σ_0= contact pressure (Pa)

υ= Poisson's ratio

V= vehicle speed (m/s)

η_p= viscosity at peak phase angle (Pa s)

z= depth from road surface (m)

x= distance from loading center (m)

a= radius of contact area (m)

i=$\sqrt{-1}$

The first portion of the presented equation is employed to predict the effect of post-compaction and the last portion estimates shear deformation of AC mixtures (Oscarsson, 2011). The viscosity of AC layers at peak phase angle obtained from the dynamic shear modulus test is the key material input in PEDRO (Jelagin et al., 2018; Said et al., 2020, 2016). The shear modulus (G*) and phase angle (δ) of AC mixtures are used to generate master curves for different temperatures. AC Mixture (G*) at peak phase angle is evaluated

from the master curve and used to assess the viscosity following Equation 4.3. The evaluated viscosities are plotted against temperatures to get the input parameters of PEDRO following the second-degree polynomial and Equation 4.4.

$$\eta^* = \frac{G^*}{\omega} \quad 4.3$$

$$log(\eta^*) = a_1 T^2 + a_2 T + a_3 \quad 4.4$$

Where,

η^*= Complex viscosity (Pa.s)

G^*= Complex shear modulus in Pa

ω = Angular frequency at peak phase angle (rad/s)

PEDRO also predicts the profile of the rutting along the cross-section of the road. The PEDRO program directly considers the effect of traffic speed, rather than loading frequency, on rutting evaluation. The software has another important feature to control the lateral positioning of traffic loading by changing standard deviation values (Jelagin et al., 2018; Said et al., 2011). The inability to integrate a multilayer pavement system is one of the major limitations of the current PEDRO (Said et al., 2020).

4.6 Study Objective and Contribution

The objective of this study is to evaluate the effect of the autonomous trucks on distresses of AC pavement and determine the influence of the induced distresses on traffic safety factors in wet weather conditions. AC rutting was the basis for pavement distresses, and skid number and hydroplaning potential were examined as traffic safety factors. Permanent Deformation of Asphalt Concrete Layer for Roads, PEDRO, was employed to assess the

rutting of AC pavement due to the movement of AT. The program, PEDRO, having special features to incorporate lateral positioning of the vehicle on the lane of a road was engaged in this study in rutting prediction. AT was simulated by different standard deviation values of traffic distribution to estimate rutting on the pavement. Different vehicle speeds for each standard deviation were replicated for rutting prediction. A comparative study was performed with human-driven traffic to observe the effect of AT implementation on predicted rutting of AC pavement. The effect of a wide range of AT was also studied for all simulations. The predicted rutting was made use of to estimate skid resistance and hydroplaning potential in wet weather conditions and the obtained results were also compared with the baseline simulation. Also, an attempt has been made to minimize the impacts of AT AC pavement by scheduling AT traffic in the low-temperature period of the day.

4.7 Methodology

The goal of this research is to assess the impacts of AT's implementation on pavement rutting in asphalt pavement. Evaluation of traffic safety factors of a road section in wet weather condition for the predicted rutting is another aim of this study. Based on truck traffic loading distribution on the lane, traffic was divided into two scenarios: baseline and autonomous. A baseline scenario was simulated for the human-driven vehicle. The autonomous scenario was simulated based on different values of the standard deviation of truck traffic in non-human-driven vehicles. All simulations of baseline and autonomous scenarios were replicated for different speeds of the vehicles. The methodology in this research mainly consists of four main phases. In the first phase, the material properties and

climate inputs were collected from different sources. The collected data were processed for inputting in the PEDRO program. In the second phase, rutting was predicted using PEDRO for all replications and then compared in order to observe the effect of the autonomous truck. In the third phase, traffic safety factors were estimated based on predicted rutting and compared with the baseline. In the fourth phase, an attempt was made to minimize the effects of AT on pavement performance by changing the hourly frequency of truck traffic over the course of a day. The framework for the evaluation of rutting and traffic safety factors is presented in Figure 4.1.

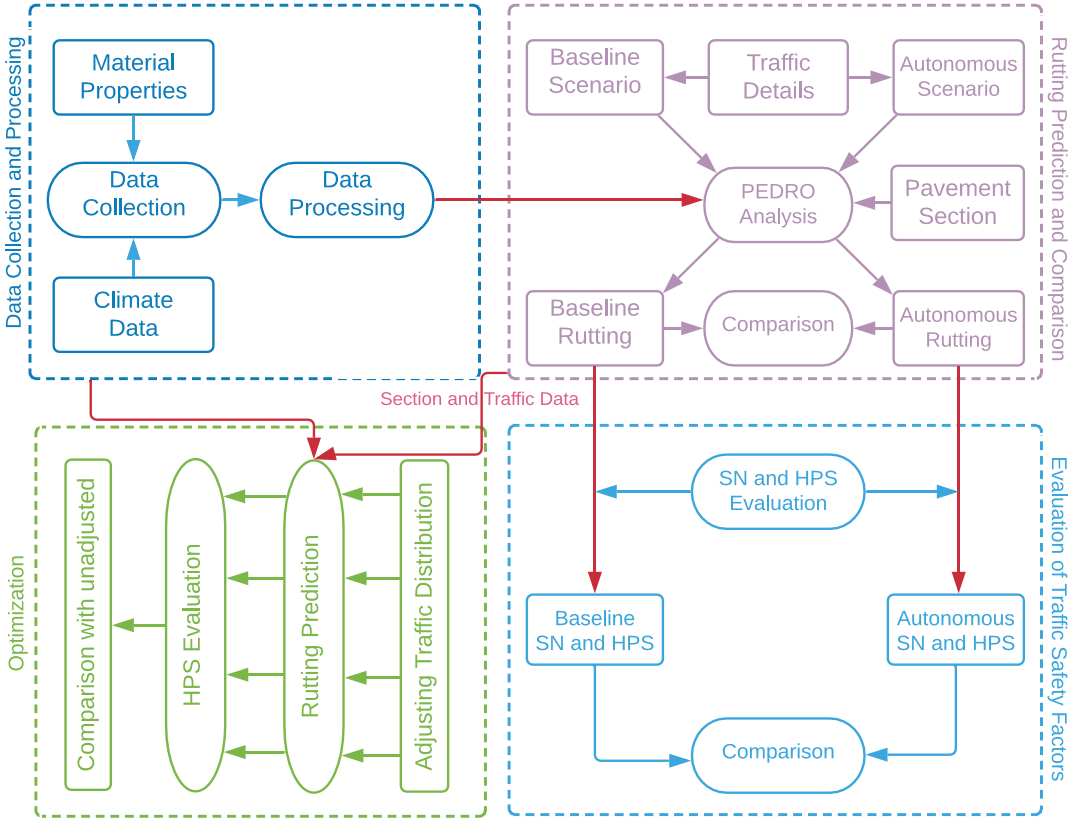

Figure 4.1 Framework for rutting and traffic safety factors evaluation

4.7.1 Data Collection and Processing

In the first phase, material properties, structural design and traffic data were collected from the Ph.D. dissertation of Harran (2009) for one road section in Winnipeg, Manitoba (Harran, 2009). Detail material properties were taken for two layers of AC layers of the pavement section. This data set consists of volumetric properties and laboratory conducted dynamic modulus (E*) of AC mixture. The collected material properties of both layers are presented in Table 4.1.

Table 4.1 Material properties

Layer/Components	**Layer 1**	**Layer 2**
Asphalt Grade (PG)	58-28	58-28
Nominal size of aggregate (mm)	12.5	12.5
Asphalt content (%)	5.5	5.0
Effective binder content, P_{be} (%)	4.8	4.2
Air voids, V_a (%)	4.5	4.8
Voids in mineral aggregate, VMA (%)	15.0	14.1
Voids filled with asphalt, VFA (%)	70.2	65.9

The dynamic modulus (E*) values of both AC mixtures are presented in Figure 4.2. Figure 4.2 shows the laboratory-measured E* values for two layers of AC mixes conducted at a frequency of 0.1, 0.5, 1, 5, 10 and 25 (Hz) for -10 (°C), 5 (°C), 10 (°C) and 25 (°C). This E* of AC mixes is a Level-1 input for robust pavement Mechanistic-Empirical Pavement Design Guide, AASHTOWare. Level 2 and level 3 input in AASHTOWare uses the Witzack model to estimate E* of AC mixes.

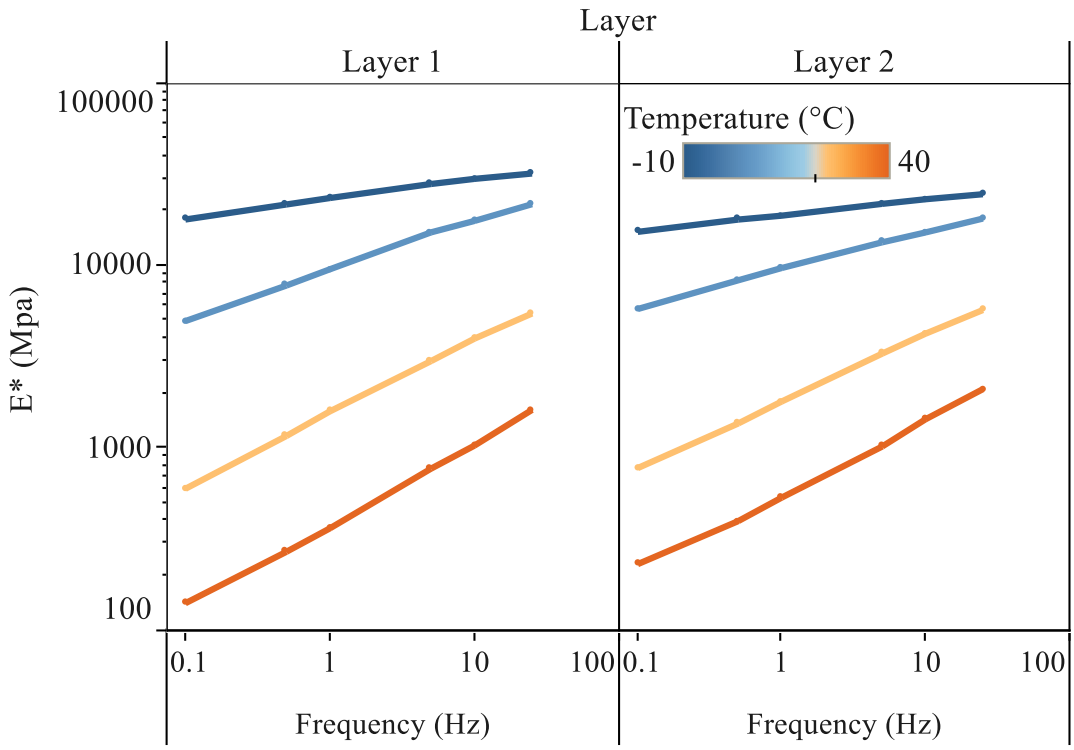

Figure 4.2 Dynamic modulus (E*) values for layer 1 and layer 2 of AC pavement

The viscosity of the AC layer is the key material input in the linear viscoelastic program, PEDRO. This model evaluates the viscosity of AC mixes generating a master curve for the dynamic shear modulus and phase angle. Zhu et al. suggested to use the Hirsch model to evaluate G*mix from of G*binder (Zhu et al., 2020). To make use of E* of AC mixes in the PEDRO material input, the dynamic shear moduli (G*) of asphalt binder was evaluated using the Hirsch E* model. Moduli, G* of the binder was back-calculated using the Equation 4.5-4.6.

$$P_c = \frac{\left(20+\frac{VFA\times G^*_{binder}}{VMA}\right)^{0.58}}{650+\left(\frac{VFA\times G^*_{binder}}{VMA}\right)^{0.58}} \quad 4.5$$

$$E^*_{mix} = P_c\left[4200000\left(1-\frac{VMA}{100}\right)+3G^*_{binder}\left(\frac{VFA\times VMA}{10000}\right)\right]+(1-P_c)\left[\frac{1-\frac{VMA}{100}}{4200000}+\frac{VMA}{3VFA\times G^*_{binder}}\right]^{-1} \quad 4.6$$

Where,

E^*_{mix} = Dynamic modulus of AC mixes (psi)

G^*_{binder}= Dynamic modulus of binder (psi)

P_c = contact factor (unitless)

VFA =voids fill with asphalt (%)

VMA = voids in mineral aggregates (%)

The obtained G* of the binder with other volumetric properties were inputted in the Hirsch model of AC mixes to obtain G* of the mix (Christensen et al., 2004). The following Equation 4.7-4.8 were used to calculate G* of AC mix.

$$P_c = \frac{\left(3+\frac{VFA\times G^*_{binder}}{VMA}\right)^{0.678}}{396+\left(\frac{VFA\times G^*_{binder}}{VMA}\right)^{0.678}} \quad 4.7$$

$$G^*_{mix} = P_c\left[601000\left(1-\frac{VMA}{100}\right)+3G^*_{binder}\left(\frac{VFA\times VMA}{10000}\right)\right]+(1-P_c)\left[\frac{1-\frac{VMA}{100}}{601000}+\frac{VMA}{3VFA\times G^*_{binder}}\right]^{-1} \quad 4.8$$

Christensen et al. developed two empirical relationships to estimate the phase angle from volumetric properties (Christensen et al., 2004). The empirical relation presented in Equation 4.9 was used for the phase angle estimation.

$$\emptyset = -21(logP_c)^2 - 55P_c \quad 4.9$$

The dynamic shear modulus and phase angles calculated following the mentioned procedures are used to generate master curves. Dynamic shear modulus and phase angles were fitted using the sigmoidal function presented in Equation 10 and fitting functions shown in Equation 11. Equations 4.12-4.13 were used to calculate the shifting function (Jelagin et al., 2018).

$$log(G^*_{mix}) = \delta + \frac{\alpha}{1+exp[\beta-\gamma \log(f_r)]} \quad 4.10$$

$$\varphi = d\left(1 - \frac{e^{\frac{f_r-a}{e}}}{1+e^{\frac{f_r-a}{e}}}\right) + \frac{c}{1+\left(\frac{f_r-a}{b}\right)^2} \quad 4.11$$

$$log(a_T) = R\left(\frac{1}{T+273} - \frac{1}{T_{ref}+273}\right) \quad 4.12$$

$$a_T = \left(\frac{f_r}{f_T}\right) \quad 4.13$$

Where,

G^*_{mix} = Dynamic shear modulus of AC mixes

φ= Phase angle

a, b, c, d, e = Fitting parameters for phase angle

$\alpha, \beta, \gamma, \delta$ = Sigmoidal fitting parameters for dynamic shear modulus

a_T = Shift factor

f_r, f_T = Frequency at reference and T temperature

Master curves for the dynamic shear modulus of two AC mixes at 10°C reference temperature is presented in Figure 4.3. The dynamic shear modulus G* of the AC mixes at the maximum phase angle is obtained from Figure 4.3.

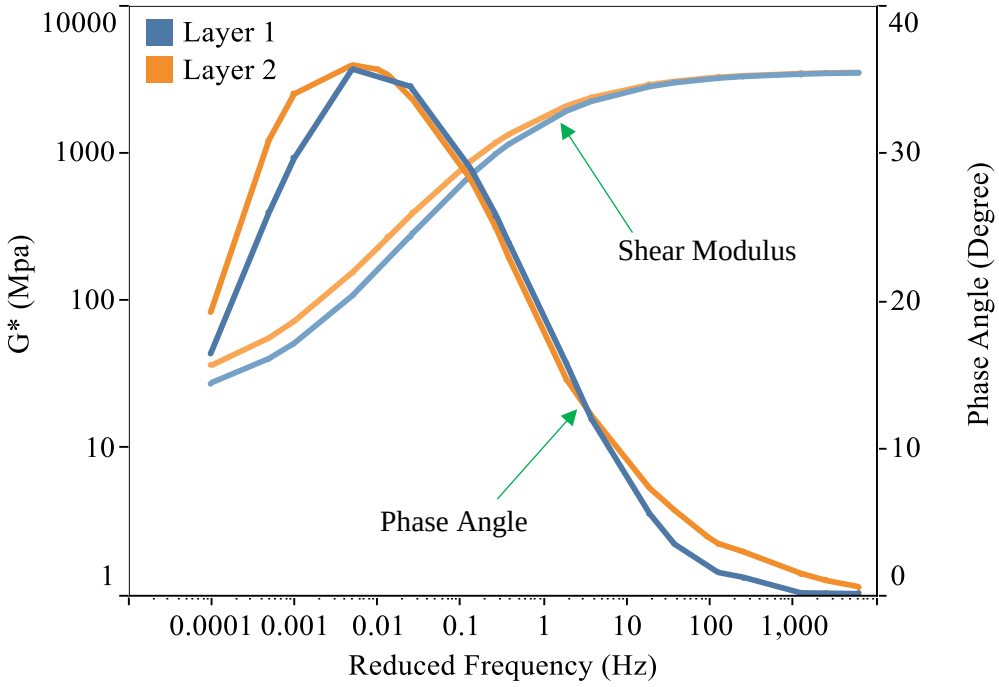

Figure 4.3 Master curves for dynamic shear modulus and phase angle at 10°C reference temperature

Master curves at reference temperatures of 5°C, 10°C, 15°C and 25°C were generated and viscosity at the specified temperatures are evaluated. The obtained viscosity vs temperature was plotted in Figure 4.4 to determine the input for PEDRO. The co-efficient of the AC mixes for layer 1 are 0.000428, -0.121 and 4.54 and for layer 2 are -0.00074, -0.104 and 4.77. These coefficients were given as input in PEDRO for layers 1 and 2 with thicknesses of 65 mm and 90 mm, respectively.

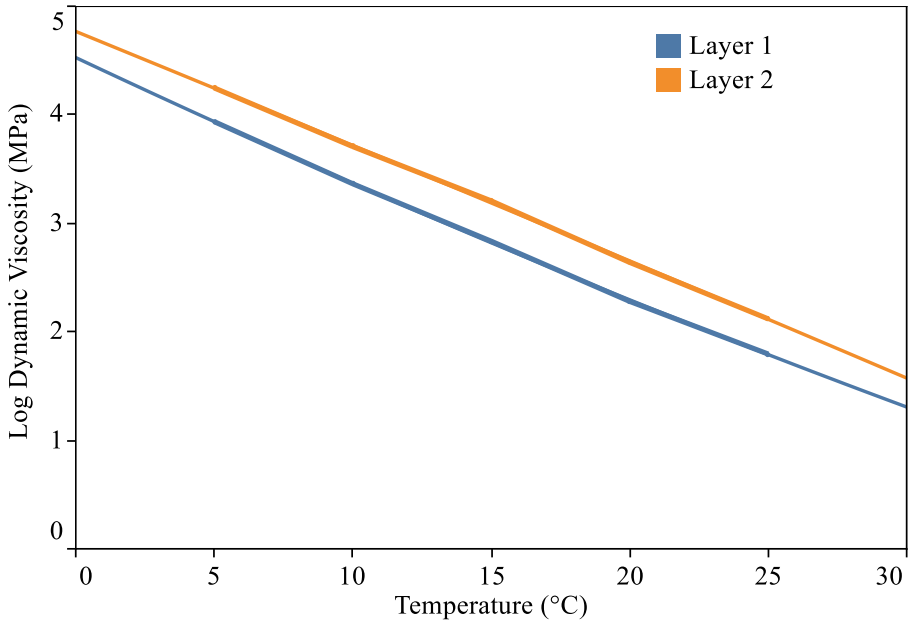

Figure 4.4 Dynamic Viscosity-Temperature curves

Climate data is collected from the Long-Term Pavement Performance (LTPP) database for the studied road section in Winnipeg, Manitoba. Climate data in the PEDRO model consists of an hourly average of monthly pavement temperature. The pavement temperature of both AC layers is evaluated using the LTPP high pavement temperature model from May to October and the LTPP low pavement temperature model from November to April for the year 2019. The temperature for layer 1 as inputted in this study is presented in Figure 4.5.

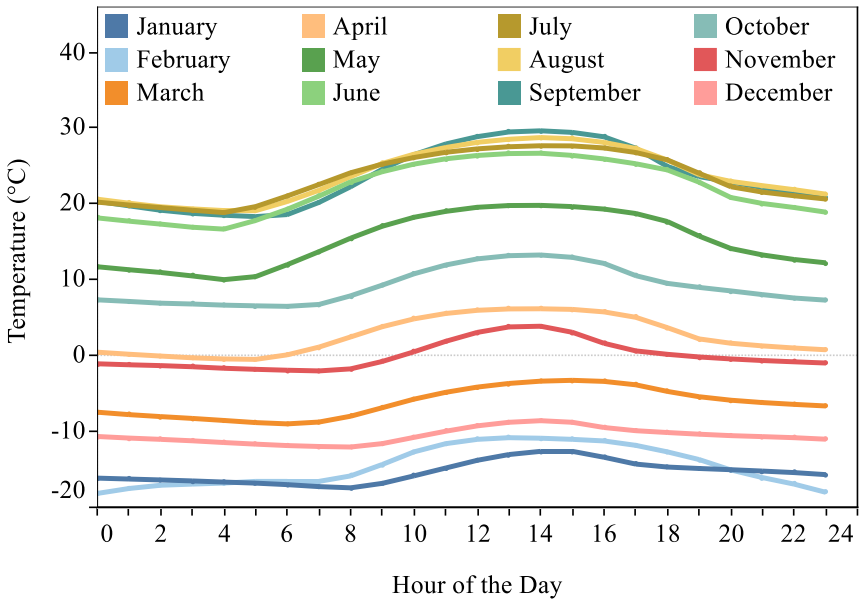

Figure 4.5 Temperature distribution over 24 hours for this study

Traffic detail is another important parameter of asphalt pavement design. In this study, annual average daily truck traffic (AADTT) was considered as 2000 with 3.5% annual traffic growth rate. Standard axle load, 80 kN for dual wheel with tire pressure 0.8 MPa, was given as input in this study. The hourly distribution of traffic load was the default value from PEDRO.

An attempt to simulate a similar section, analyzed by Harran, was made using AASHTOWare. The author analyzed the pavement section mainly for Class 9 trucks. ESAL was evaluated from AADTT by adopting the Ontario method ("Pavement Design and Rehabilitation Manual," 2013). Pavement temperature data was obtained using the same technique mentioned in the climate data paragraph. The factors used in this analysis were the same for all studies in this research. The comparison of the AC rutting between

both data is presented in Figure 4.6. There is a negligible difference observed from this comparison. This might be due to differences in traffic loading and temperature input between both analyses.

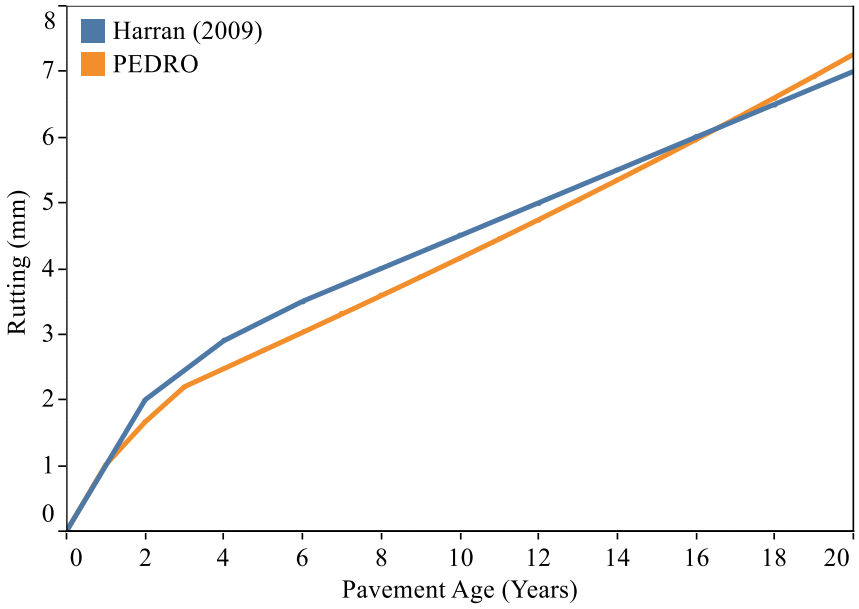

Figure 4.6 Comparison of AC rutting between PEDRO and Harran (2009**)**

4.7.2 Rutting Prediction and Comparison

PEDRO was used for predicting pavement rutting for different simulations of baseline and autonomous scenarios. The autonomous scenario was characterized by reducing the standard deviation of loading distribution, also known as traffic wandering. The effect of the wide range of AT speed on rutting for every wander was also determined. The material properties, traffic, structural design, and climate data, collected from different sources, were given as inputs in PEDRO. Material properties, structural design, and climate data were kept constant to evaluate the effect of wheel wandering and speed for the AT's

implementation on the AC rutting. AC rutting for the different wandering of traffic was compared with data for the baseline scenario. The effect of speed variation was compared within each wandering.

4.7.3 Evaluation of Traffic Safety Factors

The major traffic safety factors, hydroplaning potential speed and skid number were estimated from the predicted rutting. Skid number (SN), the measuring unit of skid resistance, was estimated using a well-established relationship proposed by Gallaway et al. (Gallaway et al., 1974). The analytical approaches introduced by Gallaway et al. (Gallaway et al., 1979) and Huebner et al. (Huebner et al., 1987) were implemented to evaluate hydroplaning speed (HPS). HPS and SN were measured for all the predicted rutting for different simulations. Comparative analyses were performed to observe the effect of autonomous trucks on HPS and SN.

4.7.4 Optimization of AC Rutting and Traffic Safety Factors

An attempt was made to minimize the effect of AT implementation on AC rutting and traffic safety factors by redistributing the hourly frequency of traffic loading. Traffic loading frequency was adjusted to get the benefit of a low-temperature duration of a day on rutting accumulation. AC rutting and traffic safety factors were reevaluated in this stage. Comparative analyses were performed to quantify the optimized performance.

4.8 Results and Discussions

The impact of autonomous trucks on AC rutting and subsequent traffic safety factors were investigated in this study. AC rutting and traffic safety factors were quantified and compared to human-driven truck traffic. Pavement performance prediction generally considers the loading distribution of a human-driven truck as normally distributed with a standard deviation of 25.0 cm (10 inches). AC rutting predicted for a standard deviation of 25.0 cm is considered a baseline scenario in this analysis. A different loading distribution of AT was regarded as autonomous scenarios in this study. The autonomous scenario was characterized by reducing the standard deviation of loading distribution to 0, 2.54 cm (1 inch), 5.1 cm (2 inches), 7.6 cm (3 inches), and 10.0 cm (4 inches). This lane-centering tendency of AT with reduced standard deviation is also represented as traffic wander. Baseline and simulations of the autonomous scenario were replicated for a wide range of truck speeds, ranging from 60 km/hr. to 120 km/hr., at an interval of 10 km/hr. Skid resistance and hydroplaning potential in wet conditions were also estimated for all simulations of the baseline and autonomous scenarios. Simulations of distress and traffic safety factors explored in this analysis are presented in Table 4.2 with nomenclature. Simulations were designated by purpose to shorten the name and permit efficient explanation in the next sections.

Table 4.2 Nomenclature of the scenarios used in the analysis

Scenario	Standard Deviation of Truck Deviation of Truck Loading Distribution (cm)	Designation
Baseline	25.0	Baseline
Autonomous	0	SD0
	2.5	SD2.5
	5.1	SD5.1
	7.6	SD7.6
	10.2	SD10.2

4.8.1 AC Rutting Prediction

The linear viscoelastic program, PEDRO, requires fundamental input regarding the typical pavement section to predict the AC rutting. Material properties and temperature data of the typical sections, significant for rutting prediction, are described in detail in the data collection and processing section and are given as input in this study. The default hourly traffic loading distribution incorporated in PEDRO was selected for this analysis. The other analysis parameters used in this study are presented in Table 4.3.

Table 4.3 Analysis parameters

AADTT	2000
Traffic growth rate (%)	3.5
Analysis period (years)	20
Axle load (kN)	80
Dual wheel (%)	100
Tyre pressure (kPa)	800
Standard deviation (cm)	25,0,2.5,5.1,7.6,10.2
Vehicle speed (km/hr)	60,70,80,90,100,110,120

The pavement section was analyzed with constant material properties, structural design data, climate data and traffic details, except traffic wander and vehicle speeds, for all simulations of baseline and autonomous scenarios. AC rutting for SD0, SD2.5, SD5.1, SD7.6, and SD10.2 simulations were compared with baseline scenarios for different speeds of truck traffic. A comparison of the AC rutting between the baseline and autonomous scenarios are presented in Figure 4.7.

Predicted AC rutting of the baseline and autonomous scenarios for different simulations of AT over the pavement life is illustrated in Figure 4.7. The presented AC rutting in Figure 4.7 was measured at a speed of 90 (km/hr) only. The AC rutting for all simulations is in increasing trend with the increment of pavement life. Based on induced AC rutting, the simulations can be presented from highest to lowest order as: SD0>SD2.5>SD5.1>SD7.6>SD10.2>Baseline. AC rutting is increasing with the reduction of the standard deviation of truck traffic distribution. At the end of the analysis period, AC rutting of Baseline, SD10.2, SD7.6, SD5.1, SD2.5, and SD0 was found to be as 6.01 (mm), 9.98 (mm), 13.09 (mm), 17.23 (mm), 20.69 (mm), and 21.85 (mm), respectively. The maximum percentage increase of rutting, 263.6 (%), is observed for zero wander conditions. It is perceptible that the lane-centering tendency of AT is a significant contributor to the increment of AC rutting.

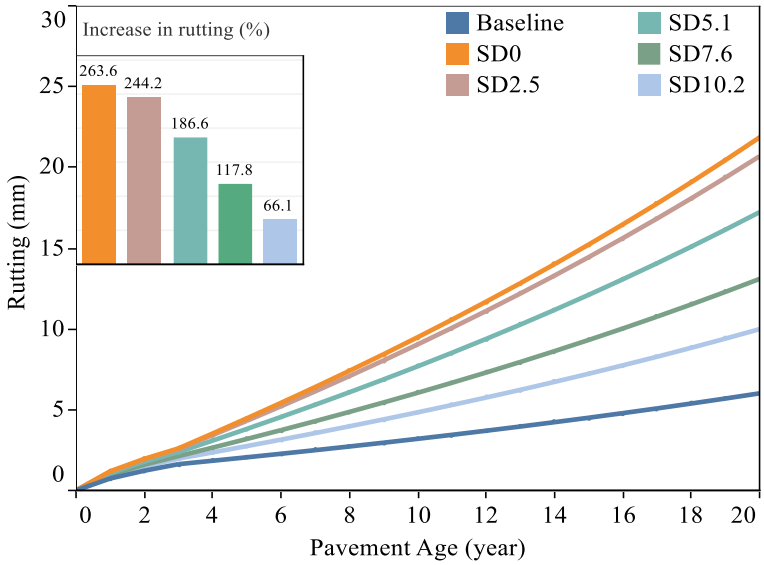

Figure 4.7 Predicted Rutting for different simulations

Rutting profiles in the transverse direction of pavement for different simulations are illustrated in Figure 4.8. Presented AC rutting in Figure 4.8 was measured at speed of 90 (km/hr). Maximum rutting is observed in the center of the dual wheel in the baseline scenario. The maximum rutting point in autonomous scenarios moves under each wheel. Upheaval in wheel path increases with decreasing standard distribution of the loading distribution of AT. The upheaval has reached to about 21% compared to the highest rutting at the baseline scenario. Jeginal et al. mentioned that upheaval might be developed by up to 15% (Jelagin et al., 2018). Overestimation of upheaval is observed from PEDRO analysis. Remarkably, the spreading of the rutting profile is becoming narrower with a decreasing standard deviation of AT loading. Predicted rutting reached to zero value at the distance of 0.46 (m), 0.26 (m), 0.28 (m), 0.29 (m), 0.30 (m), and 0.33 (m) from the center for baseline, SD0, SD2.5, SD5.1, SD7.6, SD10.2 simulations, respectively.

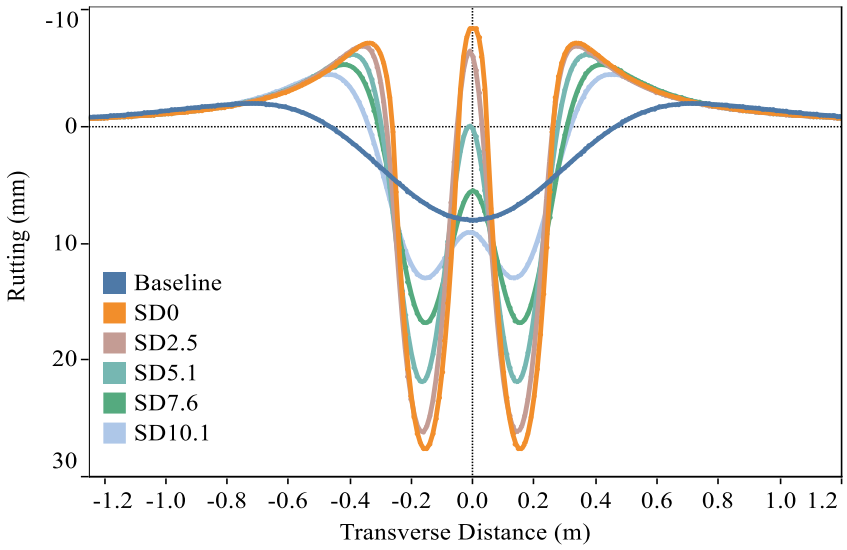

Figure 4.8 Rutting profile in transverse direction for different simulations

Compared to the baseline scenario, change in rutting due to variation of truck traffic speed for different simulations is shown in Figure 4.9. It is found that the reduction of truck traffic speed significantly increases the rutting accumulation in the pavement section. Increase in rutting at zero wander is observed as 14.98 (mm), 12.84 (mm), 11.23 (mm), 8.98 (mm), 8.16 (mm), and 7.45 (mm) for speed of vehicle at 60 (km/hr), 70 (km/hr), 80 (km/hr), 90 (km/hr), 100 (km/hr), 110 (km/hr), and 120 (km/hr), respectively. It can be summarized as increasing AT speed might be beneficial for pavement design due to a significant reduction in rutting accumulation.

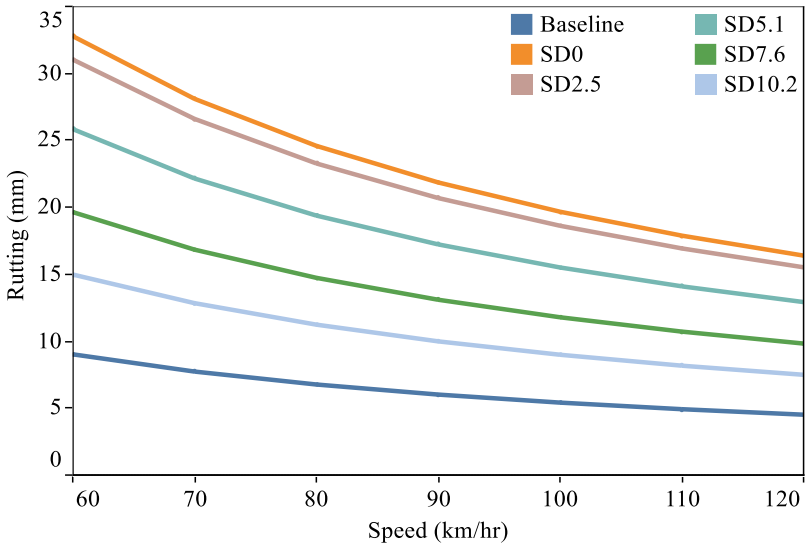

Figure 4.9 Effect of vehicle speed on rutting accumulation of different simulations

4.8.2 Evaluation of Road Safety Factors

The analysis focused on the utilization of AT-induced rutting on the evaluation of two road safety factors, hydroplaning potential and skid resistance, in wet weather conditions. Before analysis, relevant literature has been consulted to obtain the susceptibility of HPS and skid resistance to passenger car and truck traffic. Horne et al. performed a series of research on the effect of truck tire on HPS and provided the following Equation 4.14 (Horne et al., 1986).

$$HPS = 25(p_{tire})^{0.21}\left(\frac{1.4}{FAR}\right)^{0.5} \quad 4.14$$

Where,

HPS=Hydroplaning speed

p_{tire} = Tire inflation pressure

FAR= Footprint aspect ratio

The author concluded with high hydroplaning speed and lower hydroplaning risk of a truck tire having lower FAR value (Horne et al., 1986). Ong and Fwa investigated truck hydroplaning and found a higher hydroplaning risk for an empty truck, rather than a loaded truck (Ong & Fwa, 2007). Passenger cars also depicted lower hydroplaning speed for normal operational traffic on the highway. Ong and Fwa studied skid resistance for truck traffic on the highway and found reduced skid resistance for an empty truck (Ong & Fwa, 2010). Changyong found that truck tire moving on normal highway speed incorporates lower skid resistance than passenger cars (Changyong, 2010). From the above discussion, it is noticeable that hydroplaning potential and skid resistance are more susceptible to the passenger car. HPS and skid of resistance of passenger cars are investigated in this study from the accumulated rutting from the AT.

Gallaway et al. developed an empirical relationship for evaluating skid number (indicator for frictional resistance of pavements) from the experimental studies and provided the following Equation 4.15 for ASTM standard tire with 165.5 kPa (24 psi) inflation pressure (Gallaway et al., 1974).

$$SN = \frac{154}{V^{0.77}}\left[TD^{0.05} + \frac{4.71TXD^{0.09}}{(25.4WFD+2.5)^{0.09}}\right] \quad 4.15$$

Where,

SN = Skid number at the vehicle speed

V= Vehicle speed (mile/hr)

TD= Tyre thread depth (inch)

TXD= Pavement surface texture depth (inch)

WFD= Water film thickness (inch)

Most of the asphalt pavement considers the typical TXD value as 0.91 mm (0.036 inches) (Zhou et al., 2019). Tire thread depth (TD) is regarded as 2.36 mm (2/32 inch) for this analysis. Glennon provided Equation 4.16 to evaluate WFD considering the effect of the cross slope of pavement (Glennon, 2015).

$$WFD = Rutting - CS \times L \quad 4.16$$

Where,

CS = Cross slope

L = Half-length of rutting zone

Most of the US Department of Transportation considers SN value measured at 65 km/hr (40 miles/hr) as a reference line and it is symbolized as SN_{40}. The acceptance limit of SN_{40} is 30 and it is necessary to apply corrective measures lower than the limiting value (National Cooperative Highway Research Program, 1983; Oh et al., 2010). WFD is calculated for a wide range of vehicle speeds for all simulations of baseline and autonomous scenario using equation 16. CS is assumed as 0.5% for this analysis and half-length of the rutting zone is taken from the predicted rutting profile. It is mentionable that CS is not considered for rutting prediction in this study. SN_{40} values for all simulations with different speeds are evaluated using the calculated WFD and presented in Table 4.4. Presented SN_{40} values are within the acceptable range. Compared to baseline scenario, percentage decrease in SN_{40} is 8.6%, 8.3%, 7.2%, 5.6%, and 3.9% for SD0, SD2.5, SD5.1, SD7.6, SD10.2 simulations, respectively. It can be concluded that the implementation of AT has a negligible effect on the skid resistance of asphalt pavement.

Table 4.4 SN_{40} of all simulations with different truck speed

Simulations	Truck Speed (km/hr)						
	60	**70**	**80**	**90**	**100**	**110**	**120**
Baseline	33.7	34.1	34.4	34.6	34.9	35.1	35.3
SD0	30.9	31.2	31.4	31.7	31.9	32.1	32.3
SD2.5	31.0	31.3	31.6	31.8	32.0	32.2	32.4
SD5.1	31.3	31.7	31.9	32.2	32.4	32.6	32.8
SD7.6	31.9	32.2	32.5	32.7	33.0	33.2	33.3
SD10.2	32.5	32.8	33.1	33.3	33.6	33.8	33.9

Gallaway et al. conducted the extensive tests and using multilinear regression analysis provided the following relationships presented in Equations 4.17-4.19 for predicting HPS (Gallaway et al., 1979).

$$HPS = SD^{0.04} P_{tire}^{0.3} (TD + 1)^{0.06} A \quad 4.17$$

$$A = \frac{10.409}{WFD^{0.06}} + 3.507 \quad 4.18$$

$$A = \left(\frac{28.952}{WFD^{0.06}} - 7.817\right) (TXD)^{0.14} \quad 4.19$$

Where,

SD = Spin down (%)

It is recommended to choose a greater A value from Equations 3.18 and 3.19. Authors found 10% spin down is the indicating point of HPS and this equation is valid for WFD>2.54 mm (0.10 (inch) (Gallaway et al., 1979). Huebner et al. introduced a new formula, presented in Equation 4.20, to estimate HPS for WFD<2.54 mm (0.10 inch) (Huebner et al., 1987).

$$HPS = 26.04WFT^{-0.259} \quad 4.\ 20$$

HPS for different simulations with various speeds was evaluated using Equations 3.17-3.20 for ASTM standard tire considering inflation pressure, spin down, TXD, and TD as 165.5 kPa (24 psi), 10%, 0.91 mm (0.036 inches), and 2.36 mm (2/32 inch), respectively. The obtained WFD and HPS were evaluated for rutting predicted at the end of the analysis period.

Predicted WFD and HPS for AC pavement, measured at the end of the pavement life, of all simulations with various vehicle speeds, are illustrated in Figure 4.10. There is decreasing WFD values with increasing AT speeds for all simulations. WFD varies from 6.7-2.2 (mm), 31.5-15.1 (mm), 29.6-14.1 (mm), 24.4-11.5 (mm), 18.1-8.3 (mm), and 13.3-5.8 (mm) for AT speed ranging 60-120 (km/hr) for baseline, SD0, SD2.5, SD5.1, SD7.6, and SD10.2, respectively. It can be concluded that the incorporation of AT by reduced standard deviation has a significant influence on the HPS of passenger cars, compared to the baseline scenario. Graphical representation of HPS using a multi-color single line showed the increasing HPS with decreased WFD values for all simulations with different AT speeds. Each color band of a single line is showing HPS for each vehicle simulations. HPS is found to be maximum as 91 (km/hr) for 2.2 (mm) WFD and minimum as 74 (km/hr) at 31.1 (mm) WFD. HPS is reduced to the range of 74-91 (km/hr) compared to AT speed ranging from 60-120 (km/hr). Low hydroplaning potential (high HPS) is noticed up to 74 (km/hr) AT speed with SD0 simulation.

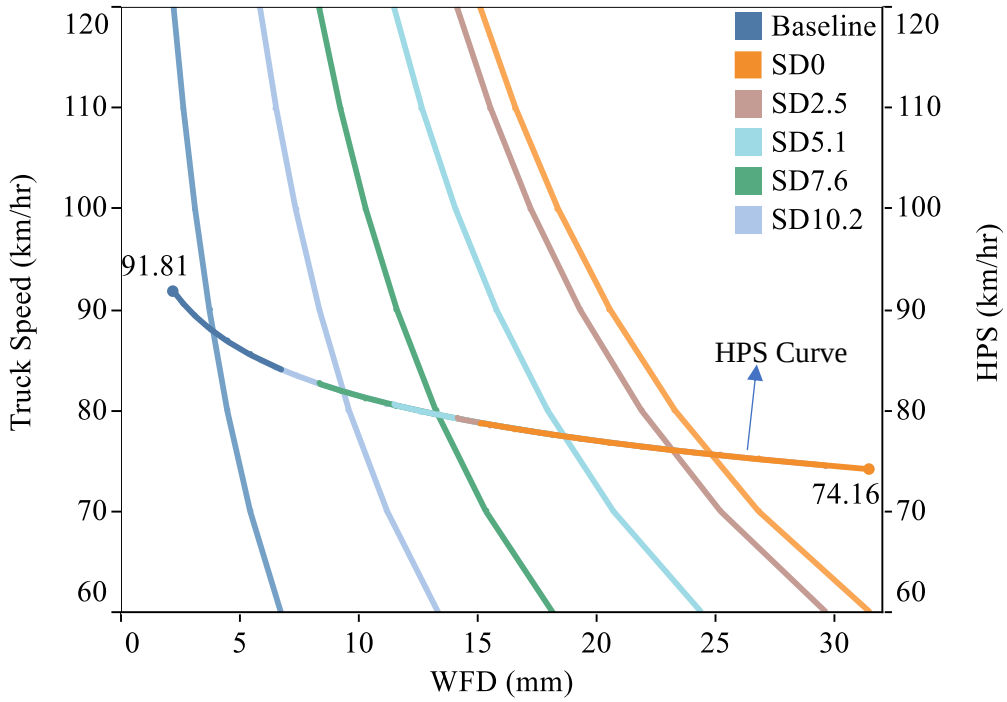

Figure 4.10 Predicted WFT and HPS for all simulations with various truck speeds

It is highly expected that the incorporation of AV, along with AT, will significantly reduce road accidents and improve roadway capacity with higher speed. Analyzed data depicted that increasing AT speed has a positive effect on rutting in AC pavement and a negative effect on HPS after a certain limit. This reverse phenomenon was observed for the implementation of AT. The critical point has been established among AT speed, HPS (mainly car speed), and WFD (can be presented rutting also) to remove the contradictory conclusion between pavement distress and traffic safety factor. HPS curve intersected the individual graph of traffic simulation at different points and that is the critical point of AT speed, HPS and rutting. For example, the HPS curve intersects the SD5.1 curve at one point with about 80 (km/hr) AT speed and 13.2 (mm) WFD. An increment of AT speed beyond

this point will reduce the rutting, but HPS will be lower and will be intending hydroplaning risk. At this critical point, both HPS and AT speed are equal. The critical point in this study indicates the speed of AT to induce optimum rutting with the safest HPS for passenger cars. Critical points for all the simulations have been established and tabulated in Table 4.5.

Table 4.5 Critical WFD and HPS

Simulations	HPS (km/hr)			Optimum WFD (mm)
	Minimum	Maximum	Critical	
Baseline	84.1	91.8	88.1	3.7
SD0	74.2	78.8	75.6	25.1
SD2.5	74.5	79.2	76.0	23.2
SD5.1	75.7	80.5	77.5	18.4
SD7.6	77.6	82.7	79.6	13.2
SD10.2	79.6	85.0	81.9	9.2

4.9 Rescheduling Hourly Traffic Distribution

Climate factors have a significant influence on asphalt pavement performance. Pavement temperature, induced from air temperature and other factors, significantly affects the AC pavement performance by changing the resilient modulus of asphalt material. Resilient modulus is the critical variable in asphalt pavement design, increases at low temperatures (Ghao et al., 2019; Zhao et al., 2020a). An attempt has been made in this study to minimize the effects of autonomous vehicles by scheduling vehicle movement in the period of low-temperature duration of a day. The model, PEDRO, uses Equation 4.21-4.22 for the hourly distribution of different vehicles.

$$\varphi = 2 * \pi * \frac{t+\beta 3}{24} \quad 4.21$$

$$Y = \beta 0 + \beta 1 * \left[\frac{\beta 2}{1+x^2} + sign[\sin(\varphi)] * \sqrt{\left(\frac{\beta 2}{1+x^2}\right)^2 - \frac{\beta 2^2 - x^2}{x^2+1}}\right] \quad 4.22$$

Where,

Y= Frequency of daily traffic distribution

$x = \tan(\varphi)$

t= O'clock in hours

$\beta 0,\ \beta 1,\ \beta 2,\ \beta 4$= Fitting functions

Fitting functions are adjusted to reschedule the frequency of hourly traffic distribution shown in Figure 4.11. Figure 4.11 represents the average hourly pavement temperature variation of 24 hours for the month of January and the hourly distribution of normal traffic and adjusted traffic. Temperature variation showed significantly reduced value from 11 PM to 8 AM of a day. At the same duration of the day, traffic flow is in the minimal stage. The fully autonomous truck will be moving without the assistance of the driver, especially for the shipment of goods. There is no possibility of mental stress for movement at nighttime. So, allowing AT to move on low-temperature duration might be beneficial for the pavement performance perspectives. The frequency of hourly traffic distribution was adjusted by using equal frequency for all hours in adjusted-1 and high frequency was used for the lower temperature zone in adjusted-2 condition.

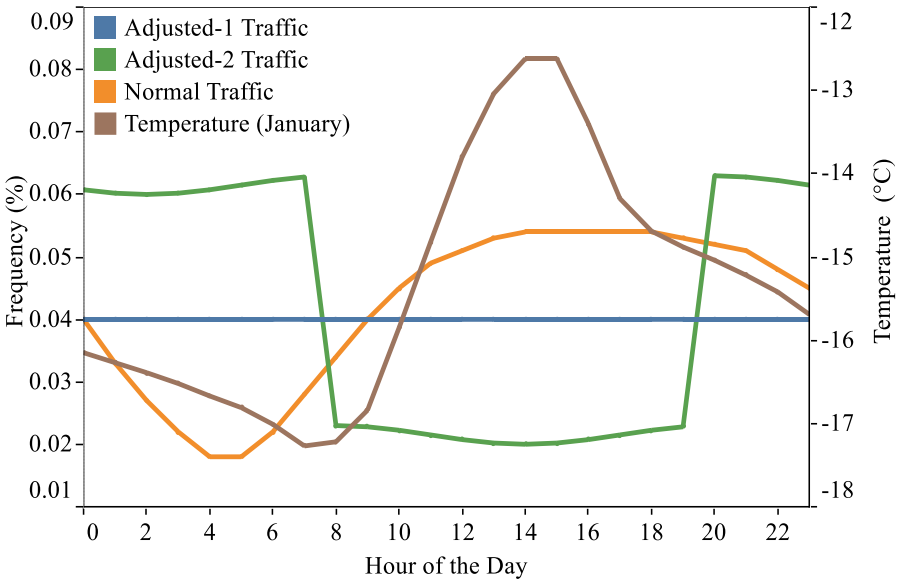

Figure 4.11 Hourly temperature variation of a day and frequency of traffic distribution

Compared to normal traffic distribution, the percentage decrease in rutting and improvement in HPS for rescheduled hourly traffic distribution for 90 (km/hr) AT speed are presented in Figures 4.12-4.13. Significant reduction in predicted rutting, 24.2% for SD0 of adjusted-1 and 44.1% for SD0 of adjusted-2 traffic, was observed. Percentage improvement in HPS for adjusted-1 and adjusted-2 traffic scenario was observed to be as about 3.0%, and 5.1% for all autonomous simulations. It can be summarized that the utilization of low-temperature duration for the movement of AT might be an option for optimizing the effect of AT on pavement rutting and traffic safety factors.

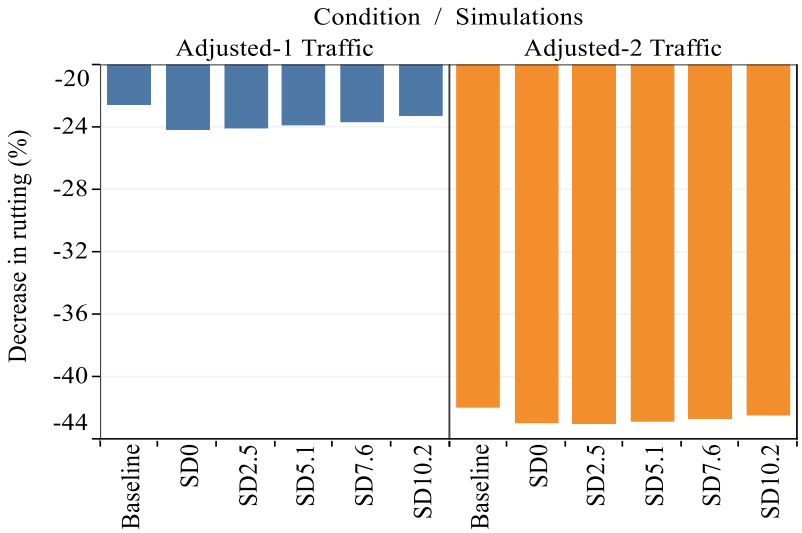

Figure 4.12 Percentage decrease in rutting for rescheduling hourly traffic distribution

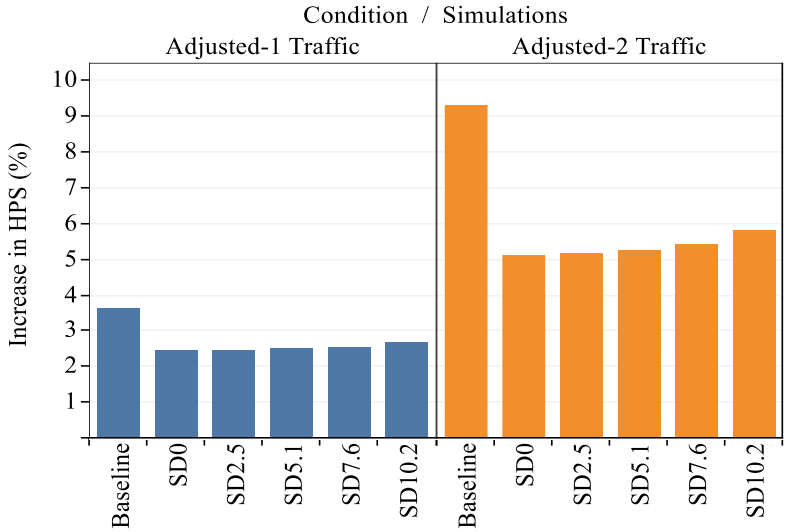

Figure 4.13 Percentage improvement in HPS for rescheduling hourly traffic distribution

4.10 Concluding Remarks

This current study focuses on quantifying the impact of autonomous truck (AT) implementation on asphalt pavement rutting and consequent traffic safety parameters in wet weather conditions. Scenarios were fabricated based on the standard deviation of normally distributed truck loading distribution or traffic wander on-road section. Based on standard deviation, baseline, and autonomous scenarios were considered in this study. The baseline scenario was designated for the movement of the non-autonomous or human-driven truck. Human-driven vehicles were simulated as normally distributed with a standard deviation of 25 cm (10"). Autonomous scenarios were simulated for truck loading with standard deviation of 0, 0.25 cm (1"), 0.51 cm (2"), 0.76 cm (3"), and 1.02 cm (4") and designated as SD0, SD2.5, SD5.1, SD7.6, and SD10.2, respectively. The typical pavement section was considered to analyze for simulations of baseline and autonomous scenarios.

Asphalt concrete mixtures volumetric and mechanical properties data were collected from Harran (2009), which were then processed using Hirsch E* and G* models to obtain dynamic shear modulus and phase angles. Masters curves of evaluated dynamic shear modulus and phase angles were generated to compute the necessary parameters to give input in PEDRO. Climate data was also processed for use in this analysis. Material, structural design, and climate input was kept constant for prediction of pavement rutting for all simulations. All traffic input details, except standard deviation and speed, were also the same for these analyses. The predicted rutting of autonomous simulations was compared with the baseline scenario to estimate the effect of AT. Traffic safety parameters,

hydroplaning potential and skid resistance were evaluated for passenger car for AT induced rutting. The passenger car, being more susceptible to hydroplaning and skid resistance, was considered for this study. Also, the pavement section was analyzed by scheduling AT in the low-temperature period of all the days of the analysis period. The conclusions drawn from the comparative pavement analyses are as presented below.

- The AC rutting for all autonomous truck scenarios increased. Compared to the baseline scenario, the maximum percentage increase of rutting is found to be 263.6 (%) for zero wander conditions. It is suspected that the lane centering tendency of AT is a significant contributor to the increment of AC rutting from the increased load repetition on a single point.
- From the analysis, it is remarkably discovered that the spread of the rutting profile from autonomous trafficking becomes narrower with decreasing standard deviation of AT loading. It is determined that rut width reduced to 0.52 m, 0.56 m, 0.58 m, 0.60 m, and 0.66 m for SD0, SD2.5, SD5.1, SD7.6, and SD10.2 for the applied loadings on the wheel path, respectively.
- Overestimation of upheaval is observed from the Permanent Deformation of Asphalt Concrete Layer for Roads (PEDRO) model analysis. Therefore, the model developers are recommended to recalibrate their models.
- The analysis clearly shows that a reduction of truck traffic speed negatively affects the rutting accumulation in the pavement section for all simulations. It suggests that the decision-maker should consider an increased speed for autonomous traffic road

or lane. This will be beneficial from a pavement durability perspective due to a significant reduction in rutting accumulation.

- Implementation of AT negligibly affects the skid resistance of asphalt pavement. Skid number (SN_{40}) decreases with decreasing standard deviation. But all the values are within the limiting range.
- Analyzed data clearly showed that hydroplaning speed (HPS) increases with AT speed and is bound to be in a safe zone up to a certain limit. Beyond this point, HPS intended to hydroplane with increased AT speed inducing lower rutting. These contradictions of pavement performance and traffic safety have been attempted to remove by presenting graphical relationships among AT speed, HPS (mainly car speed) and WFD. Furthermore, this research has developed critical values (threshold values) for truck speed, WFD and HPS parameters for a wide range of autonomous scenarios and presented in Table 4.5. This might be useful to consider traffic safety factors in pavement design.
- A countermeasure, i.e., optimal scheduling of AT loading over a low-temperature day, is introduced in this paper to reduce pavement rutting from autonomous traffic. Significant improvement in pavement distresses is found to occur for controlling the movement of AT at the low-temperature period of each day. Significant reduction in predicted rutting, 24.2% for SD0 of adjusted-1 and 44.1% for SD0 of adjusted-2 traffic, was observed. Percentage improvement in HPS for adjusted-1 and adjusted-2 traffic scenario was about 3.0%, and 5.1% for all autonomous simulations.

4.11 References

Agrawal, S. K., & Henry, J. J. (1977). Technique for evaluating hydroplaning potential of pavements. *Transportation Research Record, 633*, 1–7.

Ahmed, A. W., Said, S. F., Lu, X., & Carlsson, H. (2012). Pavement performance follow-up and evaluation of polymer-modified test sections. *International Journal of Pavement Engineering*, *20*(12), 1474–1487.

Rödin, A., & Andersson, E. U. (2017). *Implementation of the permanent deformation model PEDRO for pavement structures* [Master's thesis, Chalmers University of Technology]. Proquest Dissertations and Theses.

ARA, Inc. (2004). *Guide for mechanistic-empirical design of new and rehabilitated pavement structures*. Final Rep., NCHRP Project 1-37A

Blab, R., & Litzka, J. (1995). Measurements of the lateral distribution of heavy vehicles and its effects on the design of road pavements. *Proceedings of the International Symposium on Heavy Vehicle Weights and Dimensions*, 389–395.

Buiter, R., Cortenraad, W. M. H., Eck, A. C., & Rij, H. (1989). Effects of transverse distribution of heavy vehicles on thickness design of full-depth asphalt pavements. *Transportation Research Record*, *1227*, 66–74.

Changyong, C. (2010). *Skid resistance and hydroplaning of rib truck tires* [Master's thesis, National University of Singapore]. Proquest Dissertations and Theses.

Chen, F., Balieu, R., & Kringos, N. (2016). Potential influences on long-term service

performance of road infrastructure by automated vehicles. *Transportation Research Record*, *2550*(January 2016), 72–79. https://doi.org/10.3141/2550-10

Chen, F., Song, M., Ma, X., & Zhu, X. (2019). Assess the impacts of different autonomous trucks' lateral control modes on asphalt pavement performance. *Transportation Research Part C: Emerging Technologies*, *103*(September 2018), 17–29. https://doi.org/10.1016/j.trc.2019.04.001

Christensen Jr, D. W., Pellinen, T., & Bonaquist, R. F. (2003). Hirsch model for estimating the modulus of asphalt concrete. *Journal of the Association of Asphalt Paving Technologists*, *72*.

Chu, L., & Fwa, T. F. (2016). Incorporating pavement skid resistance and hydroplaning risk considerations in asphalt mix design. *Journal of Transportation Engineering*, *142*(10). https://doi.org/10.1061/(ASCE)TE.1943-5436.0000872

Chu, L., & Ong, G. P. (2015). Evaluating Hydroplaning potential of rutted highway pavements. *Journal of the Eastern Asia Society for Transportation Studies*, *11*(December), 1613–1622. https://doi.org/10.11175/easts.11.1613

Erlingsson, S. (2012). Rutting development in a flexible pavement structure. *Road Materials and Pavement Design*, *13*(2), 218–234.

Fee, G. (2020). Preparing for autonomous vehicles. *Asphalt Magazine*. http://asphaltmagazine.com/autonomous-vehicles/

Gallaway, B. M., Ivey, D. L., Hayes, G., Ledbetter, W. B., Olson, R. M., Woods, D. L., & Schiller Jr, R. F. (1979). *Pavement and geometric design criteria for minimizing*

hydroplaning (No. FHWA-RD-79-31 Final Rpt.).

Gallaway, B. M., Rose, J. G., Hankins, K. D., Scott Jr, W. W., & Schiller Jr, R. E. (1974). *Influence of water depths on friction properties of various pavement types*. Texas Transportation Institute, Res. Rept.

Ghao, L., Hong, F., & Ren, Y. (2019). Impact of seasonal and annual weather variations on network-level pavement performance. *Infrastructures*, *4*(27), 1–13.

Glennon, J. C. (2015). *Roadway hydroplaning ? Measuring pavement wheel rut depths to determine maximum water depths*. Crash Forensics.Com. http://www.crash-forensics.com/papers.cfm?PaperID=55

Gungor, O. E. (2018). *Final report: A literature review on wheel wander*. https://il-asphalt.org/files/2915/1743/1516/Erman_Gungor_2017_UIUC.

Gungor, O. E., & Al-Qadi, I. L. (2020a). All for one: Centralized optimization of truck platoons to improve roadway infrastructure sustainability. *Transportation Research Part C: Emerging Technologies*, *114*(January), 84–98.

Gungor, O. E., & Al-Qadi, I. L. (2020b). Wander 2D: a flexible pavement design framework for autonomous and connected trucks. *International Journal of Pavement Engineering*, *0*(0), 1–16. https://doi.org/10.1080/10298436.2020.1735636

Halstead, W. J., Copas, T. L., Pennock, H. A., & Shipman, A. (1983). Criteria for use of asphalt friction surfaces. Transportation Research Board.

Harran, G. (2011). *Improving the determination of the dynamic modulus of asphalt*

concrete for mechanistic-empirical pavement design [Ph.D. thesis, University of Manitoba, Winnipeg, Manitoba, Canada]. Proquest Dissertations and Theses.

Hills, R. & Lee, J. (2012). *Model based predictive control for automated lane centerng/changing control systems*. ((US Patent No. 8,190,330 B2). U.S. Patent and Trademark Office.

Horne, W. B., Yager, T. J., & Ivey, D. L. (1986). Recent studies to investigate effects of tire footprint aspect ratio on dynamic hydroplaning speed. *In The tire pavement interface*. ASTM International.

Huebner, R. S., Reed, J. R., & Henry, J. J. (1987). Criteria for predicting hydroplaning potential. *journal of transportation engineering*, *112*(5), 549–553.

Jelagin, D., Ahmed, A., Lu, X., & Said, S. (2018). *Asphalt layer rutting performance prediction tools.* VTI rapport 968A (Issue September).

Linder, C. (2019). Self- Driving freight trucks - Autonomous trucks. *Popular Mechanics*. https://www.popularmechanics.com/technology/infrastructure/a30196644/self-driving-truck-cross-country/

Litman, T. (2020). *Autonomous vehicle implementation predictions: Implications for transport planning*. In Victoria Transport Policy Institute (Issue January 2014).

Lu, Q., Tettamanti, T., Hörcher, D., & Varga, I. (2020). The impact of autonomous vehicles on urban traffic network capacity: An experimental analysis by microscopic traffic simulation. *Transportation Letters*, *12*(8), 540–549.

Mounce, M. J., & Bartoskewitz, T. R. (1993). Hydroplaning and roadway tort liability. *Transportation Research Record*, *1401*, 117--124.

Noorvand, H., Karnati, G., & Underwood, B. S. (2017). Autonomous vehicles: Assessment of the implications of truck positioning on flexible pavement performance and design. *Transportation Research Record*, *2640*(April 2018), 21–28.

Oh, S., Madanat, S., Ragland, D. R., & Chan, C. (2010). Evaluation of traffic and environment effects on skid resistance in California. *Transportation Research Record*, *510*.

Ong, G. P., & Fwa, T. F. (2006). Analysis of effectiveness of longitudinal grooving against hydroplaning. *Transportation Research Record: Journal of the Transportation Research Board*, *1949*(1), 112–125. https://doi.org/10.1177/0361198106194900110

Ong, G. P., & Fwa, T. F. (2007). Prediction of wet-pavement skid resistance and hydroplaning potential. *Transportation Research Record*, *2005*, 160–171. https://doi.org/10.3141/2005-17

Ong, G. P., & Fwa, T. F. (2010). Modeling skid resistance of commercial trucks on highways. *Journal of Transportation Engineering*, *136*(6), 510–517. https://doi.org/10.1061/(ASCE)TE.1943-5436.0000116

Ong, G. P., Fwa, T. F., & Guo, J. (2005). Modeling hydroplaning and effects of pavement microtexture. *Transportation Research Record: Journal of the Transportation Research Board*, *1905*(1), 166–176. https://doi.org/10.1177/0361198105190500118

Oscarsson, E. (2011). *Mechanistic-empirical modeling of permanent deformation in*

asphalt concrete layers (Vol. 259). Department of Technology and Society, Lund University.

Pavement design and rehabilitation manual. (2013). In *Materials Engineering and Research Office, Ministry of Transportation, Ontario, Canada*.

Peng, J., Chu, L., & Fwa, T. F. (2020). Determination of safe vehicle speeds on wet horizontal pavement curves. *Road Materials and Pavement Design*, *0629*. https://doi.org/10.1080/14680629.2020.1772350

Said, S. F., Hakim, H., & Eriksson, O. (2013). Rheological characterization of asphalt concrete using a shear box. *Journal of Testing and Evaluation*, *41*(4), 602–610. https://doi.org/10.1520/JTE20120177

Said, S. F., Hakim, H., Oscarsson, E., & Hjort, M. (2011). Prediction of flow rutting in asphalt concrete layers. *International Journal of Pavement Engineering*, *12*(6), 519–532. https://doi.org/10.1080/10298436.2011.559549

Said, S. F., Worake, A., & Carlsson, H. (2016). Evaluation of rutting of asphalt concrete pavement under field-like conditions. *E&E Congress 2016*, *June*. https://doi.org/10.14311/ee.2016.167

Said, S. F., Ahmed, A., Jelagin, D., Lu, X., Gudmarsson, A., Nilsson, R., Oscarsson, E., & Jarlsson, H. (2020). *Prediction of rutting in asphalt concrete pavements – the PEDRO model*. VTI rapport 1016A (Issue April)

Shafiee, M. H., Nassiri, S., & Bayat, A. (2014). Field investigation of the effect of operational speed and lateral wheel wander on flexible pavement mechanistic

responses. *2014 Transportation Association of Canada Conference and Exhibition: Past, Present, Future, ATC 2014, 5112*.

Shladover, S. E., Su, D., & Lu, X. Y. (2012). Impacts of cooperative adaptive cruise control on freeway traffic flow. *Transportation Research Record*, *2324*(Idm), 63–70. https://doi.org/10.3141/2324-08

Siddharthan, R. V., Nasimifar, M., Tan, X., & Hajj, E. Y. (2017). Investigation of impact of wheel wander on pavement performance. *Road Materials and Pavement Design*, *18*(2), 390–407. https://doi.org/10.1080/14680629.2016.1162730

Sillem, A. (2008). Feasibility study of a tire hydroplaning simulation in a monolithic finite element code using a coupled Eulerian-Lagrangian method. *Delft University of Technology*, *October*, 1–133.

Simko, D. J. (2016). Increasing road infrastructure capacity through the use of autonomous vehicles [Master's thesis, Naval Postgraduate School]. Proquest Dissertations and Theses.

Steyn, W. J. v. M., & Maina, J. W. (2019). Guidelines for the use of accelerated pavement testing data in autonomous vehicle infrastructure research. *Journal of Traffic and Transportation Engineering (English Edition)*, *6*(3), 273–281.

Tientrakool, P., Ho, Y. C., & Maxemchuk, N. F. (2011). Highway capacity benefits from using vehicle-to-vehicle communication and sensors for collision avoidance. *IEEE Vehicular Technology Conference*, 0–4.

Wanek-Libman, M. (2020). CTDOT scheduled to deploy first full-size automated transit

bus in North America. *Mass Transport*. https://www.masstransitmag.com/alt-mobility/autonomous-vehicles/article/21143509/ctdot-scheduled-to-deploy-first-fullsize-automated-transit-bus-in-north-america

Wu, R. (2008). Evaluation of the effect of wander on rutting performance in hvs tests. *Third International Conference on Accelerated Pavement Testing October 2008, Madrid, Spain*.

Zhao, X., Shen, A., & Ma, B. (2020). Temperature response of asphalt pavement to low temperatures and large temperature differences. *International Journal of Pavement Engineering*, *21*(1), 49–62. https://doi.org/10.1080/10298436.2018.1435883

Zhou, F., Hu, S., Chrysler, S. T., Kim, Y., Damnjanovic, I., Talebpour, A., & Espejo, A. (2019). Optimization of lateral wandering of automated vehicles to improve traffic safety and pavement life. *Transportation Research Record*, 1–9.

Zhu, J., Ghafoori, E., & Dinegdae, Y. (2020). *Characterization of asphalt mixtures and bitumen to minimize shear-related distresses in asphalt pavement*. VTI rapport 1056A

Zhu, S., Liu, X., Cao, Q., & Huang, X. (2017). Numerical study of tire hydroplaning based on power spectrum of asphalt pavement and kinetic friction coefficient. *Advances in Materials Science and Engineering*, *2017*. https://doi.org/10.1155/2017/5843061

Chapter 5 Conclusions and Recommendations

5.1 Overview

The movement of autonomous trucks (AT) will bring potential improvements in transportation sectors. Implementation of AT will reduce traffic deaths significantly and maximize roadway capacity. AT has some negative impacts on the performance of asphalt concrete (AC) pavement. along with many advantages. The lane-centering tendency of AT channelizes the wheel loading distribution on narrower width reducing wander. Compared to human-driven trucks, decreased wander of AT wheel induces more rutting and bottom-up (BU) fatigue cracking in AC pavement. Accumulated rutting might also influence the traffic safety factors in wet weather.

Evaluation of additional distresses from AT in AC pavement and their optimization have been studied in this research and presented in Chapter 3. Distribution of wheel load on traffic lane and positioning of trucks on different lanes of a road section was modified to optimize pavement distresses. Distribution of wheel load was applied for a wide range of wheel wander starting from zero. Performance has been studied for a dedicated lane for AT and mixing of AT with human-driven trucks. Pavement distresses induced from AT and their optimization were evaluated by devising traffic input in Mechanistic-Empirical Pavement Design Guide software, AASHTOWare. The load equivalency factor (LEF) was evaluated for different wheel loading distribution in a pavement lane. LEF for distribution of loading and lane distribution factor for vehicle positioning on different lanes were used to modify traffic inputs. Pavement performance was evaluated for modified traffic input and constant structural design, material properties, climate factors to observe pavement

distresses and their optimization. Besides, an attempt was made to allow the AT movement on a lower temperature period only to minimize pavement distresses. Climate data was modified in this study to get the benefit of lower temperature in predicting pavement distresses. The major findings of these studies are presented in clause 5.2 of this chapter.

Presented in Chapter 4, the effect of AT on AC rutting for different wheel wander was investigated using the permanent deformation of the asphalt concrete layer for roads (PEDRO) program. This program can evaluate the AC rutting for a wide range of wheel wander and vehicle speeds. Master curves of the dynamic shear modulus and phase angle of asphalt mixtures were generated to obtain input in PEDRO. Rutting in AC pavement was evaluated for a wide range of wheel wanders and vehicle speeds. Structural design, material properties and climate data were kept constant to observe the effect of AT. AC rutting was also predicted for different vehicle speeds for each wander condition to obtain optimized distress. Traffic safety factors in wet weather conditions were evaluated for predicted rutting of different simulations. An attempt was made to improve the pavement distresses by placing all the ATs in the low-temperature duration of a day. The specific findings of this study are summarized in clause 5.3 of this chapter. General conclusions from the studies presented in this thesis are presented here. Besides, the limitations of this research and the recommendations for future research are also presented.

5.2 Major Findings from the Optimization of AT Movement and Distress

- The explicit control of AT to follow the uniform distribution of the wheel load on a pavement lane significantly reduces the pavement distresses. This reduction

scenario is observed compared to zero wander (full autonomous condition). The uniform distribution covers the full width of the lane and spreads loading repetition in a wide range of areas. Reduction of AC rutting and BU fatigue cracking, for uniform distribution of ATs is found to be by 30.7%, and 93.9%, respectively. The coverage of the full width of a traffic lane might have negative effects. The negative effects were not analyzed in this study.

- Significant improvement in rutting and fatigue cracking was observed for equal distribution of the full AT in different pavement lanes with human-driven trucks. This equal distribution proportionately distributes the additional distress in different lanes. AC rutting and BU cracking reduce by 14.7%, and 69.0%., respectively for equally distributed trucks compared to the disproportionately distributed trucks.
- It is also noticeable that the incorporation of field wander (0.76 cm) might allow a certain additional percentage of AT movement at specific pavement distresses. The increased wander prevents the single point distribution of the wheel load from AT. The percentage decrease in AC rutting and BU cracking for 0.76 cm standard deviation of wheel loading is 2.62%, and 10.8%, respectively.
- Explicit control of AT to specific loading pattern or distribution or low-temperature time might bring remarkable minimization of the detrimental effects of AT on the pavement section. The control of AT at a low-temperature period is advantageous due to having a higher modulus of AC mixtures at low temperatures. This control reduces AC rutting for different scenarios up to 23.9%.

5.3 Major Findings from Rutting and Traffic Safety Analysis

- Predicted AC rutting was found to be increasing with decreasing wheel wander. The highest percentage of 263.6 (%) was observed for fully AT loading with zero wander conditions. The lane centering tendency of AT permits the vehicles to move on a channelized path. This type of channelization increases the wheel load repetition on a single point. Increased wheel load repetition is a significant contributor to the increment of AC rutting.
- Maximum rutting is observed in the center of the dual-wheel in the baseline scenario. The maximum rutting point in autonomous scenarios moves under each wheel. Upheaval in wheel path increases with decreasing standard distribution of the loading distribution of AT. The upheaval has reached to about 21% compared to the highest rutting at the baseline scenario. Overestimation of upheaval is observed from PEDRO analysis. Remarkably, the spreading of the rutting profile is becoming narrower with a decreasing standard deviation of AT loading. Compared to the human-driven truck, rut width reduces by 0.26 m for AT.
- The increasing truck speed is beneficial from a pavement durability perspective due to a significant reduction in rutting accumulation. The predicted rutting at zero wander condition is about 33 (mm) at a speed of 60 (km/hr) and about 19 mm at the speed of 120 (km/hr). It suggests that the decision-maker should consider an increased speed for autonomous traffic road or lane.
- Increasing truck speed reduces rutting continuously and increases hydroplaning speed up to a critical point. Beyond that critical point, hydroplaning speed and

rutting accumulation becomes contradictory. These contradictions of pavement performance and traffic safety have been attempted to remove by presenting graphical relationships among AT speed, hydroplaning speed (HPS) (mainly car speed) and water film depth (WFD). Furthermore, this research has developed critical values (threshold values) for truck speed, WFD and HPS parameters for a wide range of autonomous scenarios. This might be useful to consider traffic safety factors in pavement design.

- There is a remarkable reduction in AC rutting by scheduling all ATs in the low-temperature duration of a day. This also reduces the hydroplaning risk of light-weight vehicles, originated from rutting induced from AT traffic. Adjustment of traffic loading frequency significantly reduces AC rutting and HPS for full autonomous trucks up to 44.1% and 5.1%, respectively. The allocation of AT at low temperatures is beneficial due to the improved properties of AC mixtures.

5.4 Recommendations for Future Works

- The studies presented in this thesis is entirely based on simulation. Most pavement design software can not predict pavement performance for autonomous vehicles. It will be a good research option to modify pavement design software to incorporate autonomous scenario. The uniform distribution of wheel loading on a road section might have negative effects due to covering the whole width of the lane. It will be a great contribution to pavement designers to study these effects.
- Auto manufacturers are performing field experiments on autonomous vehicles to observe the operational capability of autonomous vehicles. It might be a good

option to observe the pavement performance for the movement of the autonomous truck. Along with simulation or computer modeling, it could be better to develop laboratory experimental procedures to determine the impact of the autonomous truck on asphalt concrete pavement.

- Different organizations are currently conducting field study for commercial launching of autonomous passenger and freight transport. It will take longer to occupy the road lane completely with fully autonomous vehicles. Numerical, empirical, and experimental procedures to evaluate pavement performance directly might be an important contribution in the field of pavement engineering.
- Relaxation modulus is an essential parameter for the accumulation of asphalt pavement distress. The higher relaxation ability of asphalt mixtures can easily release the thermal stress without exceeding the allowable limit. Optimization of pavement distress has been presented in this study by placing autonomous trucks on the low-temperature period of a day. The effects of this placement on the relaxation modulus and cracking in asphalt pavement need to investigate carefully.
- The movement of autonomous trucks on a road is entirely dependent on the marking, signals, or communication technology. In the lack of proper infrastructures in the traveling lane, the behavior of autonomous vehicles can be obtained from transportation sectors easily. The additional impact of this misconduct of vehicles on pavement performance can be modeled.
- There is more possibility to occur truck platooning for the movement of the autonomous truck in the road. This truck platooning increases highway capacity.

Increased highway capacity might have significant negative effects on asphalt pavement. This can be studied in the future.

Appendix

Table A1.1 Raw data from multi-linear elastic analysis for layer=1, z=0 (unit is in micro-strain)

Y	Normal Strain X-X	Normal Strain Y-Y	Normal Strain Z-Z	Shear Strain XY	Shear Strain XZ	Shear Strain YZ
-32	-0.012285	0.056139	-0.024037	-0.26833	-1.8131E-12	-1.8156E-11
-24	0.015843	0.036075	-0.026961	-0.32862	-3.2178E-13	1.5585E-11
-16	0.060013	-0.0054949	-0.0262	-0.36382	-6.7899E-14	-1.9478E-11
-8	0.11597	-0.068881	-0.017791	-0.34403	5.5697E-12	2.7644E-11
-4	0.13596	-0.11472	-0.026035	-0.30168	3.1488E-12	-1.7957E-11
0	0.12942	-0.14066	-0.037072	-0.24611	-3.6184E-12	-1.1345E-12
3.54	0.41548	-0.18454	0.2179	-0.17654	-0.014808	-0.014808
7.08	0.14936	-0.19681	-0.057047	-0.08494	-0.014808	-0.014808
8.95	0.18428	-0.19802	-0.023879	-0.037882	-1.8879E-12	2.9204E-11
10.8	0.18921	-0.19438	-0.015665	-0.00072169	-0.014808	-0.014808

Table A1.2 Raw data from multi-linear elastic analysis for layer=1, z=0.25" (unit is in micro-strain)

Y	Normal Strain X-X	Normal Strain Y-Y	Normal Strain Z-Z	Shear Strain XY	Shear Strain XZ	Shear Strain YZ
-32	-0.012189	0.052232	-0.02185	-0.25023	0.0006783	-0.0037856
-24	0.012884	0.032577	-0.02391	-0.30552	0.00056009	-0.0040245
-16	0.052298	-0.0074641	-0.022279	-0.33717	-0.00047882	-0.0034903
-8	0.10119	-0.069001	-0.012843	-0.31733	-0.0035043	-0.002311
-4	0.13287	-0.098514	-0.027265	-0.28262	0.0027497	0.0082872
0	0.18001	-0.14846	-0.053014	-0.21861	0.039496	-0.012348
3.54	-0.035958	-0.16058	0.35938	-0.14806	-0.31478	-0.041897
7.08	0.21207	-0.16481	-0.081708	-0.080742	0.037604	-0.0074894
8.95	0.18723	-0.16603	-0.029973	-0.04061	0.011052	0.0061221
10.8	0.18421	-0.17032	-0.018415	0.0086299	-0.0085998	-0.034841

Table A1.3 Raw data from multi-linear elastic analysis for layer=1, z=0.75" (unit is in micro-strain)

Y	Normal Strain X-X	Normal Strain Y-Y	Normal Strain Z-Z	Shear Strain XY	Shear Strain XZ	Shear Strain YZ
-32	-0.012382	0.043892	-0.017111	-0.21241	0.0018311	-0.0027148
-24	0.0085586	0.027223	-0.019302	-0.2588	0.00098348	-0.001795
-16	0.0416	-0.0065184	-0.018774	-0.2851	-0.0012242	0.00037131
-8	0.08296	-0.057938	-0.013044	-0.26801	-0.0053615	0.0042415
-4	0.10522	-0.08702	-0.011179	-0.2368	-0.0065715	0.0080858
0	0.14164	-0.12167	-0.025738	-0.18971	0.010535	0.019469
3.54	0.029873	-0.13937	0.12184	-0.13224	-0.15108	-0.0129
7.08	0.15968	-0.14735	-0.020746	-0.065667	-0.0081998	-0.024715
8.95	0.14724	-0.14772	-0.0023599	-0.032977	-0.010049	0.00049483
10.8	0.14708	-0.14869	-0.00079932	0.0044194	-0.025698	-0.018448

Table A1.4 Raw data from multi-linear elastic analysis for layer=1, z=1.5" (unit is in micro-strain)

Y	Normal Strain X-X	Normal Strain Y-Y	Normal Strain Z-Z	Shear Strain XY	Shear Strain XZ	Shear Strain YZ
-32	-0.012469	0.031517	-0.010459	-0.15605	0.0028874	-0.0034038
-24	0.0019997	0.018998	-0.011598	-0.18901	0.0011974	-0.0015395
-16	0.025047	-0.0058126	-0.010793	-0.20714	-0.0027691	0.0023486
-8	0.054073	-0.043173	-0.0064996	-0.19379	-0.0096941	0.0090811
-4	0.068639	-0.065522	-0.0024257	-0.17041	-0.014315	0.013427
0	0.083666	-0.086838	-0.0036643	-0.13483	-0.017552	0.023703
3.54	0.079519	-0.098017	0.0062466	-0.095112	-0.051232	-0.0093139
7.08	0.097424	-0.10894	0.0021233	-0.048964	-0.037176	-0.024972
8.95	0.097316	-0.11059	0.0060868	-0.023558	-0.02373	-0.0028191
10.8	0.097712	-0.11059	0.0059498	0.0024596	-0.03851	-0.014641

Table A1.5 Raw data from multi-linear elastic analysis for layer=1, z=2.5" (unit is in micro-strain)

Y	Normal Strain X-X	Normal Strain Y-Y	Normal Strain Z-Z	Shear Strain XY	Shear Strain XZ	Shear Strain YZ
-32	-0.012406	0.015105	-0.0018241	-0.081105	0.0030903	-0.0038399
-24	-0.0065391	0.0080565	-0.0014487	-0.096269	0.00045571	-0.001143
-16	0.0032298	-0.0049413	-0.00011548	-0.10363	-0.0053407	0.0042256
-8	0.015745	-0.02379	0.002752	-0.095407	-0.015172	0.01331
-4	0.022029	-0.035072	0.0051956	-0.083171	-0.02175	0.019521
0	0.027617	-0.043966	0.0037582	-0.064974	-0.029523	0.02701
3.54	0.031026	-0.047066	-0.00054966	-0.046231	-0.050301	-0.0075561
7.08	0.033848	-0.055222	0.0068811	-0.024602	-0.05028	-0.023817
8.95	0.034459	-0.057314	0.0096724	-0.011845	-0.035069	-0.0043151
10.8	0.034644	-0.057464	0.0098467	0.0011307	-0.049775	-0.01433

Table A1.6 Raw data from multi-linear elastic analysis for layer=1, z=3.5" (unit is in micro-strain)

Y	Normal Strain X-X	Normal Strain Y-Y	Normal Strain Z-Z	Shear Strain XY	Shear Strain XZ	Shear Strain YZ
-32	-0.012253	-0.0012538	0.0066937	-0.0062904	0.0019594	-0.0029264
-24	-0.014907	-0.0028008	0.0084946	-0.003771	-0.0014323	0.0002378
-16	-0.018288	-0.0039497	0.010226	-0.00051338	-0.0083508	0.0061647
-8	-0.022114	-0.004235	0.011489	0.0024311	-0.019662	0.015864
-4	-0.023968	-0.0041529	0.011946	0.0034118	-0.027121	0.022735
0	-0.025608	-0.001592	0.0088293	0.0037001	-0.03578	0.027841
3.54	-0.026734	0.0019362	0.0045336	0.0020161	-0.056487	-0.0061236
7.08	-0.027386	-0.0017925	0.0097957	0.00024203	-0.057334	-0.022138
8.95	-0.027556	-0.0033473	0.012148	-4.6927E-05	-0.042146	-0.0044475
10.8	-0.027609	-0.003585	0.012503	-0.00017849	-0.056849	-0.014261

Table A1.7 Raw data from multi-linear elastic analysis for layer=1, z=5.3" (unit is in micro-strain)

Y	Normal Strain X-X	Normal Strain Y-Y	Normal Strain Z-Z	Shear Strain XY	Shear Strain XZ	Shear Strain YZ
-32	-0.012057	-0.030614	0.022026	0.12804	-0.0034097	0.0021565
-24	-0.030086	-0.022314	0.026473	0.16237	-0.0076796	0.0052389
-16	-0.057199	-0.0022549	0.029073	0.18477	-0.014813	0.0098407
-8	-0.090529	0.030695	0.027664	0.17836	-0.025147	0.016156
-4	-0.10708	0.051444	0.024492	0.15914	-0.03149	0.020473
0	-0.12165	0.074401	0.018494	0.12725	-0.038432	0.021918
3.54	-0.13163	0.090034	0.014181	0.088773	-0.057872	-0.0061601
7.08	-0.13793	0.093853	0.015985	0.044929	-0.059025	-0.017697
8.95	-0.1396	0.093585	0.017418	0.021209	-0.044088	-0.0023239
10.8	-0.14009	0.093443	0.017766	-0.0025398	-0.058872	-0.014445

Table A1.8 Raw data from multi-linear elastic analysis for layer=1, z=6.6" (unit is in micro-strain)

Y	Normal Strain X-X	Normal Strain Y-Y	Normal Strain Z-Z	Shear Strain XY	Shear Strain XZ	Shear Strain YZ
-32	-0.012242	-0.051787	0.033348	0.22478	-0.010012	0.008652
-24	-0.041617	-0.036547	0.040045	0.28228	-0.014595	0.010997
-16	-0.086257	-0.0014575	0.04383	0.31889	-0.020546	0.01286
-8	-0.14143	0.055013	0.041323	0.3063	-0.027418	0.013201
-4	-0.1689	0.090437	0.036009	0.27289	-0.030846	0.012331
0	-0.19309	0.12984	0.026758	0.21792	-0.033926	0.010199
3.54	-0.20967	0.15633	0.020687	0.15194	-0.050835	-0.0080438
7.08	-0.22014	0.16277	0.022592	0.076912	-0.051998	-0.011717
8.95	-0.22291	0.16214	0.024465	0.036352	-0.037424	0.0014893
10.8	-0.22371	0.16179	0.02501	-0.004222	-0.052349	-0.014868

Table A1.9 AADTT for integrated scenario with different simulations

AT (%)/ Simulations	AADTT for Integrated Scenario					
	EFW0	EFW3	EFWU	ERW0	ERW3	ERWU
0	2000	2000	2000	2000	2000	2000
10	1930	1930	1889	2055	2033	1867
20	1860	1838	1778	2111	2066	1733
30	1790	1757	1667	2167	2100	1600
40	1720	1676	1556	2222	2133	1467
50	1650	1594	1445	2277	2166	1333
60	1580	1513	1333	2333	2200	1200
70	1510	1432	1222	2389	2233	1067
80	1440	1351	1111	2445	2266	933
90	1370	1270	1000	2500	2300	800
100	1300	1189	889	2556	2333	667

Table A1.10 AADTT for integrated scenario with different simulations (last part)

AT (%)/ Simulations	AADTT for Integrated Scenario					
	DFW0	DFW3	DFWU	DRW0	DRW3	DRWU
0	2000	2000	2000	2000	2000	2000
10	2034	2014	1960	2260	2220	1920
20	2068	2028	1920	2520	2440	1840
30	2102	2042	1880	2780	2660	1760
40	2136	2056	1840	3040	2880	1680
50	2170	2070	1800	3300	3100	1600
60	2204	2084	1760	3560	3320	1520
70	2238	2098	1720	3820	3540	1440
80	2272	2112	1680	4080	3760	1360
90	2306	2126	1640	4340	3980	1280
100	2340	2140	1600	4600	4200	1200

Table A1.11 AADTT for separated scenario with different simulations

AV (%)/ Simulations	AADTT for Separated Scenario						
	Baseline	SFW0	SFW3	SFWU	SRW0	SRW3	SRWU
0	0	0	0	0	0	0	0
10	200	234	214	160	460	420	120
20	400	468	428	320	920	840	240
30	600	702	642	480	1380	1260	360
40	800	936	856	640	1840	1680	480
50	1000	1170	1070	800	2300	2100	600
60	1200	1404	1284	960	2760	2520	720
70	1400	1638	1498	1120	3220	2940	840
80	1600	1872	1712	1280	3680	3360	960
90	1800	2106	1926	1440	4140	3780	1080
100	2000	2340	2140	1600	4600	4200	1200

Table A2.1 Collected properties for asphalt mixtures

Temp. (℃)	Freq. (Hz)	Layer 1		Layer 2	
		E* (ksi)	Phase Angle (°)	E* (ksi)	Phase Angle (°)
-10	0.1	2598.4	16.1	1932.9	15.1
-10	0.5	3141.4	13.4	2597.2	10.9
-10	1	3263.5	12.1	2727.6	9.2
-10	5	4155.6	9.6	3166.8	7.1
-10	10	4268.6	8.3	3356.6	6.7
-10	25	4498.6	6.9	3575.5	3.5
5	0.1	720.8	27.4	839.5	24.6
5	0.5	1129.0	24.5	1206.6	21.6
5	1	1604.0	21.3	1408.3	19.8
5	5	2208.6	17.1	1948.9	16.2
5	10	2407.5	15.3	2062.4	15.1
5	25	3153.1	11.2	2339.3	13.1
25	0.1	86.7	32.7	112.7	30.0
25	0.5	169.0	34.4	198.0	32.4
25	1	245.1	31.8	271.8	31.3
25	5	449.3	29.9	478.0	29.9
25	10	577.7	29.2	615.0	29.3
25	25	778.6	26.4	814.2	26.9
40	0.1	24.8	24.8	33.5	27.9
40	0.5	39.2	29.4	57.7	31.2
40	1	52.6	29.6	79.0	30.7
40	5	111.8	30.1	147.9	32.8
40	10	164.2	30.1	208.7	32.7
40	25	235.0	31.4	305.2	31.5

Table A2.2 Calculated properties for asphalt mixtures

Temp. (°C)	Freq. (Hz)	Layer 1			Layer 2		
		Pc	G* (ksi)	Phase Angle (°)	Pc	G* (ksi)	Phase Angle (°)
-10	0.1	0.859	443.9	3.5	0.720	367.9	7.4
-10	0.5	0.935	492.0	1.6	0.859	443.8	3.5
-10	1	0.948	502.6	1.3	0.880	456.2	3.0
-10	5	0.992	730.1	0.2	0.938	494.2	1.5
-10	10	0.993	774.5	0.2	0.957	511.4	1.0
-10	25	0.994	865.5	0.1	0.975	540.6	0.6
5	0.1	0.307	154.9	22.7	0.357	180.4	20.4
5	0.5	0.471	238.5	15.7	0.499	253.0	14.7
5	1	0.630	320.5	10.2	0.568	288.7	12.2
5	5	0.784	402.3	5.6	0.724	370.0	7.3
5	10	0.825	424.5	4.5	0.751	384.6	6.5
5	25	0.937	493.0	1.5	0.811	417.1	4.8
25	0.1	0.027	13.6	34.6	0.038	18.9	35.7
25	0.5	0.061	30.8	35.8	0.074	37.1	35.3
25	1	0.095	47.6	34.3	0.107	53.6	33.6
25	5	0.187	94.0	28.9	0.200	100.6	28.2
25	10	0.244	123.2	25.8	0.261	131.5	24.9
25	25	0.332	167.4	21.5	0.347	175.0	20.9
40	0.1	0.005	2.7	16.5	0.006	3.1	19.3
40	0.5	0.009	4.3	23.9	0.016	7.9	30.9
40	1	0.014	6.9	29.7	0.024	12.1	34.0
40	5	0.037	18.7	35.7	0.052	26.3	36.0
40	10	0.059	29.8	35.9	0.079	39.5	35.1
40	25	0.090	45.3	34.5	0.122	61.1	32.7

Table A2.3 Pavement temperature data used in rutting prediction from PEDRO for layer 1 (January to June)

Month/Hour	January	February	March	April	May	June
0	-16.15	-18.17	-7.46	0.45	11.71	18.15
1	-16.27	-17.52	-7.78	0.18	11.32	17.72
2	-16.39	-17.09	-8.04	-0.06	10.96	17.33
3	-16.52	-16.94	-8.28	-0.29	10.5	16.92
4	-16.67	-16.8	-8.55	-0.44	10.01	16.67
5	-16.81	-16.58	-8.83	-0.5	10.41	17.81
6	-17.01	-16.58	-9	0.1	11.99	19.29
7	-17.27	-16.58	-8.76	1.12	13.7	21.02
8	-17.43	-15.86	-7.99	2.46	15.48	22.9
9	-16.84	-14.35	-6.87	3.81	17.05	24.24
10	-15.85	-12.69	-5.74	4.84	18.23	25.24
11	-14.82	-11.61	-4.84	5.55	19.01	25.94
12	-13.8	-11.04	-4.15	5.97	19.55	26.38
13	-13.04	-10.82	-3.67	6.15	19.78	26.63
14	-12.62	-10.89	-3.37	6.17	19.8	26.67
15	-12.62	-11.04	-3.26	6.09	19.64	26.39
16	-13.4	-11.25	-3.4	5.76	19.31	25.92
17	-14.3	-11.83	-3.85	5.05	18.73	25.29
18	-14.69	-12.69	-4.72	3.68	17.67	24.47
19	-14.88	-13.7	-5.42	2.2	15.75	22.86
20	-15.04	-15.07	-5.88	1.63	14.12	20.84
21	-15.22	-16.08	-6.19	1.28	13.27	20.05
22	-15.42	-16.94	-6.43	1	12.67	19.52
23	-15.69	-18.02	-6.64	0.77	12.23	18.91

Table A2.4 Pavement temperature data used in rutting prediction from PEDRO for layer 1 (July to December)

Month/Hour	July	August	September	October	November	December
0	20.23	20.62	20.34	7.35	-1.08	-10.66
1	19.85	20.09	19.74	7.14	-1.21	-10.87
2	19.51	19.62	19.16	6.91	-1.32	-11.04
3	19.16	19.34	18.75	6.8	-1.47	-11.23
4	18.85	19.12	18.5	6.65	-1.67	-11.46
5	19.64	19.1	18.32	6.56	-1.81	-11.67
6	21.04	20.31	18.59	6.49	-1.93	-11.86
7	22.55	21.79	20.19	6.74	-2.02	-11.98
8	24.1	23.59	22.26	7.88	-1.75	-12.05
9	25.24	25.33	24.56	9.29	-0.77	-11.6
10	26.11	26.55	26.49	10.78	0.5	-10.78
11	26.8	27.43	27.89	11.94	1.88	-9.97
12	27.25	28.11	28.86	12.75	3.06	-9.26
13	27.53	28.52	29.48	13.17	3.78	-8.79
14	27.66	28.74	29.63	13.26	3.87	-8.58
15	27.64	28.58	29.42	12.95	3.07	-8.79
16	27.37	28.1	28.84	12.15	1.62	-9.48
17	26.77	27.3	27.34	10.54	0.62	-9.9
18	25.79	25.77	24.93	9.52	0.17	-10.14
19	24.04	23.85	23.59	8.99	-0.18	-10.36
20	22.26	22.96	22.89	8.53	-0.44	-10.55
21	21.55	22.4	22.16	8.04	-0.65	-10.68
22	21.07	21.87	21.43	7.59	-0.82	-10.82
23	20.64	21.28	20.76	7.31	-0.98	-11.02

Table A2.5 Pavement temperature data used in rutting prediction from PEDRO for layer 2 (January to June)

Month/Hour	January	February	March	April	May	June
0	-13.91	-15.92	-5.22	2.69	9.71	16.15
1	-14.03	-15.28	-5.53	2.42	9.32	15.72
2	-14.15	-14.84	-5.8	2.18	8.96	15.33
3	-14.28	-14.7	-6.04	1.95	8.5	14.92
4	-14.42	-14.56	-6.31	1.81	8.01	14.67
5	-14.57	-14.34	-6.59	1.75	8.41	15.81
6	-14.77	-14.34	-6.76	2.34	9.99	17.29
7	-15.02	-14.34	-6.52	3.36	11.7	19.02
8	-15.18	-13.62	-5.75	4.7	13.48	20.9
9	-14.6	-12.11	-4.63	6.05	15.05	22.24
10	-13.61	-10.45	-3.5	7.08	16.23	23.24
11	-12.58	-9.37	-2.6	7.79	17.01	23.94
12	-11.56	-8.8	-1.91	8.21	17.55	24.38
13	-10.8	-8.58	-1.42	8.39	17.78	24.63
14	-10.38	-8.65	-1.13	8.42	17.8	24.67
15	-10.38	-8.8	-1.02	8.33	17.64	24.39
16	-11.16	-9.01	-1.16	8	17.31	23.92
17	-12.06	-9.59	-1.61	7.3	16.73	23.29
18	-12.45	-10.45	-2.48	5.92	15.67	22.47
19	-12.64	-11.46	-3.18	4.44	13.75	20.86
20	-12.8	-12.83	-3.64	3.87	12.12	18.84
21	-12.98	-13.84	-3.94	3.52	11.27	18.05
22	-13.18	-14.7	-4.19	3.24	10.67	17.52
23	-13.45	-15.78	-4.4	3.01	10.23	16.91

Table A2.6 Pavement temperature data used in rutting prediction from PEDRO for layer 2 (July to December)

Month/Hour	July	August	September	October	November	December
0	18.23	18.62	18.34	5.35	1.16	-8.42
1	17.85	18.09	17.74	5.14	1.03	-8.63
2	17.51	17.62	17.16	4.91	0.92	-8.79
3	17.16	17.34	16.75	4.8	0.77	-8.99
4	16.85	17.12	16.5	4.65	0.57	-9.22
5	17.64	17.1	16.32	4.56	0.43	-9.43
6	19.04	18.31	16.59	4.49	0.31	-9.62
7	20.55	19.79	18.19	4.74	0.22	-9.74
8	22.1	21.59	20.26	5.88	0.49	-9.81
9	23.24	23.33	22.56	7.29	1.47	-9.36
10	24.11	24.55	24.49	8.78	2.74	-8.53
11	24.8	25.43	25.89	9.94	4.12	-7.72
12	25.25	26.11	26.86	10.75	5.31	-7.02
13	25.53	26.52	27.48	11.17	6.02	-6.54
14	25.66	26.74	27.63	11.26	6.11	-6.33
15	25.64	26.58	27.42	10.95	5.31	-6.55
16	25.37	26.1	26.84	10.15	3.86	-7.24
17	24.77	25.3	25.34	8.54	2.86	-7.66
18	23.79	23.77	22.93	7.52	2.41	-7.9
19	22.04	21.85	21.59	6.99	2.06	-8.12
20	20.26	20.96	20.89	6.53	1.81	-8.31
21	19.55	20.4	20.16	6.04	1.59	-8.43
22	19.07	19.87	19.43	5.59	1.42	-8.58
23	18.64	19.28	18.76	5.31	1.27	-8.78

Table A2.7 Frequency of traffic loading distribution used in PEDRO

Hour of a Day	Frequency		
	Normal Condition	Adjusted-01	Adjusted-02
0	0.040	0.040	0.061
1	0.033	0.040	0.060
2	0.027	0.040	0.060
3	0.022	0.040	0.060
4	0.018	0.040	0.061
5	0.018	0.040	0.062
6	0.022	0.040	0.062
7	0.028	0.040	0.063
8	0.034	0.040	0.023
9	0.040	0.040	0.023
10	0.045	0.040	0.022
11	0.049	0.040	0.021
12	0.051	0.040	0.021
13	0.053	0.040	0.020
14	0.054	0.040	0.020
15	0.054	0.040	0.020
16	0.054	0.040	0.021
17	0.054	0.040	0.022
18	0.054	0.040	0.022
19	0.053	0.040	0.023
20	0.052	0.040	0.063
21	0.051	0.040	0.063
22	0.048	0.040	0.062
23	0.045	0.040	0.061
24	0.040	0.040	0.061